Optimal Design of Combined Reaction Distillation Processes

Dissertation

zur Erlangung des akademischen Grades

Doktoringenieur
(Dr.-Ing.)

von M. Tech. Jignesh Gangadwala

geb. am 11. October 1978 in Surat, Indien

genehmigt durch die Fakultät für Elektrotechnik und Informationstechnik
der Otto-von-Guericke-Universität Magdeburg

Gutachter: Prof. Dr.-Ing. Achim Kienle
Prof. Dr.-Ing. Sanjay M. Mahajani

Promotionskolloquium am 03. Mai 2007

Forschungsberichte aus dem Max-Planck-Institut
für Dynamik komplexer technischer Systeme

Band 17

Jignesh Gangadwala

Optimal Design of Combined Reaction Distillation Processes

Shaker Verlag
Aachen 2007

Bibliographic information published by the Deutsche Nationalbibliothek
The Deutsche Nationalbibliothek lists this publication in the Deutsche Nationalbibliografie; detailed bibliographic data are available in the Internet at http://dnb.d-nb.de.

Zugl.: Magdeburg, Univ., Diss., 2007

Printed in Germany.

ISBN 978-3-8322-6261-7
ISSN 1439-4804

Shaker Verlag GmbH • P.O. BOX 101818 • D-52018 Aachen
Phone: 0049/2407/9596-0 • Telefax: 0049/2407/9596-9
Internet: www.shaker.de • e-mail: info@shaker.de

Acknowledgments

This thesis originated while I was working as a research assistant at the Max Planck Institute for Dynamics of Complex Technical Systems, Magdeburg. I could not have arrived at this remarkable milestone of my career alone. Many individuals have supported me in my way to this accomplishment.

First of all, my sincere thanks to my supervisor Prof. Dr.-Ing. Achim Kienle for allowing me to work on this interesting topic and permitting to access lavish facilities of the institute. Moreover, I am truly appreciative of his continuous scientific help, many in-depth discussions and his critiques in final stages of the thesis which gave it a perfect finishing touch. I will always feel proud about being an alumnus of his group. I would also like to thank Prof. Sanjay Mahajani for his selfless help on various aspects of this work. At the same time, I would like to recognize the support of his group members during the joint experimental work. In spite of the large physical distance, I received their prompt response whenever I shouted my queries. Further, I want to extend my gratitude to Prof. Robert Weismantel and his colleagues. Because of their support, the methodological aspects of this thesis has strengthened enormously. Not to exaggerate, I will hardly forget many interesting discussion on the topic with Utz-Uwe Haus and Dennis Michaels.

Among others, I would like to express my gratitude to Gabriel Radulescu, Frank Steyer and Erik Stein who showed up at various turning points during this thesis to help me. Next, I feel obliged to all of my group members for their kind cooperation. Here, Carolyn Mangold, Klaus Peter Zeyer and Malte Kaspereit are worth mentioning for their help in the proof reading. Among other group members, I want to thank Michael Mangold and Ilknur Disli-Uslu for their readiness to sort out many of my routine problems.

Further, my cordial gratitude to all my Indian friends in Magdeburg. The relaxed moments we enjoyed and trips we made across the cities of Europe together are a few of the best memories that I will remember for a long time.

Finally, I would like to thank my parents and my two adoring sisters for giving me the much needed love and moral support. In my heart, they belong forever and I know very well that the reverse is also true. I am also grateful to my love Rita for staying close to my heart and supporting me through difficult times. A final word of thanks also for her parents for their love and encouragement.

Magdeburg, May 2007 Jignesh Gangadwala

To my parents

Contents

Notation

A	heat transfer area	m^2
a	activity	
B	bottom flow rate	kmol/hr
$\mathbb{C}$	capital cost	money unit
C	cost factors	[-] or money unit
D	distillate flow rate	kmol/hr
$\mathcal{D}$	diameter	m
Da	Damköhler number	
E	activation energy	kJ/kmol
F	feed flow rate	kmol/hr
F_c	F-factor	$Pa^{0.5}$
fb	tray number into which the recycle is entering	
H^0	height accounted for reboiler and condenser	m
H	enthalpy	kJ/kmol
H^v	enthalpy of vaporization	kJ/kmol
$\mathcal{H}$	height	m
I	binary variable acting as a switch 1 = ON, 0 = OFF	
K_{eq}	equilibrium constant	
k_f	forward reaction rate constant	kmol/kg hr or kmol/kg s
K_s	adsorption constant	
K_W	heat transfer coefficient	kJ/s m^2 K
L	liquid flow	kmol/hr
$Mcat$	total catalyst mass	kg cat
MW	molecular weight	kg/kmol
N_R	number of reactive stages	
N_{Rx}	number of reactors	
N_T	number of column stages	
n_c	number of components	
$\mathbb{O}$	operating cost	money unit
P	pressure	bar
Q	heat duty	kJ/s
r	reaction rate	kmol/s
R	gas constant	kJ/kmol K

Rf	reflux ratio	
sd	tray number from which sidedraw is withdrawn	
$\mathbb{T}$	total cost (capital + operating)	money unit
T	temperature	K
V	vapor flow rate	kmol/hr
$\mathcal{V}$	volume	m^3
x	liquid mole fraction	
y	vapor mole fraction	

Greek Letters

α	relative volatility	
γ	activity coefficient	
ν	stoichiometric coefficient	
ρ_{cat}	catalyst density	kg/m^3
ϕ	phase split fraction	

Subscripts

B	bottom
CON	condenser
col	column
CW	cooling water
D	distillate
F	feed
HW	steam
he	heat exchanger
p	nonreactive packing
R	reactor or reflux
REB	reboiler
rp	reactive packing
s	stage
sh	column shell
T	total

Superscripts

g	vapor
I	input
l	liquid
O	output
org	organic phase

Abbreviations

CMO	constant molar overflow
FTL	feed tray location
NPHSP	column model without consideration of liquid-liquid phase split
PHSP	column model with consideration of liquid-liquid phase split
RDC	reactive distillation column
RDCSR	reactive distillation column coupled with a side reactor
RPLUSC	reactor coupled with a distillation column
REACREB	reactive reboiler at the bottom of the distillation column
nSRC	”n” side reactors coupled to the column

Zusammenfassung

Kontinuierliche Produktionsanlagen mit chemischen Reaktions- und Destillationsprozessen spielen in der chemischen Industrie eine wichtige Rolle. Eine Frage, die oft auftritt, ist, wie diese Funktionseinheiten in optimaler Weise kombiniert werden sollen. Typische Möglichkeiten sind beispielsweise konventionelle Reaktor-Destillations-Systeme mit Recycle, Reaktivdestillationskolonnen oder Seitenreaktor-Konfigurationen.

Um diese Frage zu beantworten, wird ein algorithmischer Ansatz basierend auf mathematischer Modellierung und Optimierung in dieser Doktorarbeit verfolgt. Die Modelle basieren auf Mengen- und Energiebilanzen. Sie sind typischerweise nichtlinear. Mögliche Quellen für Nichtlinearitäten sind beispielsweise die Reaktionskinetik oder das Dampf-Flüssig-Gleichgewicht. Typische Design-Variablen sind entweder kontinuierliche Variablen, wie z.B. Rücklauf- und Aufdampfverhältnisse, Katalysatorbeladungen und Recycle-Flüsse; oder diskrete Variablen, wie z.B. die Anzahl und die Position der Feedböden, die Anzahl und Position von reaktiven Zonen und die Gesamtzahl der Kolonnenböden. Dies führt zu gemischt ganzzahligen Nichtlinearen Optimierungsproblemen (*Mixed-Integer-Nonlinear-Problems* (MINLP)), die in der Regel schwer zu lösen sind.

In der vorliegenden Doktorarbeit wurden neue Lösungsstrategien für die vorliegende Klasse von Problemen untersucht. Die vorgeschlagene Designstrategie folgt einem dreistufigem Ansatz. In einem ersten Schritt werden geeignete Prozesskandidaten mit Hilfe von graphischen Methoden, wie beispielsweise Rückstandskurven, und unter physikalisch-chemischen Gesichtspunkten, ausgewählt. In einem zweiten Schritt wird durch Modellierung und Simulation der Einfluss der Prozessparameter auf die Prozessperformance untersucht. In diesem Stadium ist oft eine experimentelle Validierung des Modells erforderlich. In einem dritten Schritt wird das endgültige optimale Design durch rigorose Optimierung erhalten. Dazu werden zunächst etablierte lokale Optimierungsverfahren eingesetzt, um ein schnelles vorläufiges Ranking der Prozesskandidaten zu erhalten. Der Vorteil lokaler Optimierer ist, dass sie große MINLP-Probleme effizient behandeln können, gleichwohl haben sie eine Tendenz, bei lokalen Optima steckenzubleiben. Um diese Schwierigkeit zu überwinden, werden anschließend globale Methoden eingesetzt. Dabei handelt es sich um eine große Herausforderung, die bisher wenig untersucht wurde. Erste Schritte in dieser Richtung werden im Rahmen dieser Doktorarbeit durch Anwendung von zwei verschiedenen Ansätzen untersucht. Der erste Ansatz basiert auf der Kombination von stochastischen und deterministischen Methoden. Dabei handelt es sich um den Multi-Start-Algorithmus OQNLP [Greenberg & Lasdon, *J. Glob. Op-*

tim., 36:319-338, 2006]. Der zweite Ansatz ist rein deterministischer Art und bestimmt eine globale Schranke für die Zielfunktion eines gegebenen MINLP-Problems durch Benutzung von polyedrischen Relaxierungen. Der letztere Ansatz wurde im Rahmen einer DFG-Forschergruppe in der Gruppe von Herrn Prof. Weismantel an der Otto-von-Guericke-Universität Magdeburg entwickelt. In gemeinsamer Forschungsarbeit wurde er auf ein Fallbeispiel, das in dieser Doktorarbeit betrachtet wird, angewandt.

Zur Illustration der oben erwähnten modellbasierten Design-Strategien werden im Rahmen der vorliegenden Arbeit drei Fallbeispiele mit steigender Komplexität betrachtet. Als ein erstes innovatives Fallbeispiel, wird die Isomerisierung von 2,3-Dimethyl-2-buten (DMB-2) zu 2,3-Dimethyl-1-buten (DMB-1) betrachtet. DMB-1 ist ein hochwertiges Lösungsmittel für die Fein- und Spezialchemie. Diese Isomerisierung ist das einfachste Reaktionssystem, das man sich vorstellen kann. Es ist ein Zweikomponenten-System mit einem idealen Dampf-Flüssigkeitsgleichgewicht und linearer chemischer Kinetik. Als ein zweites Standard-Beispiel, wird die Veresterung von Essigsäure mit Butanol betrachtet. Im Vergleich zum ersten Beispiel hat die Komplexität deutlich zugenommen. Dieses System hat fünf Komponenten, dies bedeutet eine höhere Dimensionalität, ein hochgradig nichtideales Phasengleichgewicht und eine nichtlineare chemische Kinetik. Gleichwohl kann für beide Beispiele eine homogene Flüssigphase angenommen werden. Daher wird ein drittes Fallbeispiel eingeführt, welches das Auftreten eines möglichen Phasenzerfalls der Flüssigphase berücksichtigt. Als chemische Reaktion wird wiederum die Veresterung von Essigsäure mit Butanol betrachtet, die in diesem Falle aber zur Abwasserreinigung eingesetzt wird. Durch die veränderten Rahmenbedingungen kann es bei diesem Anwendungsbeispiel zu dem erwähnten Flüssig-Flüssig-Phasenzerfall kommen. Es wird gezeigt, dass die Reaktivdestillation eine elegante und ökonomisch attraktive Technologie ist, um Essigsäure aus Industrieabwässern zu entfernen. Zu der Komplexität durch die Wechselwirkung zwischen Reaktion und Destillation, kommt bei diesem Prozess die Komplexität durch einen möglichen Phasenzerfall der Flüssigphase hinzu, was ein zusätzliches Umschalten der zugrundeliegenden Modellstruktur erfordert.

Durch die modellbasierte Designstrategie werden im Rahmen der Arbeit für alle drei Fallbeispiele verbesserte und innovative Prozessentwürfe erhalten. Shortcut-Methoden, Modellierung und Simulation funktionieren bei allen drei Fallbeispielen gut. Für die Optimierung treten jedoch Einschränkungen auf. Die lokalen Optimierungsmethoden sind effizient für ein vorbereitendes Prozess-Screening, jedoch versagen sie oft bei der Ermittlung des globalen Optimums. Für ihre effektive Anwendung ist es notwendig, eine gute Initialisierung, geeignete obere und untere Schranken für alle Variablen und

eine geeignete Modellformulierung zu erstellen. Durch den Einsatz des Multi-Start-Optimierungsalgorithmus wurde gezeigt, dass mehrfache lokale Lösungen mit unterschiedlichen Designs existieren. Der Multi-Start-Algorithmus konnte z.T. verbesserte lokale Lösungen ermitteln. Diese Methode kann jedoch keine Garantie für die Globalität der gefundenen Lösung geben. Im Gegensatz dazu, liefert die auf polyedrischen Relaxierungen basierende Methode rigorose globale Schranken für die optimale Lösung. Sie ist jedoch auf Grund der kombinatorischen Komplexität rechenzeitaufwändig. Eine Anwendung war nur für den Isomerisierungsprozess möglich. Für die Anwendung auf komplexere Beispiele sind Weiterentwicklungen erforderlich, die jedoch den Rahmen der Arbeit übersteigen.

Zusätzliche Komplexität tritt im dritten Fallbeispiel durch Modellumschaltung auf. Es konnten daher nur vorläufige Simulationsergebnisse erhalten werden, die jedoch die Attraktivität der vorgeschlagenen Technologie belegen. Eine Optimierung, weder lokal noch global, war nicht möglich und erfordert ebenfalls Weiterentwicklungen, die deutlich über den Rahmen dieser Doktorarbeit hinausgehen.

Abstract

Continuous production plants involving chemical reaction and distillation functionalities have vast applications in the chemical engineering world. A question that often arises is how these functionalities should be combined in an optimal way. Typical possibilities are conventional reactor-distillation systems with recycles, reactive distillation columns or side reactor configurations, for example.

To answer this question, an algorithmic approach based on mathematical modeling and optimization is applied in this thesis. The models are derived from first principles. They are typically nonlinear. Potential sources for nonlinearities are either reaction kinetics or vapor-liquid equilibrium, for example. Typical design variables are either continuous variables such as reflux and reboil ratios, catalyst loading and recycle flows; or discrete variables such as the number and position of feeds, the number and position of reactive zones and the total number of column stages, for example. This will lead to *mixed integer nonlinear problems* (MINLP), which are usually difficult to solve.

In the present thesis, new solution strategies for this class of problems are explored. The proposed design strategy follows a three step approach. In a first step, suitable process candidates are selected based on graphical methods such as residue curve maps and physical/chemical insight. In a second step, the influence of process parameters on process performance is studied through modeling and simulation. At this stage, experimental validation of the model is often required. In a third step, the final optimal design is obtained through rigorous optimization. In the beginning state-of-the-art local optimizers are applied in order to get a quick ranking of the process candidates. The advantage of local optimizers is that they can handle large MINLP problems efficiently, nonetheless, they have a tendency of getting stuck at some inferior local optimum. In order to overcome this difficulty, global methods are applied to perform exhaustive optimization for the promising candidates. This, however, is a challenging task, which has hardly been tackled so far. First steps in this direction are explored in this thesis by applying two different approaches. The first approach is based on the combination of stochastic and deterministic methods, namely, the multi-start algorithm OQNLP [Greenberg & Lasdon, *J. Glob. Optim.*, 36:319-338, 2006]. The second approach is fully deterministic in nature and it determines a global bound of a given MINLP problem by using polyhedral relaxations. The latter approach was developed within a joint DFG research project by the group of Prof. Weismantel from the Otto-von-Guericke-University Magdeburg. In joint research it was applied to the benchmark problems considered in this thesis.

To demonstrate the above-mentioned model based design strategy the following three benchmark problems are considered with increasing level of complexity. As a first innovative benchmark problem isomerization of 2,3-dimethylbutene-2 (DMB-2) to 2,3-dimethylbutene-1 (DMB-1) is considered. DMB-1 is a high value added solvent, which is used in the fine and speciality chemistry. This isomerization system is the most simple reaction system one can think of. It is a two component system with an ideal vapor-liquid equilibrium and linear chemical kinetics. As a second benchmark example, esterification of acetic acid with butanol is considered. Compared to the first example, complexity has increased considerably. This system has five components, i.e. higher dimensionality, highly non-ideal phase equilibrium and nonlinear chemical kinetics. Nevertheless, in both examples, a homogeneous liquid phase can be assumed. Therefore, a third benchmark example is introduced, which accounts for a potential phase split of the liquid phase. Again, esterification of acetic acid with butanol is considered as a chemical reaction. However, the application is concerned with waste water treatment, which can lead to liquid-liquid phase split. It is shown, that reactive distillation is a rather elegant and economically attractive technology for removing acetic acid from waste waters. However, apart from the complexity due to the interaction between reaction and distillation, in this process, complexity is further increased due to the potential phase splitting of the liquid phase, which requires additional switching of the underlying model structure.

Through the model based design procedure innovative and improved designs are obtained for all three benchmark problems. Shortcut methods, modeling and simulation work well for all three benchmark examples. However, limitations occur for the optimization. The local optimization methods are efficient for preliminary process screening but often fail to provide the global optimum. It is necessary to provide a good initialization, appropriate upper and lower bounds on all variables and an appropriate model formulation for their efficient use. It has been shown by the use of the multi-start optimization algorithm that multiple local solutions exist which correspond to different designs. The multi-start algorithm can provide improved local solutions. However, this method can not give any guarantee for the globality of the solution. In contrast to this, the method based on polyhedral relaxations provides rigorous global bounds for the optimal solution. However, it is computationally expensive due to combinatorial complexity. Application was only possible for the isomerization process. Further research is required for application to more challenging process applications.

Additional complexity arises in the third benchmark problem due to model switching. Hence, only preliminary simulation results could be obtained, which indicate the attrac-

tiveness of the proposed technology. Optimization was not yet possible, neither local nor global, and requires further developments, which are clearly beyond the scope of this thesis.

Chapter 1

Introduction

1.1 Problem outline

The concept of combining reaction and distillation functionalities in a fully or partially integrated fashion has become popular in the chemical engineering world. By combining these prime functionalities, for many reaction systems chemical equilibrium limitation can be surpassed due to simultaneous removal of products from the reaction. Further, due to the synergistic effects additional advantages like selectivity improvement and elimination of azeotropes are possible. Some simple candidates for combined reaction distillation processes are shown in Fig. 1.1. These include: on the left, a reactor coupled with a nonreactive distillation column by a recycle loop; on the middle, a reactive distillation column; and on the right, a side reactor coupled with a nonreactive distillation column. Depending on the properties of a reaction system more complex combinations may arise, for example multiple side reactors as indicated in the right of Fig. 1.1. The configurations with a recycle reactor or side reactors are examples of a partial integration whereas the reactive distillation column is an example of a full integration.

The recycle reactor configuration is typically a conventional process where unreacted reactants from the reactor are separated in a distillation unit and are recycled to the reactor. The reactive distillation (RD) combines chemical reaction and distillation in a single processing unit. The commercial success of RD has been demonstrated for the production of MTBE [73, 81] and methyl acetate [1] which showcase RD's ability to render cost-effectiveness and compactness to chemical plants. Lately, RD has been explored as a potentially important process for several other industrial applications. A detailed survey

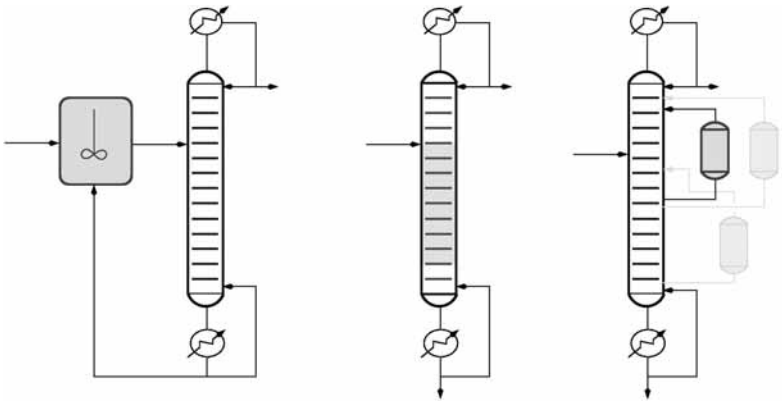

Figure 1.1: Some simple process alternatives for combined reaction distillation processes. Left - a reactor coupled with a distillation column by a recycle stream, middle - a reactive distillation column and right - a side reactor configuration.

of the present RD applications and new potential applications is given in Sharma and Mahajani [71]. A fully integrated multifunctional reactor like RD may not always be advantageous, as sometimes partial integration of reaction and distillation functionalities may exhibit an economical and commercial edge over RD [80]. The side reactor configuration is a prominent alternative to RD as it offers advantages like easy replacement of the spent catalyst without disturbing the process operation and easy column hardware design [3, 69].

The focus of this thesis is to determine the best process design with the best set of operating conditions for a given reaction system and given constraints (production rate, product purities etc.). For this purpose, potential process candidates are evaluated based on their performance in terms of feasibility, economy and operability. The design strategy considered in this thesis is based on mathematical modeling and optimization. The models are derived from first principles. Nevertheless, they may contain varying degrees of detail depending on the complexity of the process. Typical design variables for combined reaction distillation processes can be continuous or discrete in nature. Examples of continuous decision variables are reflux and reboil ratios, catalyst loading and recycle flows. Examples of discrete decision variables are the number and position of feeds, the number and position of reactive trays for an RD, the number and position of reactors for a recycle reactor or a side reactor configuration as well as the total number of column stages. In addition

to these, for detailed design, suitable column internals including reactive and nonreactive packing (or tray specifications) are important [47]. However, their design is usually done in a separate step and, therefore, will not be considered in this thesis.

1.2 Solution approaches

Combination of reaction and distillation can lead to several benefits. However, the complexity introduced by their interaction makes the design procedure a difficult task. There are many alternative design approaches which have been proposed in the literature to handle design complexity.

The first approach in that series consists of conceptual design methods, which gain insight into an RD process based only on the physico-chemical properties of a reacting system. These methods often try to answer following basic questions: 1. whether RD is a feasible option for a given reaction system; 2. what are the feasible design alternatives; and 3. how the optimal design structure look like. Over the years researchers have modified and extended the concept of residue curve maps, fixed point method or distillation lines [88, 87, 6, 21]. Several additional graphical approaches include the difference point method [38], attainable region methods [55, 57, 22], the static analysis method [28] and the rectification body method [50].

In another approach, designs are achieved based on numerical simulation or experiments. Simulation are performed repeatedly while continuously changing the design parameters such as number of stages, feed stage, reaction zone, catalyst loading and reflux and reboil ratio etc., until the desired product specifications are matched. Although it requires many trials, simulation studies are relatively inexpensive. In a similar way experimental-based RD designs are obtained by varying various design parameters to attain a feasible set of operating parameters giving the desired products. Since experimental-based designs are in general expensive, often simulation results are used contemporarily in order to reduce experimental efforts. Customarily, simulation and experiments are aided by heuristics so that the number of trials to be performed can be reduced [5].

A last possible approach is based on mathematical programming. In this approach, mixed-integer nonlinear programming (MINLP) models are written for alternative superstructures generated based on thermodynamic principles [20]. The final design is determined by performing simultaneous optimization of all design variables. The following section briefly discusses aspects of MINLP optimization concerned with RD design.

The generic form of MINLP model reads

$$\begin{array}{ll} \min & f(\mathbf{x}, \mathbf{y}) \\ \text{s.t.} & g(\mathbf{x}, \mathbf{y}) = 0 \\ & h(\mathbf{x}, \mathbf{y}) \leq 0 \\ & \mathbf{x} \in \mathbf{R}^n \\ & \mathbf{y} \in \{0,\ 1\}^m \end{array} \tag{1.1}$$

where f is an objective function to be minimized, $\mathbf{x}$ is a vector of continuous variables and $\mathbf{y}$ is a vector of discrete variables. In case of RD, continuous variables $\mathbf{x}$ are related to the geometrical dimensions or operating variables and discrete variables $\mathbf{y}$ are related to the structural decisions as discussed in section 1.1. Appropriate objective functions to be minimized are either product impurities, energy costs or more rigorously, total annualized costs, including energy and equipment costs. Typically, g is a set of linear and nonlinear equality constraints and h is a set of inequality constraints. Examples of the former are model equations like mass and energy balances, phase equilibrium, reaction rate etc., whereas of the latter are product purity and safety constraints.

MINLP optimization is a powerful and theoretically well-founded methodology to achieve an optimal RD design. The solution algorithms are typically gradient based methods augmented by enumerative procedures dealing with discrete variables. These include state-of-the-art MINLP solvers available in GAMS [9]. In particular, standard branch and bound (SBB) solver or outer-approximation [18] based solver DICOPT can be used. SBB requires a nonlinear solver (NLP) for the examination of the nonlinear subproblem at each node. For that purpose, a widely known implementation of generalized reduced gradient method CONOPT [17] can be used. In addition to a NLP solver, DICOPT requires a MILP solver to deal with discrete variables. For that purpose, the most efficient MILP solver CPLEX [41] can be used. GAMS provides interface to MILP, NLP and MINLP solvers.

These methods have already been applied with some success to reactive distillation processes [13, 79, 76]. The classical techniques, nevertheless, face difficulty in determining the optimal solution due to presence of nonlinearities in RD models. Major sources of the nonlinearities are the reaction kinetics and phase equilibrium equations. These nonlinearities lead to nonconvexity of the MINLP model which in turn leads to multiple local optima in the solution space. In order to overcome the problem of getting stuck into a local solution, a good starting point in the vicinity of the global optimum should be used. This might be obtained by using physical insight or shortcut methods. However, gener-

ally there is no guarantee that the solution represents a global optimum. The alternative approach is to apply new solution strategies capable of finding a global solution.

Methods capable of finding a global solution belong to two different categories, namely, deterministic methods and stochastic methods. An excellent review of these methods has been published by Grossmann and Biegler [32]. Deterministic methods are rigorous methods. They require the calculation of gradients to perform exhaustive search yielding a global solution. The deterministic methods appearing in the literature are interval methods [36] or branch and bound methods employing underestimators. In the latter method, to treat general nonlinear functions occurring in MINLP model, convex underestimators are applied for the corresponding functions. This ensures that relaxations of MINLP can be defined that only involve convex functions. Following this approach, interesting global bounds on the optimal value of a synthesis problem can be given if one is able to derive good convex underestimators. For special functions convex underestimators have been given by Tawarmalani and Sahinidis [84]. Due to the high computational effort required by these methods, they are not yet capable to solve large-scale process engineering problems.

Stochastic methods on the other hand are heuristic based methods. They do not require gradient information and their implementation is conceptually easy. They basically operate in three steps: a sampling step, an evaluation or optimization step and a termination step. The most simple form of stochastic method randomly selects starting points in the solution space. However, this usually requires very high number of starting points to determine the global solution. Advanced stochastic methods, for example population based evolutionary algorithms like, genetic algorithms [54] or probabilistic meta-heuristics like simulated annealing [11], make use of refined heuristic rules and information from the previous search results to determine the global solution in a finite number of steps. On the average these methods are computationally very demanding. Further, due to the probabilistic approach they can also not guarantee the global optimality.

1.3 Thesis outline

The main objective of this thesis is to explore new solution strategies for the optimal design of combined reaction distillation processes. To achieve this the following approach is devised.

- ► Selection of suitable process candidates based on graphical methods.

  For a given reaction system, suitable process candidates can be generated by using physical/chemical insight together with graphical methods.

- ► Exploration of the solution space by using simulation and/or continuation methods.

  Mathematical models can be developed based on first principles for each of the process candidate. The main task here is to perform parameter studies in order to gain insight into the influence of design parameters on process performance. In this thesis, all simulation are performed using the process simulation environment DIVA [52].

- ► Application of optimization techniques, from local methods to global methods, to determine the final design for a given reaction system with given constraints. This should be characterized by the best process configuration with the best set of operating conditions.

  A corresponding MINLP model can be written for each process candidate which is then solved using the following strategy. At first, state-of-the-art local MINLP solvers available in GAMS are used to obtain local results. In particular, SBB is used to solve MINLPs and CONOPT is used to solve NLP subproblems. In a second step global methods are applied. However, the global optimization of RD design problems is a challenging task. In this thesis, first steps in this direction are explored. Two alternative global approaches are investigated. The first approach is based on the combination of stochastic and deterministic methods, namely, multi-start algorithm OQNLP [31, 86]. The second approach is fully deterministic in nature and determines global bounds by using polyhedral relaxations [24].

To demonstrate the above-mentioned model based design strategy, the following three benchmark problems are considered. They are ordered top-down with increasing level of complexity.

- $\rightsquigarrow$ As a first innovative benchmark problem, isomerization of 2,3-dimethylbutene-2 to 2,3-dimethylbutene-1 is considered. This is the most simple reaction system. It is a binary system with ideal vapor-liquid equilibrium and linear kinetics expression.
- $\rightsquigarrow$ In a second step, esterification processes are investigated. These represent an important field of application for combined reaction separation processes. As a practical benchmark problem synthesis of butyl acetate (BuAc) is considered. Compared

to the previous isomerization process, complexity has increased significantly. This system is a five component system, i.e. higher dimensionality, with highly non-ideal phase equilibrium behavior and nonlinear kinetics involving two parallel reactions.

In principle highly non-ideal thermodynamics can also lead to liquid-liquid phase splitting for the BuAc system. However, this effect is not significant for standard production process with approximately equimolar reactants [72, 77]. Additional complexity arising from liquid-liquid phase splitting forms the basis for the next application.

$\rightsquigarrow$ In a third step, reactive distillation processes with potential phase splitting of the liquid phase are addressed. As an interesting technical application example, new process for the removal of acetic acid from waste waters through esterification with BuOH is developed. Unlike the standard BuAc synthesis process, in this process high amount of water enters the column as feed potentially leading to the occurrence of liquid-liquid phase splitting on many column stages.

The isomerization example represents a class of RD applications of binary systems. Common examples of binary systems are dimerization and trimerization reactions. Beside this, its simplicity allows to perform number of inexpensive modeling experiments and thereby provides valuable insight on various solution methods which is also valid for more complex examples. The esterification problem is a good representative of another important class of RD applications including etherification, transesterification, hydrolysis, acetalization, hydration etc. The proposed design strategy can be readily applied to these vast applications provided reliable reaction kinetics and thermodynamics are known. The waste water treatment problem represents an untouched class of RD applications where potential phase splitting of the liquid phase may occur. A few applications exhibiting this phenomena are known, C3 and higher ester synthesis in a batch mode [10], cyclohexanol production from cyclohexene by hydration [60] and recovery of lactic acid from the fermentation broth [48].

This thesis is organized in the following order. At first, chapter 2 considers the isomerization process. For the present example, details on reaction kinetics and thermodynamics are not available in the open literature. These are examined in section 2.2. Section 2.3 deals with the local optimization of alternative process candidates. This section also presents detailed MINLP models and cost functions. The global optimization of these problems is addressed in section 2.4. In section 2.5, the global sensitivity analysis (GSA) is applied to investigate the effects of uncertainty in model parameters on total annual

costs of the final design. There, the concept of GSA is explained and the method is demonstrated by considering parameter uncertainty in two kinetic parameters.

In chapter 3 the esterification process of acetic acid with butanol is investigated. Details on reaction kinetics and phase equilibrium are presented in section 3.2 and 3.3, respectively. Section 3.4 covers the modeling of a reactive distillation column and presents results on experimental validation. Parameter studies are performed for each process candidate in order to gain insight of the parameter domain. The results are discussed in section 3.5, which also provide suitable initializations for rigorous optimization to be applied in section 3.6. There, the MINLP model formulations, cost functions and results of local optimizations for different process candidates are presented. Finally, the global optimization of the underlying MINLP problems is studied in section 3.7.

Chapter 4 considers the reactive distillation process for acetic acid removal, which exhibits potential phase splitting of the liquid phase. In this case, it is difficult to derive a MINLP model which switches between vapor-liquid-liquid-equilibrium equations and vapor-liquid-equilibrium equations based on the phase splitting calculations. As a result, the final designs are obtained by simulation performed in DIVA. Nevertheless, the preliminary MINLP modeling via GAMS is extensively used to generate promising initial states. Section 4.2 is devoted to the model formulation, model verification and solution procedure. In section 4.3. various process candidates are introduced and simulation results for the same are presented. Based on these results, two promising process candidates giving close to 100 % conversion of acetic acid are selected. Finally, in section 4.4 these two configurations are investigated in detail with respect to steady state simulation, open loop dynamic simulation, economical aspects and adaptability to handle acetic acid streams from dilute to very high concentrations.

Finally, in chapter 5 conclusions and future directions are presented.

Chapter 2

Isomerization process

2.1 Introduction

Isomerization systems are, in general, the most simple reaction systems. They can be characterized by low dimensionality, i.e two component systems, ideal thermodynamics and linear kinetics. This chapter considers such a practical as well as innovative example, isomerization of 2,3-dimethylbutene-2 (DMB-2) to 2,3-dimethylbutene-1 (DMB-1). This is an important step in the production of DMB-1 from propylene [45]. In the latter process, propylene is regioselectively dimerized to DMB-2 at first. DMB-2 is a heavy boiling component, which is easy to separate from other undesired dimerization products such as methyl pentenes, hexenes etc. Thereafter, DMB-2 undergoes an isomerization reaction to produce valuable DMB-1.

DMB-1 is used as a key component in the production of musk fragrances and insecticides [68]. The difference in boiling point temperatures of the two isomers DMB-1 (57 ^{o}C) and DMB-2 (73 ^{o}C) is significant. Further, the rate of reaction is sufficiently high for the operating conditions usually employed in a distillation column, so that reactive distillation seems to be a suitable process candidate. Suitable heterogeneous catalysts are sodium/potassium on alumina support or strongly acidic macroporous cation exchange resins, like Amberlyst 15 (see for example [45]).

The outline of the chapter is as follows: first, isomerization kinetics over Amberlyst 15 catalyst is experimentally determined and the binary vapor-liquid equilibrium is studied. Afterwards suitable reactive distillation process candidates capable of performing the isomerization reaction are presented. A preliminary ranking of the process candidates is

obtained using local MINLP optimization methods. The results are subsequently confirmed with two alternative global approaches. Finally, as an outlook a global sensitivity analysis of the final designs with respect to parameter uncertainty is presented.

2.2 Reaction kinetics and phase equilibrium

The reaction kinetics were studied in a batch reactor in a temperature range of 50 - 70 ^{o}C, catalyst loadings between 0.30 - 1.82 gm/gmol DMB-2, and stirrer speeds between 500 - 1500 rpm. The widely known Amberlyst 15 is used as a catalyst.

2.2.1 Materials

DMB-1 ($>$ 98 %) is obtained from the Fluka Chemica AG and DMB-2 ($>$ 98 %) is obtained from the Aldrich Chemica AG. The catalyst Amberlyst 15 is obtained from Rohm & Hass. The catalyst was used in the supplied form for the kinetics experiments.

2.2.2 Experimental procedure and analysis

The reaction was performed in a 100 ml batch mode autoclave provided with a magnetic stirrer, sampling valves, temperature and pressure sensors. Nitrogen pressure is applied to maintain the reactor at 4 bar in order to keep all the reacting components in the liquid phase. The reaction temperature was controlled by immersing the reactor in a water or oil bath. This provides a very good temperature control within $\pm$ 1 ^{o}C. Once the desired reaction temperature was attained, samples were withdrawn through sampling valves at regular time intervals. The composition of the reaction mixture is analyzed by a gas chromatography using FID/TCD combined detectors with a 30m x 250 μm x 0.25 μm INNOWAX column (Hewlett Packard 6890). The column temperature was maintained at 50 ^{o}C. The reaction mixture was also analyzed to check the presence of side products in a separate gas chromatography analyzer using GC/MSD detector with 60m x 250 μm x 0.1 μm DB5ms column (Agilent 6890N).

2.2.3 Side product analysis

The side products detected using a GC/MSD column are shown in Table 2.1. Table 2.1 also shows their normal boiling points. The cumulative amount of these substances is less than 3 %. Since, most of the side products are heavy boiling components, in combined reaction distillation processes, they can be kept in lower concentrations by purging them from the bottom of the column. The desired product DMB-1 is a light boiling component which is obtained at the column top. For simplicity of the following treatments, the side products will not be taken further into account.

Table 2.1: Side products and their normal boiling points (T_b)

	Components	T_b [K]
desired product	2,3-dimethyl-1-butene	328.6
	2-penten-4-methyl (cis)	329.6
	2-penten-4-methyl (trans)	331.8
	2-penten-2-methyl	340.5
	2-penten-3-methyl	340.9
	2-hexene	342.0
reactant	2,3-dimethyl-2-butene	346.4
	2-butanone-3,3-dimethyl	379.0
	2-butanol-2,3-dimethyl	392.0
	pinacolyl alcohol	393.0
	3-butenol-2,3-dimethyl	NA

Values taken from Reid et al. [62] and http://webbook.nist.gov/chemistry/

2.2.4 Influence of mass transport

Fig. 2.1 (a) shows the reaction rates at three different rotation speeds of the magnetic stirrer in the batch reactor. It is obvious from the figure that rotation speed has no significant effect on the reaction rate. In other words, external mass transport resistance from liquid bulk to external catalyst surface has been eliminated. The rest of the experiments were performed at 1500 rpm only.

To check the diffusional resistance inside the catalyst pores, experiments with different catalyst sizes have been performed. From Fig. 2.1 (b) it can be seen that different catalyst particle sizes do not owe significant effect on the overall rate, therefore, internal diffusion

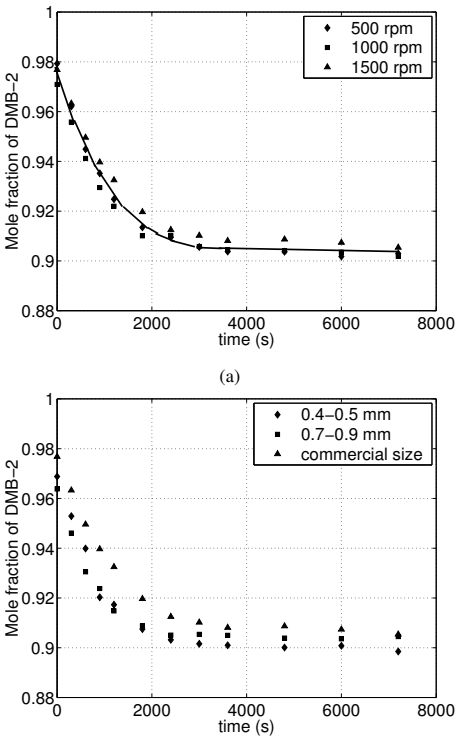

Figure 2.1: For a 333.15 K and 0.6 gm/gmol catalyst loading (a) effect of stirrer speed on the reaction rate; (b) effect of catalyst size on the reaction rate, commercial catalyst has a size of 0.1-0.9 mm

is not playing a key role here. The rest of the experiments were conducted using the commercially available catalyst size.

2.2.5 Kinetics data fitting

A simple pseudo-homogeneous model is used for fitting the kinetics data obtained from the batch experiments. The reaction mechanism and the rate model is given by

$$\text{DMB-2 (1)} \rightleftharpoons \text{DMB-1 (2)}$$

$$r_0 = \frac{1}{\nu_i} \cdot \frac{dn_i}{dt} = McatK_f \cdot (x_1 - \frac{1}{K_{eq}} x_2) \tag{2.1}$$

where, ν_i is the stoichiometric coefficient of i^{th} component, n_i is the number of moles of i^{th} component in $kmol$, $Mcat$ is the catalyst mass in kg, x_1 and x_2 are the mole fractions of DMB-2 and DMB-1. $K_{eq} = \frac{K_f}{K_b} = \frac{x_2^{eq}}{x_1^{eq}}$, where x_1^{eq}, x_2^{eq} are the mole fractions of DMB-2 and DMB-1 at equilibrium.

The temperature dependency of the forward rate constant K_f follows from the Arrhenius equation and that of the chemical equilibrium constant K_{eq} follows from the Van't Hoff equation:

$$K_f = K_f^0 exp(-\frac{E_f^0}{RT}) \quad \text{and} \quad K_{eq} = K_{eq}^0 exp(-\frac{E_{eq}^0}{RT}) \tag{2.2}$$

Where, K_f^0 and K_{eq}^0 are the pre-exponential factors, E_f^0 is the activation energy of the forward reaction and E_{eq}^0 is the difference of the activation energies of the forward and backward reaction. A total of four parameters had to be identified for the pseudo-homogeneous rate expression, namely, K_f^0, E_f^0, K_{eq}^0, and E_{eq}^0. The parameters are obtained by minimizing the square of the difference between the experimental and the calculated mole fractions of DMB-2. For that purpose a standard SQP (sequential quadratic programming) method is used in combination with SDASAC integrator (see also [26]). The rate constants obtained by parameter identification are shown in Table 2.2. Table 2.2 also shows the sum of residuals, which is the square difference between calculated values of mole fraction of DMB-1 and that obtained through experiments. As can be seen from Figs. 2.2 (a) and (b), agreement between the pseudo-homogeneous kinetics model (Eq. - 2.1) and the experimental data is quite satisfactory.

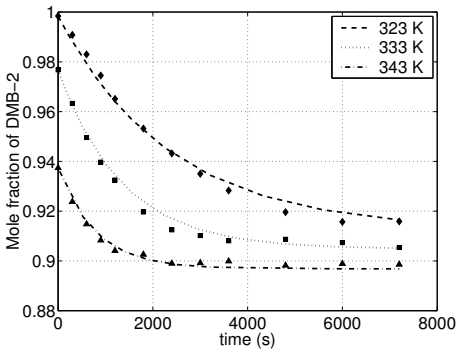

(a)

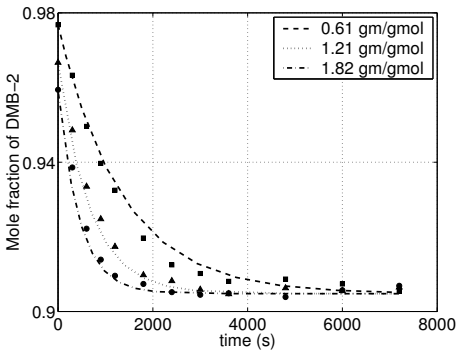

(b)

Figure 2.2: Comparison between experimental data and kinetics model (a) for different temperatures at 0.6 gm/gmol catalyst loading; (b) for different catalyst loadings (gm/gmol DMB-2) at 333.15 K

Later in the optimization section, for simplicity, the values of the rate constant K_f and equilibrium constant K_{eq} are set to 0.1210 $(\frac{kmol}{kg\ hr})$ and 0.1070 , respectively, corresponding to T = 335.0 K in Eq. - 2.2.

Table 2.2: Kinetics parameters for the pseudo-homogeneous model

K_f^0 $\frac{\text{kmol}}{\text{kg-cat·s}}$	E_f^0 $\frac{\text{kJ}}{\text{kmol}}$	K_{eq}^0	E_{eq}^0 $\frac{\text{kJ}}{\text{kmol}}$	Residual ϕ
33320.70	57694.10	2.24547	8476.92	1.80e-4

2.2.6 Phase equilibrium

For the present two component system, experimental VLE data are not available in the open literature. Therefore, in a first step a modified UNIFAC group contribution method [29] is used for the prediction of the VLE. Vapor pressures are calculated using the Antoine equation with parameters from Himmelblau [39]. As shown in Fig. 2.3, McCabe-Thiele diagram is obtained at a constant atmospheric pressure. From this figure it is concluded that the phase equilibrium is almost ideal from the thermodynamic point of view. It compares very well with a much simpler VLE model with a constant relative volatility α, which is also shown in Fig. 2.3. In particular, a value of 1.8 for the α is used. Hereafter, the constant relative volatility VLE model will be used.

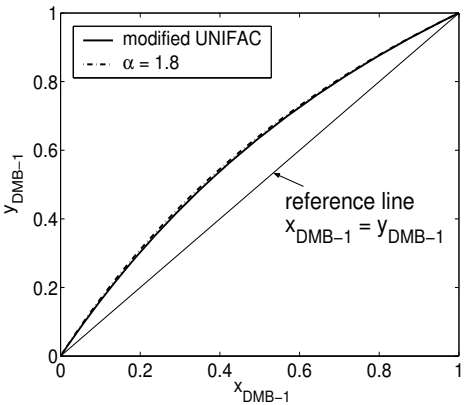

Figure 2.3: McCabe-Thiele diagram comparing the constant relative volatility model with the modified UNIFAC model

2.3 Local optimization

2.3.1 Suitable process candidates

Due to relative high difference in boiling points, a reactive distillation column (RDC) seems to be a suitable process candidate for the production of DMB-1. Other process candidates are a liquid phase reactor coupled to a nonreactive distillation column (RPLUSC)

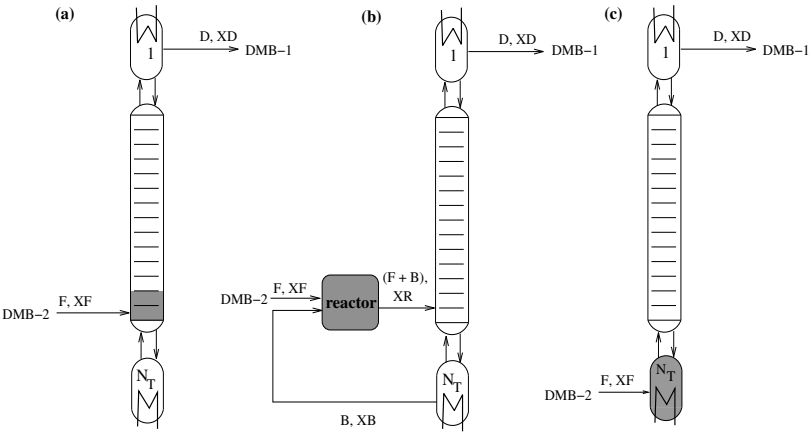

Figure 2.4: Superstructures: (a) reactive distillation column (RDC), (b) reactor coupled with a nonreactive distillation column (RPLUSC) and (c) nonreactive distillation column with reactive reboiler (REACREB)

and a reactive reboiler, i.e. a two-phase reactor, with a nonreactive distillation column on top (REACREB). Fig. 2.4 shows the schematics of these configurations. In all three cases pure DMB-2 is used as a process feed. The integer design variables to be determined for the RDC configuration are the location of the feed, the number and location of the reactive and nonreactive stages. In contrast to this, the reaction zone is fixed for the other two configurations within the reactor. Therefore, the feed location to the column and the number of stages inside the column are the only integer variables to be optimized for these configurations. Continuous design variables are the catalyst loading on the column trays or in the reactors, respectively, and the reflux ratio. For the RPLUSC configuration, a suitable bottom flow rate has to be determined in addition. The objective function is to minimize the total annual cost for a given product purity.

2.3.2 MINLP model formulations

For the distillation columns in all three process configurations, an equilibrium stage model is applied using the constant molar overflow assumption. This is a good assumption because the latent heat of vaporization of DMB-1 and DMB-2 are nearly the same and the heat of reaction is negligibly small. Further, the pressure drop across the column

height is neglected. The phase equilibrium and the reaction kinetics are modeled with the correlations discussed in section 2.2.

For the binary system, component indices are dropped by $x = x_2$ (i.e. liquid phase composition of DMB-1) and $1 - x = x_1$ (i.e. liquid phase composition of DMB-2). The index i, in the following sections, represents the stage index. The stages are numbered from top to bottom, i.e. $i = 1$ represents the condenser and $i = N_{max}$ represents the reboiler. In particular a total condenser is used in all three cases. Furthermore, since the reactant is a heavy component and the unreacted reactant has to be recycled to the column, a total reboiler is used for the RDC and the REACREB configurations with zero bottoms flow rate.

RDC model equations

Fig. 2.5 shows a schematic of the reactive distillation column showing all important design variables to be determined by solving the MINLP problem. In particular, the binary variables IN_i, $Icat_i$ and IR_i determine whether a tray 'i' is a feed tray ($IN_i = 1$), a reactive tray ($Icat_i = 1$) or the top tray receiving the reflux ($IR_i = 1$). All stages above this top tray will have no effect on the column performance, since no liquid is present there. Further a single liquid feed is assumed. Continuous design variables to be determined are the amount of catalyst on the reactive trays and the column reflux. For practical reasons an equal amount of catalyst is assumed on all reactive trays.

This kind of MINLP model formulation is first proposed by Viswanathan and Grossmann [90] for nonreactive distillation columns and is readily extended to reactive distillation. With these assumptions the following model equations are obtained for the reactive distillation column.

Reaction kinetics

$$r_i = K_f Mcat_S Icat_i \left((1 - x_i) - \frac{x_i}{K_{eq}} \right) \qquad (i = 1, \ldots, N_T) \tag{2.3}$$

Vapor-liquid equilibrium

$$y_i = \frac{\alpha x_i}{(1 + (\alpha - 1)x_i)} \qquad (i = 2, \ldots, N_T\text{-}1) \tag{2.4}$$

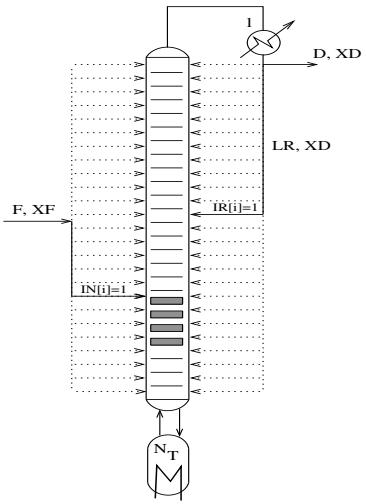

Figure 2.5: Design variables for a reactive distillation column

Component material balances

$$\begin{aligned}
&-(L_R + D)x_i + Vy_{i+1} + Fx_F IN_i + r_i = 0 && (i = 1) \\
&-L_i x_i + L_{i-1}x_{i-1} + V(y_{i+1} - y_i) + Fx_F IN_i + r_i + L_R IR_i x_1 = 0 \\
& && (i = 2, \ldots, N_T\text{-}1) \\
&-L_i x_i + L_{i-1}x_{i-1} - Vy_i + Fx_F IN_i + r_i = 0 && (i = N_T)
\end{aligned} \tag{2.5}$$

Total material balances

$$\begin{aligned}
&-(L_R + D) + V + FIN_i = 0 && (i = 1) \\
&-L_i + L_{i-1} + FIN_i + L_R IR_i = 0 && (i = 2, \ldots, N_T\text{-}1) \\
&-L_i + L_{i-1} - V + FIN_i = 0 && (i = N_T)
\end{aligned} \tag{2.6}$$

with $L_1 = 0$ because the reflux is given by the quantity L_R in this formulation and $L_{N_T} = 0$ for vanishing bottom product. Further a one tray column, with a reflux directly introduced to the reboiler is for practical reasons not taken into account in this formulation.

Constraint of single feed

$$\sum_{i=1}^{N_{max}} IN_i = 1.0 \tag{2.7}$$

Constraint on reflux flow

$$\sum_{i=1}^{N_{max}} L_R \cdot IR_i = V - D, \qquad \sum_{i=1}^{N_{max}} IR_i = 1.0 \tag{2.8}$$

Constraint on reflux location relative to feed location

$$\sum_{i=1}^{N_{max}} i \cdot IN_i \geq \sum_{i=1}^{N_{max}} i \cdot IR_i \tag{2.9}$$

Constraint on reaction zone location relative to reflux location

$$Icat_i \cdot (i \cdot Icat_i - \sum_{i=1}^{N_{max}} i \cdot IR_i) \geq 0.0 \qquad (i = 1, \ldots, N_T) \tag{2.10}$$

Purity constraint

$$x_1 \geq 0.9916 \tag{2.11}$$

RPLUSC model equations

The reactor in the RPLUSC configuration is modeled as a CSTR. For the nonreactive column model, the component material balances have to be modified by removing the reaction rates r_i. The reactor model reads:

Reaction kinetics

$$r = K_f \left((1 - x_R) - \frac{x_R}{K_{eq}} \right) \tag{2.12}$$

Component material balance

$$Fx_F + Bx_B - (F+B)x_R + Mcat_R \cdot r = 0 \tag{2.13}$$

REACREB model equations

For the REACREB configuration we can directly use the RDC model equations described above by fixing the reaction zone to the reboiler with

$$Icat_{N_T} = 1, \;\; Icat_i = 0 \quad \forall i \neq N_T \tag{2.14}$$

2.3.3 Objective function

The objective function is composed of two main costs, i.e. annual capital costs and annual operating costs. The capital costs include cost of equipment, like column shell, nonreactive packings, reactive packings and heat exchangers; and their installation costs which are estimated by multiplying the capital costs by 4. The costs of equipment can be estimated using standard relations available in the literature [16, 19]. The cost factors are adopted from Frey [19]. Though these values are not recent ones, for the qualitative investigation intended in this thesis they are sufficient. The Marshall & Swift index method [16] could be used to transform them to more recent values, which is, however, beyond the scope of this work. The operating costs include the energy costs for heating and cooling. The cost factors for steam and cooling water required to calculate the operating costs, are taken as 250 and 100 money unit / kW, respectively. The calculated yearly operation time is 8000 h. Appendix A gives the detailed cost function with necessary cost parameters.

2.3.4 Local optimization results

The optimization procedure performed on the superstructures described above yields the locally optimal solutions as shown in Table 2.3. SBB (standard branch and bound) routine from GAMS is used to solve these optimization problems [9]. The upper bound on the total number of stages for the column is assumed 60. The feed flow rate to each configuration is 1.4852 kmol/hr. The feed is pure DMB-2. The results of the optimization procedure show

that the RDC gives the lowest minimum annual total cost. The values for the important design variables obtained by the optimizer are also given in Table 2.3. The total stages required for RDC, RPLUSC and REACREB are 24, 22 and 21, respectively. The higher annual capital costs for the latter case, however, is due to the very high vapor flow ($V = (Rf + 1) \cdot F$) requirement, which in turn needs a large column diameter. The operating costs, which are directly proportional to the vapor flow, are also high in this case.

Table 2.3: Comparison of optimal total cost

	$\mathbb{T}$	$\mathbb{C}$	$\mathbb{O}$	$Mcat$	Da	Rf	N_T	N_R	FTL
RDC	183250	120692	62557	76.09	6.20	13.99	24	20 - 23	23^{rd}
RPLUSC[a]	186263	114510	71753	197.13	16.06	14.57	22	-	20^{th}
REACREB	301681	161896	139785	42.52	3.46	32.51	21	21^{st}	21^{st}

[a] B = 69.71 kmol/hr

The critical reflux ratio R_{crit} at infinite $Mcat$ for the REACREB configuration can be calculated using the thermodynamic parameters α and K_{eq} and the product specification x_D (pp. 197, eq (19) in Sundmacher and Qi [83]). Using the parameter values α = 1.8, K_{eq} = 0.1070 and x_D = 0.9916, the value of R_{crit} turns out to be 22.90. This value is already higher compared to the reported values of reflux ratios for RDC and RPLUSC configurations in Table 2.3. The reflux ratio required for REACREB case further increases at finite $Mcat$ values as can be seen from Table 2.3. However, the difference between the minimum annual total cost for RDC and RPLUSC is not significant.

In RDC the catalyst section position or in RPLUSC the reactor position determined by the optimizer is near the bottom of the column. This is obvious from the physical point of view because by providing the reaction zone near the bottom allows sufficient nonreactive trays in the column to separate a reaction mixture obtained from the reaction zone. Also note that for the RDC configuration, the feed position determined by the optimizer is at the bottom of the reaction zone. This is against the common belief that for a heavy reactant the feed position generally has to be at the top of the reaction zone. This is because, the maximum conversion that can be obtained in the reaction zone approaches the equilibrium conversion at the uppermost reactive tray. If suppose, pure reactant is introduced into this stage as feed, then composition on this stage will shift towards reactant provided internal flows are finite. This is unfavorable from the separation point of view, as it will require a higher reflux ratio to separate a reaction mixture richer in reactant (DMB-2) than the equilibrium reaction mixture. This is true in general for binary systems with

an equilibrium limited chemical reaction of a heavy reactant like the one considered in this work. The other way round, in case of binary systems with an equilibrium limited reaction of a light reactant, for example dimerization or trimerization reactions [2, 76], the reaction zone should be placed near the column top and feed should be introduced near the condenser.

2.4 Global optimization

Local optimization results from the previous section suggest that the optimal total annual cost of the RDC and RPLUSC processes are close, while that of the REACREB process is significantly higher. To make an appropriate global statement, as discussed in chapter 1 two alternate approaches are investigated. In the following sub-sections both approaches are explained in detail.

2.4.1 Local optimization from multiple starting points

The multi-start algorithm attempts to find a global solution by starting a local NLP solver from multiple starting points in the solution space. OQNLP, a stand-alone optimizer [31, 86] is one of the common multi-start algorithm. An interface to OQNLP is also provided in GAMS. The GAMS version has a flexibility of using any local NLP solvers from the list CONOPT, MINOS and SNOPT[23]. In OQNLP the potential starting points from which a NLP solver is launched are generated using a stochastic algorithm called *scatter search* (SS) [49]. SS generates new potential starting points by deterministic combinations of previous starting points. As deterministic combinations, it uses generalized path constructions in the Euclidean space. These include, for example, linear interpolation or extrapolation between the previous starting points.

OQNLP requires that each variable has a finite upper and lower bound. In the beginning, so called reference set ($R0$) contains 3 initial trial points: the lower and upper bounds and the mid point. The initial point provided by the user, if any, is also stored in $R0$. Combination of these initial points are used to generate diversified trial points in the solution space. These trial points are then subjected to local improvements in order to obtain a better set of trial points with reasonable quality and diversity. To ensure the quality, a merit filter is

applied which evaluates the trial points based on the penalty function:

$$P_i = f(\mathbf{x}) + \sum_{i=1}^{q} w_i \cdot viol(\mathcal{G}_i(\mathbf{x})) \tag{2.15}$$

where, $f(\mathbf{x})$ is the value of the objective function at point $\mathbf{x}$, w_i are nonnegative penalty weights, and $\mathcal{G}$ is vector of all constrains. The function $viol(\mathcal{G}_i(\mathbf{x}))$ is equal to the absolute amount by which the ith constraint is violated at the point $\mathbf{x}$. The merit filter prevents the NLP solver to be launched from a starting point whose exact penalty function value is greater than a threshold. To maintain the diversity of a reference set, a distance filter is applied. The distance filter prevents the NLP solver starting from a point which is located in a basin of attraction of an already found local optimum.

The advantage of this method is that it benefits on one hand from the superior accuracy and feasibility seeking behavior of gradient based local NLP solvers and on the other hand from the exploration capabilities of the scatter search. The drawback is that there is no guarantee that the final solution is a global optimum, and no bound is provided on how far the solution is from the global optimum. However, it is claimed [86] that the algorithm is effective in determining the global solution. OQNLP has also been used by Sand et al. [65, 66] to globally optimize a reactive distillation column for synthesis of MTBE.

In principle OQNLP can operate on MINLPs but it is found that the integer variables are hardly changed during generation of new starting points. Therefore, a different approach is applied here. First, all integer variables are relaxed to lie within the interval $[0,\ 1]$. This converts the original MINLP problem into a NLP problem. The solutions of a relaxed problem are the physically meaningful as:

- $IN_i \in [0,\ 1], \sum_{i=1}^{N_{max}} IN_i = 1$ means distributed feed,
- $Icat_i \in [0,\ 1]$ means distributed catalyst and
- $IR_i \in [0,\ 1], \sum_{i=1}^{N_{max}} IR_i = 1$ means distributed reflux.

To solve a relaxed problem, OQNLP is used in a combination with a local NLP solver CONOPT3. Afterwards an MINLP solver (SBB) is applied to find a close by optimal solution with single feed, constant amount of catalyst on all reactive trays and constant reflux. This solution has a high probability of being a global solution.

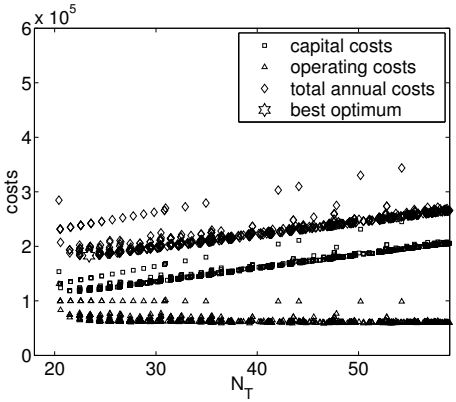

(a)

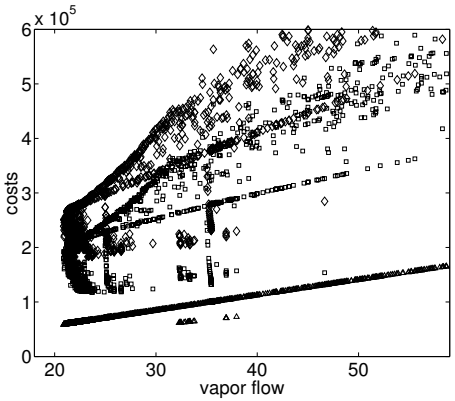

(b)

Figure 2.6: Local solutions ($\diamond$) from multiple starting points for RDC problem: local solutions plotted in terms of (a) various costs vs. number of column stages; (b) various costs vs. vapor flow

For RDC, optimizing the total annual costs by applying the combination of the OQNLP - CONOPT solvers, results in 2211 distinct local solutions of the relaxed problem. These solutions are shown in Fig. 2.6. In Fig. 2.6 (a) local solutions are presented as number of column stages vs. various costs and in Fig. 2.6 (b) they are presented as vapor flow vs. various costs. It can be seen that as the number of stages increases, capital costs tend to increase and operating costs tend to decrease. However, increment in the capital costs

dominates the decline in the operating costs. Hence, as an overall effect total annual costs increase with the number of stages. The best local solution is indicated by an open "six star". Fig. 2.6 (b) shows that there is a linear increase in the operating costs with vapor flow. However, there is no clear dependency of the capital and total annual costs.

SBB determines the best integer solution in the discrete subspace from the best local solution shown in Fig. 2.6. It turns out that the optimal solution reported in Table 2.3 - first row is the global integer solution with high probability. However, no guarantee can be given yet that the solution obtained by the combination of OQNLP - CONOPT - SBB is the global optimum.

Multiple local solutions are also generated for RPLUSC and REACREB, which confirms that the local solutions reported in Table 2.3 are the global solutions with high probability for these configurations.

2.4.2 Global bounds on optimal solution

This deterministic approach is developed in the group of Prof. Weismantel at the University of Magdeburg and together with them is applied to the isomerization problem. It is based on techniques to derive polyhedral approximations of the underlying nonlinear equations in such a way that a mixed-integer linear relaxation of the original problem is obtained, which can be solved rigorously. Since the feasible set of the original nonlinear problem lies within the feasible set of the relaxed problem, the latter provides global lower bounds for the optimal solution of the original problem. The lower bound approaches the true global optimum as the number of grid points of the relaxation is increased.

Here, a sketch of the main ideas is presented which elaborates the approximation procedure. For simplicity of the following discussion, consider $x = (x_1, ..., x_d)^\top \in \mathbf{R}^d$ be a vector of d continuous variables and a nonlinear function $\phi : \mathbf{R}^d \to \mathbf{R}$ restricted to a box $[l, u] \subseteq \mathbf{R}^d$. The relaxation procedure consists of

- a subroutine ANALYZE in which the nonlinear function $\phi(x)$ is investigated for local and global properties, e. g., local and global extrema, discontinuities, etc., using elementary differential geometry.
- a subroutine BINMOD that subdivides the domain $[l_i, u_i]$ for each variable x_i into subdomains and introduces a new binary variable for each subdomain that indicates whether x_i is contained in this subdomain or not.

- a subroutine POLYPROX that defines an *enclosing* polyhedron for the graph of $\phi(x)$ on every subregion based on the results from the subroutine ANALYZE.

The relaxation procedure is illustrated in Fig.-2.7.

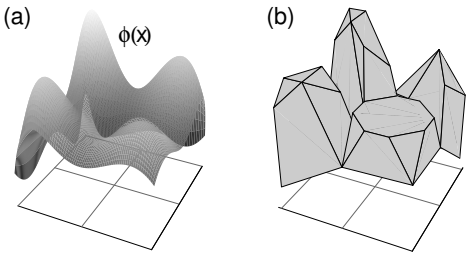

Figure 2.7: For the nonlinear function $\phi(x)$ on a box $[l, u]$ in (a), a polyhedral relaxation for the graph of $\phi(x)$ is given in (b): The domain is subdivided into four subregions. For each subregion a polyhedron is defined enclosing the graph of $\phi(x)$.

Co-workers from Prof. Weismantel's group have applied this approach to approximate the model equations of the RPLUSC configuration. The nonlinear equations appearing in the original RPLUSC model include component material balances, vapor-liquid equilibrium and the objective function. The integer variables are number of column stages, N_T (or IR) and feed tray location, IN. For a fixed value of N_T and IN, the original MINLP problem gives rise to a continuous nonconvex subproblem. Each of these subproblems are approximated through the polyhedral relaxation procedure. Rigorous solutions of approximated mixed integer linear programs can be obtained using a standard software based on simplex-based branch-and-cut algorithms.

Using sufficient discretization on the relaxation, the global lower bound of RPLUSC process is determined to be 185000. For a detailed discussion on the effect of grid fineness and solution times, readers are referred to Gangadwala et al. [24]. It can be seen from Table 2.3 that the local solution of the RDC process is superior than the global lower bound on the optimal solution of RPLUSC process. Thus, it has been confirmed that no other solution of the RPLUSC process exists, which is superior to the RDC process.

2.5 Global sensitivity analysis

The optimal total annual costs obtained in the previous section is based on the given values of the model parameters. To achieve a successful design it is required to consider uncertainty in the model parameters in the early design stages. This section deals with the uncertainty in the model parameters. Sensitivity analysis is an effective tool that gives a quantitative measure of the influence of model variances on model outputs [64]. For the underlying problem, model outputs can be the objective function (e.g. total annual costs) or constraints (e.g. product purity). Alternatively, model outputs can be referred to as Key Performance Indicators (KPIs) [33]. The uncertain parameters θs can be reaction rate constants, thermodynamic properties or cost parameters.

In practice, usually a local sensitivity analysis is used to calculate sensitivities. For a local sensitivity analysis, a specific solution KPI$^*(\theta^*)$ is considered and partial derivatives $\left(\frac{\partial KPI}{\partial \theta_i}\right)_{\theta=\theta^*}$ are determined. The obvious deficiencies of this approach are: 1. local values can not capture the KPI variability wrto. the model parameters over their entire ranges; and 2. any single measure of sensitivity is unlikely to contain sufficient information for assessing whether the uncertainty in a certain design is acceptable.

On the other hand, a global sensitivity analysis (GSA) approach is not restricted to a single specific solution. In the GSA approach the following optimization problem is solved for a fixed design d and a sequence of values of the uncertain parameters θs [33].

$$\begin{aligned} \min \quad & \Phi(d,u,x,\theta) \\ \text{s. t.} \quad & h(d,u,x,\theta) = 0 \\ & g(d,u,x,\theta) \leq 0 \end{aligned} \qquad \text{(GSAOPT}_\theta\text{)}$$

where Φ represents the objective function (e.g. total annual costs) also considered as a process KPI, u a vector of control variables that may be varied over a space $\mathcal{U}$, and x is a vector of state variables. The model equations are represented by h and constraints are represented by g.

The optimization problem GSAOPT$_\theta$ determines the best set of operating conditions u (e.g. reflux or reboil ratios, heat duty etc.) for a fixed design d under a certain realization of uncertain parameters. This is repeated for all samples θ_j obtained over a domain Θ with a given probability distribution. There are many sampling techniques available which can be used including, random sampling or stratified sampling to obtain samples

θ_j. Of major importance are quasi-random sampling techniques. As a quasi-random sampling technique, low-discrepancy sequences due to Sobol' [74] have been found to be very efficient for global sensitivity analysis problems. The quasi-random samples have a number of desirable properties. They are designed to have a high level of uniformity in multidimensional space and unlike regular grids, the projection of N sample points onto any parameter axis results in N distinct values of that parameter. Hence, accelerated convergence rates are obtained in Monte Carlo simulations by using them. The code to generate Sobol's low-discrepancy sequences is openly available as the ACM algorithm 659 [8].

The global sensitivity indices can be calculated using Monte Carlo simulations as proposed by Sobol' [75, 40]. This method is briefly described below. Let us consider, a n dimensional parameter domain $\Theta = \{\theta_1, \ldots, \theta_n\}$. In Sobol's method the parameter domain Θ is extended by extra n replicated dimensions $\Theta' = \{\theta_{n+1}, \ldots, \theta_{2n}\}$ to obtain a new domain $\widehat{\Theta} = \{\theta_1, \ldots, \theta_n, \theta_{n+1}, \ldots, \theta_{2n}\}$. For a j^{th} trial, a quasi-random sequence $Q_j = \{q_1, \ldots, q_{2n}\}$ is generated from $\widehat{\Theta}$ such that $\zeta_j = \{q_1, \ldots, q_n\}$ and $\zeta'_j = \{q_{n+1}, \ldots, q_{2n}\}$. Each Monte Carlo trial (j) requires optimization of the model GSAOPT$_\theta$ to obtain $\phi(\zeta_j)$ and $\phi(\zeta_j^{'i})$. In this notion, ζ_j is the j^{th} realization from Θ and $\zeta_j^{'i}$ is a resampling of all the parameters except the i^{th} parameter from Θ' such that $\zeta_j^{'i} = \{q_i, q_{n+m,\ \forall m \neq i}\}_j :\ i,\ m = 1, \ldots, n$. After N trials, crude Monte Carlo estimates are obtained:

$$\begin{aligned}
\lim_{N\to\infty} \frac{1}{N} \sum_{j=1}^{N} \phi(\zeta_j) &= \phi_0 \\
\lim_{N\to\infty} \frac{1}{N} \sum_{j=1}^{N} \phi^2(\zeta_j) &= D + \phi_0^2 \\
\lim_{N\to\infty} \frac{1}{N} \sum_{j=1}^{N} \phi(\zeta_j) \cdot \phi(\zeta_j^{'i}) &= D_i + \phi_0^2
\end{aligned} \tag{2.16}$$

Where, ϕ_0 is a mean of the function ϕ , D is an overall deviation and D_i is a deviation of ϕ with regards to the parameter θ_i. A first order sensitivity coefficient is defined as

$$S_i = \frac{D_i}{D}$$

Monte Carlo evaluation of the second order terms $D_{i,k}$ are obtained by a resampling of all the parameters except the i^{th} and k^{th} from Θ' such that $\zeta_j^{'i,k} = \{q_i, q_k, q_{n+m,\ \forall m \neq \{i,\ k\}}\}_j$ $i,\ k,\ m = 1, \ldots, n$.

$$\lim_{N\to\infty}\frac{1}{N}\sum_{j=1}^{N}\phi(\zeta_j)\cdot\phi(\zeta_j^{'i,k}) \quad = \quad D_i + D_k + D_{i,k} + \phi_0^2 \tag{2.17}$$

In a similar way, higher order terms $D_{1,\ldots,n}$ are obtained to calculate corresponding sensitivity indices:

$$S_{1,\ldots,n} = \frac{D_{1,\ldots,n}}{D}$$

such that $\overset{\wedge}{\sum} S_{1,\ldots,n} \equiv \sum_{i=1}^{n} S_i + \sum_{1\le i\le j\le n}\sum S_{ij} + \ldots + S_{12\ldots n} = 1.$

In case of RDC, the design d is obtained by setting the total number of column stages, feed tray location and reactive stages to their optimal values presented in Table 2.3. For a fixed design, the column diameter is set to $\mathcal{D}_{col} = 0.7350$, a slightly higher value than the optimal value in order to ensure process feasibility for all realization of uncertain parameters. For the sake of simplicity, two uncertain parameters K_f and K_{eq} are considered, i.e. $n = 2$. Further, it is assumed that these parameters have an uncertainty domain of $\pm$ 10 % wrto. their base case values of [0.1210, 0.1070] and they are constantly distributed in this domain. In principle, any type of probability distribution can be used. Sobol's sequences generated for this rectangle box ($\mathcal{S}B$) with N = 1000 sample points are shown in Fig. 2.8. As explained before, the Sobol's sequences should be generated for $\widehat{\Theta} = \{K_f, K_{eq}, K'_f, K'_{eq}\}$, i.e. in $2n$ dimensions. The $\Theta' = \{K'_f, K'_{eq}\}$ contains resamples of K_f and K_{eq}. Fig. 2.9 (a) and (b) show the plots of K'_{eq} vs. K_f and K_{eq} vs. K'_f respectively. It is easy to see that projections of the sample points on all the faces of hypercube ($\mathcal{S}B \times \mathcal{S}B$) are uniformly spaced.

For the calculation of the global sensitivity indices, $N = 5000$ sample points were selected. Thus, (2^n - 1) $\times N = 15000$ optimization of type GSAOPT$_\theta$ need to be solved. All of the optimization problems were solved in automatic loops in GAMS. The original MINLP problem has become a NLP problem because in the design d the integer variables such as N_T, FTL, N_R are fixed. Therefore, the NLP solver CONOPT3 is applied. As an initial guess, the global optimum reported in Table 2.3 is provided, which is essential for all N optimization problems to be solved to a near global solution. These problems were solved in approximately 5 hrs of CPU time on a 2.0 GHz AMD 64.0 processor.

The global sensitivity indices calculated on the basis of 15000 optimized objective values and eqs. 2.16 are reported in Table 2.4. It can be seen that the sensitivity of the total annual costs wrto. to K_{eq} is dominating, whereas the sensitivities due to K_f or due to

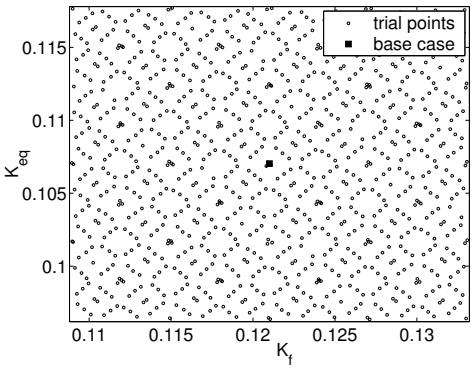

Figure 2.8: Example of Sobol's sequences for a considered $\pm$ 10 % uncertainty in both K_f and K_{eq} (1000 samples)

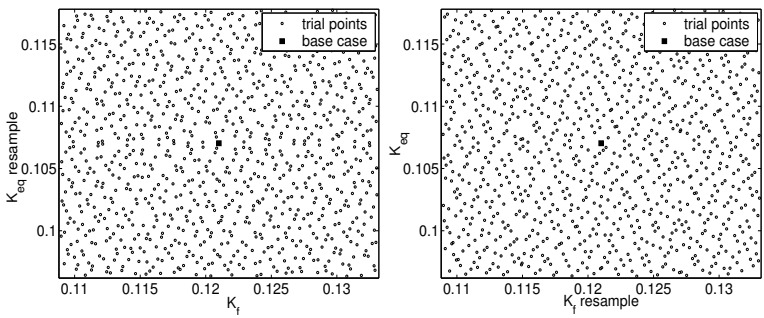

Figure 2.9: (a) K_f vs. K_{eq} re-sampled; and (b) K_f re-sampled vs. K_{eq}

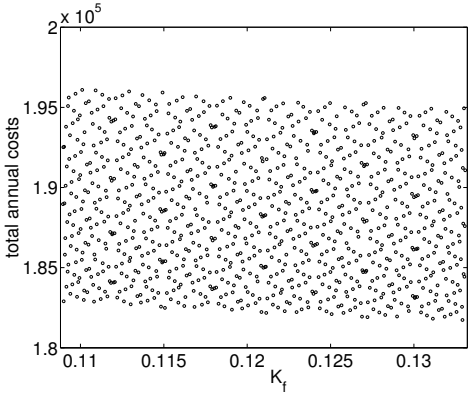

(a)

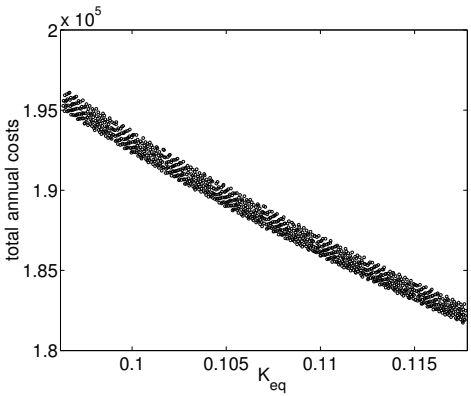

(b)

Figure 2.10: Distribution of total annual costs: (a) with respect to K_f (b) with respect to K_{eq}

interaction of K_f and K_{eq} are negligible. For comparison, Table 2.4 also shows local sensitivity values calculated using the process simulator DIVA. It can be seen that the trends are correctly predicted by the local sensitivity analysis but there is a considerable difference in the ratio of two sensitivities. The influence of K_f and K_{eq} can also be seen from Fig. 2.10 (a) and (b). The total annual costs exhibit uniform distribution for K_f whereas it tends to decrease sharply with increase in K_{eq}. This result suggests that the

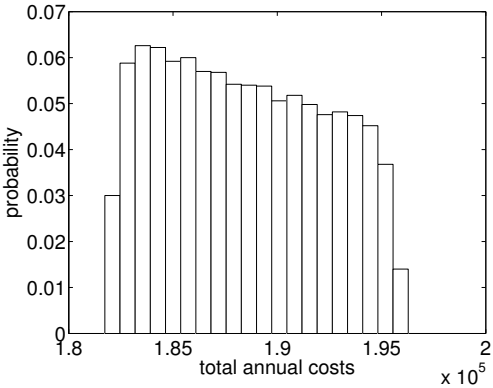

Figure 2.11: Probability distribution of total annual costs

RD column must be operated close to equilibrium. The probability distribution for total annual costs is shown in Fig. 2.11.

Table 2.4: Sensitivity indices of total annual costs for N=5,000

	ϕ_0	D	STD error	S_{K_f}	$S_{K_{eq}}$	$S_{K_f/K_{eq}}$
RDC*	-	-	-	0.3932	0.9195	-
RDC	188480	1.5167e+07	55.08	-0.0082	0.9905	0.0177
RDC[a]	188330	3.8631e+06	27.79	0.0025	0.9635	0.0340
RPLUSC	190290	2.0459e+07	63.97	-0.0075	0.9923	0.0152

* local sensitivities at[K_f^*, K_{eq}^*] = [0.1210, 0.1070] calculated using DIVA

[a] reduced parameter uncertainty domain: $K_f \pm 10$ % and $K_{eq} \pm 5$ %

One can possibly exploit this situation in the following way, imagine that more laboratory experiments are performed so that the uncertainty domain of K_{eq} is reduced to $\pm$ 5 %. Now, the sensitivity indices are calculated in the new reduced domain. As it can be seen from the third row of Table 2.4, the STD error in the new domain has reduced to the almost half of that in the original domain.

In a similar manner, the sensitivity indices are calculated for RPLUSC design which suggests that for a same parameter uncertainty domain, total annual costs in RPLUSC has more STD error than RDC. In principle, small negative value for the S_{K_f} is not possible, hence it should be considered as a small positive value.

2.6 Summary

In this chapter a new methodology is introduced for computer aided design of reaction separation processes. The production of DMB-1 is considered as an innovative benchmark problem. First, standard local MINLP solvers are applied to obtain a quick ranking of suitable process candidates. Later, two global approaches are used to provide an appropriate global analysis on the objective function value, allowing for the comparison of known local optima for different designs. Through that, it is shown that for the given constraints (production rate, product purity etc.) and costs, reactive distillation is most economic. This may, however, change with changing constraints and changing costs.

At the end, global sensitivity analysis (GSA) is applied to study the influence of parameter uncertainty on total annual costs. This analysis is especially useful to gain insight about the inherent risk in final designs. Here, the GSA is performed by considering parameter uncertainty in two kinetic parameters. For a large number of uncertain parameters, calculations of global sensitivity indices is computationally demanding. Since isomerization example is easy to solve, in principle, global sensitivity indices are computable for a large number of uncertain parameters. The GSA approach can also be applied to more complex RD applications, such as those to be addressed later in this thesis. However, due to increased complexity (large number of uncertain parameters and increased nonlinearity) those problems are difficult to solve. The study of those problems is beyond the scope of this thesis.

Chapter 3

Esterification process

3.1 Introduction

The esterification processes are characterized by high dimensionality, i.e. multi component systems, highly non-ideal thermodynamics and nonlinear reaction kinetics. Compared to the isomerization example considered in the previous chapter complexity has increased significantly. As a practical application synthesis of butyl acetate is considered.

Butyl acetate (BuAc) is an industrially important chemical with application as a versatile solvent and as an intermediate in organic synthesis. Because of its lower impact on the environment compared to some other types of solvent, its consumption is expected to grow in near future. BuAc is commonly produced by esterification of acetic acid (AcH) with n-butanol (BuOH) in the presence of a suitable acid catalyst. This reaction is reversible and the simultaneous removal of products during the course of the reaction is beneficial in view of obtaining enhanced conversion. Reactive distillation (RD) offers such a possibility of an *in situ* reaction and separation. RD has also been acknowledged by industrial partners as an economical option for many esterification reaction system [1, 43, 7, 70]. Alternatively, BuAc can be produced in a reactive extraction [56], in a reactive and extractive distillation via transesterification reaction of methyl acetate and butanol [44] or in a multifunctional trickle bed reactor [35]. However, out of all the production routes reactive distillation is a most favored means for BuAc synthesis.

In classical RD processes homogeneous acid catalyst, for example, sulfuric acid and p-toluene sulfonic acid were used [37, 89]. These catalysts have drawback due to their severe corrosiveness for the RD column material. On the contrary, solid heterogeneous

catalysts, for example, ion exchange resins offer benefits like ease of separation, less waste disposal and less corrosion problems. There have been extensive studies published in literature on the experimental/theoretical investigation of BuAc synthesis in a reactive distillation column with solid acid catalysts [72, 25, 77, 34, 7, 92, 43]. In all of these papers, the final RD process design is obtained on the basis of experimental and/or simulation results. However, none of these papers address the issue of an optimal process design. By operating a nonoptimal process, industries may suffer huge economical loss.

Reactive distillation is not the only possibility to combine reaction and distillation, but a network of side reactors coupled with a nonreactive column is also an additional possibility. Therefore, in this chapter following process alternatives are considered: a reactive distillation column (RDC) and a network of side reactors coupled to a nonreactive column (SRC) (See Fig. 3.1).

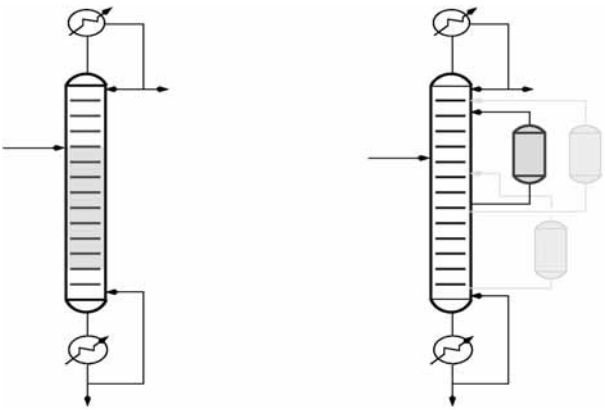

(a) (b)

Figure 3.1: Schematic examples of BuAc processes: (a) a reactive distillation column (RDC) and (b) three side reactors coupled to a nonreactive column (3SRC)

The chapter is organized as follows: at first, details of the reaction kinetics and phase equilibrium models are presented. The RD model validation is presented next. Then insight of the influence of the design parameters on RDC and SRC performance is gained via simulation in DIVA [52]. The MINLP model formulations for the RDC and SRC configurations and results of local optimization are presented next. At the end results of global optimization are presented.

3.2 Reaction kinetics

In a previous study on the RD experiments, Janowsky et al. [43] observed the presence of side products 1-butene and dibutyl ether (DBE) in the final products. It was possible then to eliminate a side product 1-butene by operating the RD column at lower pressure of 650 mbar. However, another side product DBE was found to be always present in the bottoms due to its highest boiling point. DBE forms by etherification of BuOH and because of its toxic nature, its concentration in the final product should be kept minimum. In this thesis, this important fact has been taken into account. The kinetics expressions and kinetics parameters for the esterification and the etherification adopted from Gangadwala et al. [26] are shown below. The kinetics parameters are valid for the Amberlyst - 15 catalyst.

Esterification: AcH (1) + BuOH (2) $\rightleftharpoons$ BuAc (3) + H_2O (4)

$$r^o = \frac{1}{\nu_i} \cdot \frac{dn_i}{dt} = M_{cat} K_f K_1 K_2 \frac{(a_1 a_2 - \frac{1}{K_a} a_3 a_4)}{(1 + K_1 a_1 + K_2 a_2 + K_4 a_4)^2}$$

Etherification: 2BuOH $\rightarrow$ DBE (5) + H_2O

$$r^o = \frac{1}{\nu_i} \cdot \frac{dn_i}{dt} = M_{cat} K_{DBE} \frac{(K_2 a_2)^2}{(1 + K_2 a_2 + K_4 a_4 + K_5 a_5)^2}$$

The temperature dependency of the rate constants is expressed as:

$$K_i = K_i^0 \cdot exp\left(\frac{E_i}{RT}\right)$$

K_f^0 $\frac{kmol}{kg\ s}$	E_f $\frac{kJ}{kmol}$	K_a^0	E_a $\frac{kJ}{kmol}$	K_1	K_2	K_4	K_{DBE}^0 $\frac{kmol}{kg\ s}$	E_{DBE} $\frac{kJ}{kmol}$	K_5
20.13×10^6	73410	3.82	-3580	7.09	5.06	8.81	361.89	68600	3.33

3.3 Phase equilibrium models

The vapor-liquid equilibrium for the present system has been calculated by assuming ideal vapor phase and non-ideal liquid phase. According to that, the vapor composition (y_i) in

equilibrium with the liquid composition (x_i) can be expressed as:

$$y_i = \frac{p_i^s \, \gamma_i \, x_i}{P}$$

The vapor pressures (p_i^s) are obtained by using Antoine co-relations and the total pressure (P) is assumed constant throughout the column. To calculate activity coefficients (γ_i) for inside column stages, the Wilson model is used. Though in the present system liquid-liquid miscibility gaps are present, it is reasonable to assume a single homogeneous liquid phase on all the column stages [92, 34, 77]. Nonetheless, the liquid-liquid phase split should be taken into account for a decanter model. Inside the decanter, liquid-liquid equilibrium is considered according to following equations:

$$\gamma_i^I \, x_i^I = \gamma_i^{II} \, x_i^{II}$$

$$x_i^0 = \phi \, x_i^I + (1 - \phi) \, x_i^{II}$$

$$\sum_{i=1}^{nc} (x_i^I - x_i^{II}) = 0$$

where, x_i^I and x_i^{II} are liquid compositions for phase 1 and 2 having a phase split ratio ϕ. The activity coefficient (γ_i^I and γ_i^{II}) are calculated by using the UNIQUAC model. The Wilson and UNIQUAC binary interaction parameters are obtained from DECHEMA database.

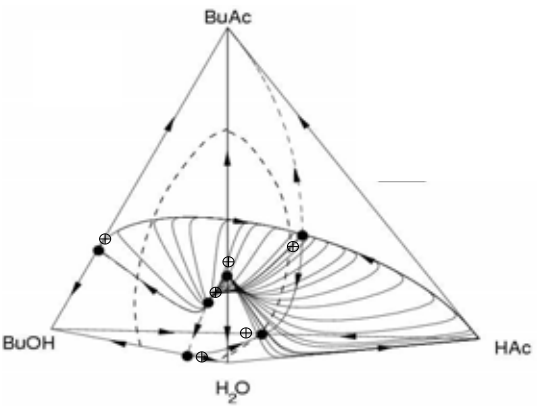

Figure 3.2: nonreactive residue curve maps in BuAc system at 1 atm, adopted from Kienle et al. [46]. $\oplus$ represents azeotropes at 650 mbar, dashed line represents a liquid-liquid equilibrium envelop

Fig. 3.2 shows the nonreactive residue curve map for a quaternary mixture of AcH, BuOH, BuAc and water, plotted at atmospheric pressure using the Wilson model. The arrows are in the directions of increasing temperatures. As can be seen this is a highly non-ideal system with a total number of six azeotropes. Out of these, there are three binary minimum azeotropes, a binary maximum azeotrope, a ternary minimum azeotrope and a ternary saddle azeotrope. The azeotropes BuOH - H_2O, BuAc - H_2O and BuOH - BuAc - H_2O are heterogeneous. The rest of the azeotropes are homogeneous. The ternary heterogeneous azeotrope (BuOH - BuAc - H_2O) is a low-boiling stationary point in the system. Hence, it is obtained at the top of the column. This azeotrope upon condensation separates into two liquid phases in the decanter. The organic phase consists of BuAc, BuOH and H_2O, which is generally completely refluxed to the column. Whereas the aqueous phase is removed as a distillate. Thus, there are no degrees of freedom at the column top (see Fig. 3.3).

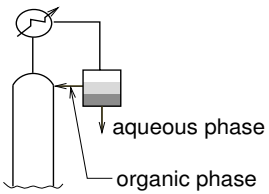

Figure 3.3: organic reflux arrangement

According to Janowsky et al. [43], the RD column should be operated at 650 mbar to avoid 1-butene formation. Therefore, in this chapter all the optimizations are performed at 650 mbar. At this pressure all azeotropes remain present ($\oplus$ in Fig. 3.2) and the qualitative behavior of residue curve map also remains unchanged.

3.4 RD model and model validation

As mentioned before, the previous studies by Zhicai et al. [92], Hanika et al. [34], Steinigeweg et al. [77] suggests that for the present reaction system, an equilibrium stage model without any provisional equations for a liquid-liquid phase splitting inside the column, predicts the experimental results well. Considering that, in this work an equilibrium stage model with detailed energy balances is developed for the reactive distillation pro-

cess, and simulation results are validated with experimental data from Singh et al. [72] (see Fig. 3.4). The reaction kinetics and phase equilibrium models are used as described in sections 3.2 and 3.3. The additional modeling assumptions are as follows: 1. phase splitting is considered only in the decanter; 2. the reactions proceed only in the liquid phase; 3. the pressure drop along the column height is assumed to be negligible; and 4. fluid dynamics of the column internals is ignored.

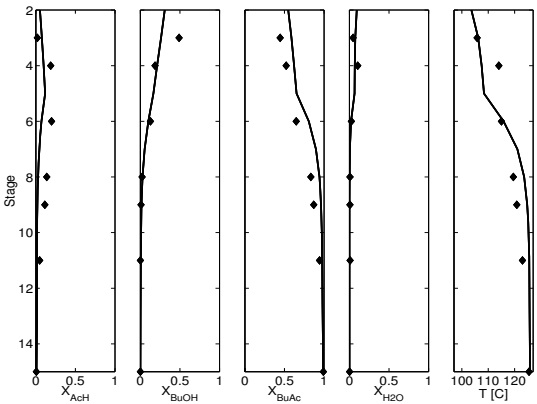

Figure 3.4: Comparison of experimental data vs. simulation for a run 9 of Singh et al. [72], experiments and simulation are performed at 1 atm., stages are numbered from top (stage 1) to bottom (stage 15)

It can be seen from Fig. 3.4 that the model predicts experimental data reasonably well. The model predictions also matched well with the results of other experimental runs performed under different input conditions [72]. This model has been also verified by Gangadwala et al. [25] with the experimental data from Janowsky et al. [43] and Hanika et al. [35].

3.5 Parameter studies for a detailed process insight

The model developed in the previous section can be used to perform simulation studies for RDC and SRC configurations (Figs. 3.5 (a) and (b)). The main objective here is to determine best suitable operating conditions for the RDC and SRC configurations so that the bottom product contains minimum of DBE and AcH. For SRC (Fig. 3.5 (b)), a

continuous stirred tank reactor is used. The catalyst loading of the reactor is comparable to that required in RDC. It has been noticed that very high pump around flow rates, higher than the feed flow rate, are required to get satisfactory performance.

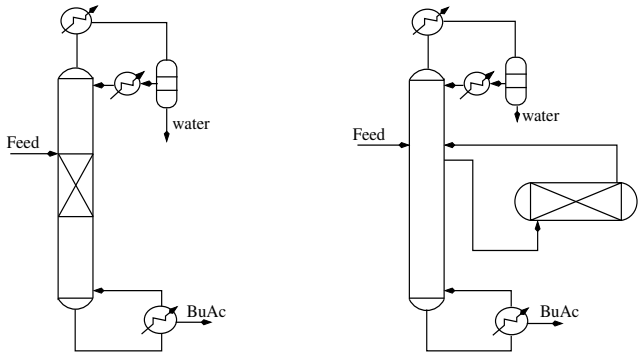

Figure 3.5: (a) RDC and (b) SRC. The reactive section is shown by a cross sign

For the purpose of this section, the reaction mixture coming from the pre-reactor is considered as a feed to the column, for which compositions are given in Table 3.1. Later, in the optimization section this restriction will be relaxed. In order to determine suitable values of the design variables, viz. reboiler duty, catalyst loading, catalyst section length and location and feed tray location, continuation methods implemented in the simulation environment DIVA [52] are used. The base case parameters for each configuration are given in Table 3.2. In this section, no attempt is made to determine the optimal number of column stages. However, it is found that the column performance is insensitive to the number of stages if more than 20 column stages are provided. Therefore, all the simulation performed in this section consider 22 column stages.

3.5.1 Reboiler heat duty

For RDC increasing the reboiler heat duty increases the BuAc concentration in the bottoms, but at the same time increases DBE concentration as well. It is even possible to get 100 % conversion of AcH at higher reboiler duty. This is expected because increasing heat duty increases reactive section temperature, which enhances the conversion but

Table 3.1: Inputs to the column from the Janowsky et al.[43]

F: 0.0215 kmol / hr and T_F = 343 K	
	x_F
x_{AcH}	0.1535
x_{BuOH}	0.1676
x_{BuAc}	0.4491
x_{H_2O}	0.2297
x_{DBE}	0.0001

Table 3.2: Base case parameters for RDC and SRC

Configuration	N_T	N_R or reactor location	FTL	Q_{REB} kW	$Mcat_s$ kg cat	F_R kmol / hr
RDC	22	9 - 17	8^{th}	0.4	0.2	-
SRC	22	6 - 7	6^{th}	1.0	4.0	0.2

reduces the selectivity (Fig. 3.6). It should be noted that each point on the curve in Fig. 3.6 corresponds to a steady state solution for a given value of the reboiler heat duty. In further simulation runs a heat duty of 0.5 kW will be used for RDC.

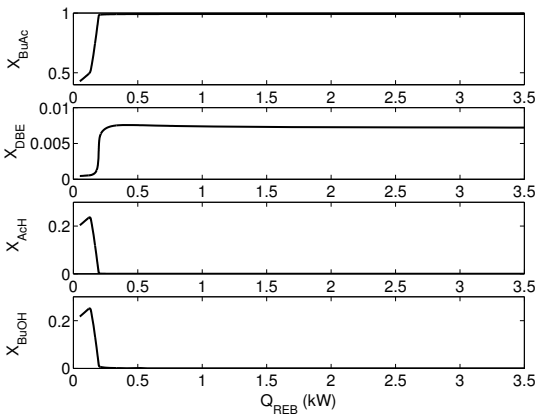

Figure 3.6: Effect of reboiler heat duty for RDC. The bottom compositions are plotted against heat duty

The model for SRC predicts multiple steady states in a range between 0.6417 and 0.7328 as shown in Fig. 3.7. In further simulation runs a heat duty of 1.0 kW will be used for the SRC.

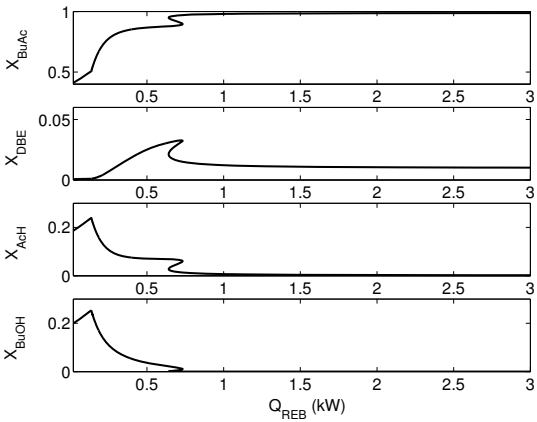

Figure 3.7: Effect of reboiler heat duty for SRC. The bottom compositions are plotted against heat duty

3.5.2 Catalyst loading

It is observed for RDC that at higher catalyst loading the side reaction forming DBE becomes favorable. In this case, the optimum catalyst loading is found to be 0.25 kg cat / tray. For SRC to avoid a multiplicity range, the optimal reactor catalyst loading is selected as 4.0 kg.

3.5.3 Feed tray location

Because the difference in the boiling points of BuOH (117.7^o C) and AcH (117.9^o C) is rather small, the idea of providing feed at two separate points is not very attractive. This has been observed from the simulation runs for RDC. Therefore, in the following discussion only the single feed case is considered. The effect of increase in the feed flow rate is also investigated and as expected, the trend is to decrease the conversion.

As the feed tray is shifted down in the reactive section, the conversion of reactants decreases leading to a decrease in BuAc concentration in the products. Moreover, high concentration of AcH in the reactive section inhibits the DBE formation. The same arguments can be applied to the shifting of the feed tray up in the rectifying section which results in the high concentration of BuAc and DBE in the bottom products. Therefore, a trade off is required between AcH and DBE concentration in bottoms. The best feed tray location for RDC is observed at the top of the reactive section. For SRC, shifting the feed tray up and down causes similar effects as for RDC. The best feed tray location is found at the tray where the pump around is fed back to the column.

3.5.4 Reaction zone location for RDC

As said earlier, providing more catalyst, degrades the product purity. Therefore, the optimum number of catalytic stage must be provided in the reactive section. For RDC, with some efforts it is found that 9 catalytic stages provided between 9 - 17 stages can give better RDC performance.

3.5.5 Pump around location for SRC

It is observed that when a gap of two stages is provided between the pump around withdrawal and its introduction to the column, better SRC performance could be obtained. The pump around position is then varied from 2 - 3 to 19 - 20 (introduction - withdrawal) maintaining the feed position at the same stage where the pump around is introduced to the column. The optimum pump around location is found at the 6 - 7 stages with the feed introduced into the 6^{th} stage.

3.5.6 Discussion

Table 3.3 shows the best suited operating conditions determined based on the one parameter continuation studies. For these parameters RDC gives 99.19 mole % BuAc in the bottom product accompanied by 0.78 mole % DBE; and SRC gives 98.72 mole % BuAc accompanied by 1.03 mole % DBE. For RDC more than 99 % AcH conversion is obtained whereas SRC gives around 98 % conversion. Based on these results, the RDC is found to be more effective than SRC. However, it can be said that SRC has a large scope for further improvement upon rigorous optimization to be performed in the next section.

Table 3.3: Operating parameters for the best of RDC and SRC

Configuration	N_T	N_R or reactor location	FTL	Q_{REB} kW	$Mcat_s$ kg cat	F_R kmol / hr
RDC	22	9 - 17	8^{th}	0.5	0.25	-
SRC	22	6 - 7	6^{th}	1.0	4.0	1.0

3.6 Local optimization

It will be interesting to investigate whether, by optimizing MINLP models for the underlined problems, any better designs could be determined. Therefore, at first, the reboiler duty is minimized as an objective function by keeping the total number of column stages fixed at 22, but reaction zone location in RDC and pump around location in SRC, feed tray location and catalyst amount are kept as free variables. For a fair comparison to the results presented in Table 3.3, the constraint on the bottom product purity, for RDC is set at $x_{BuAc} \geq 0.9919$ (mole fraction) and that for SRC is set at $x_{BuAc} \geq 0.9872$. In the next step, the whole design problem is optimized by including overall cost functions and minimizing the total annual costs of these processes, which include equipment and utility costs. The details of MINLP modeling and the optimization results will be presented in the following sections. The SBB solver from GAMS is employed to solve the optimization problems.

Provision of a suitable initialization state vector is a crucial point to perform successful optimizations of RD processes [42]. In order to generate a suitable and quick estimate of the initial values for a rigorous optimization model with variable flow rates, a constant molar overflow (CMO) model was developed. This is a reasonable choice as the heat of vaporization for all components fall in the same range. In addition, the main reaction (i.e BuAc synthesis reaction) is only mildly exothermic. The CMO models are solved using the preliminary simulation results reported in section 3.5 as starting values. In the present case, CMO model solutions provide good starting values for the rigorous model. Difference between these solutions, in general, are approximately 2-3%. Moreover, the computation time required to solve the CMO model is up to three to seven times less than that of the rigorous model.

3.6.1 MINLP models for RDC and SRC

Fig. 3.8 shows schematics of RDC and SRC with their respective design variables. The distillation column is modeled based on tray by tray mass and energy balance constraints. Binary variables related to each tray decide existence and/or type of the tray, i.e. reactive, nonreactive or feed tray. As discussed previously in section 3.5, in this section all optimization problems are solved only for a single feed column. However, one more feed stream can easily be accommodated in the model by providing an additional binary variable on each tray.

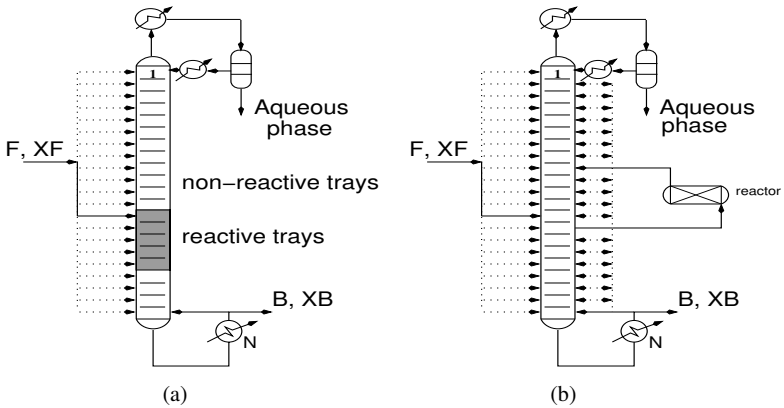

Figure 3.8: Schematic diagram for (a) RDC and (b) SRC

The SRC shown in Fig. 3.8 (b) is having a single side reactor, which will be called 1SRC in the remainder. Accordingly, a configuration with 'n' side reactors will be called nSRC. For a 1SRC configuration, determination of a reactor location requires two binary variables for each column tray, one for the reactor inlet (position of the sidedraw from the column) and the other for the reactor outlet (position of the feedback to the column), unlike the RDC where only a single binary variable is required to decide whether the tray is reactive or nonreactive. For multiple side reactors, combinatorial complexity will further increase, as for each reactor two binary variables are required on each tray. Note that in the SRCs, the column itself is a nonreactive and reactions take place only inside the reactors. The reactor type used in this study is a stirred tank reactor, however, it can easily be replaced by any other reactor type.

Appendix B shows the detailed MINLP models for the RDC and the SRC configurations. The cost functions are also given in Appendix B. When the total annual cost is minimized, the optimal values of number and location of reactive trays, feed tray location, catalyst loading on each reactive tray and reboiler duty are obtained.

3.6.2 Results and Discussions

RDC optimization

The result of a reboiler heat duty minimization problem is shown in Table 3.4 (second row). For comparison Table 3.4 also shows the result of section 3.5 (first row). There is about 5% improvement in the energy demands for the same product purity by MINLP design. The RDC design shown in section 3.5 is quite close to the optimal configuration obtained by MINLP optimization. The third row in Table 3.4 is a solution of a reboiler heat duty minimization problem subjected to a nonuniform distribution of the catalyst amount in the reaction zone. The result indicates that in the present case, only minor improvements are possible through catalyst distribution. The optimal catalyst loading profile is shown in Fig. 3.9.

Table 3.4: RDC - results of reboiler duty optimization for 22 stages column

Q_{REB}	$Mcat_s$	$\mathcal{D}_{col}$	N_R	FTL	bottoms composition			remarks
					x_{AcH}	x_{BuAc}	x_{DBE}	
0.5	0.25	0.8	9-17	8	0.0001	0.9919	0.0077	taken from section 3.5
0.4735	0.19	0.8	7-15	8	7.83e-5	0.9919	0.0076	constant catalyst loading
0.4646	-	0.8	7-15	8	6.09e-5	0.9919	0.0076	variable catalyst loading

Table 3.5 shows a total cost optimization result for the 22 stages column with the uniform catalyst distribution inside the reaction zone. The optimal configuration has 17 reactive stages from the 2^{nd} to the 18^{th} tray. The optimal feed tray position is found near the middle of the reaction zone at the 7^{th} tray. The reboiler duty requirement is found to be higher compared to that of the heat duty minimization result reported in Table 3.4 - first row. This is because of the trade off between the equipment cost (column diameter) and the operating cost (reboiler duty). Note that for the optimization performed here, the total number of column stages is fixed at 22 and is not optimized simultaneously. It has been noticed that the potential for improvements by using different number of column stages is low with this configuration (< 1 %).

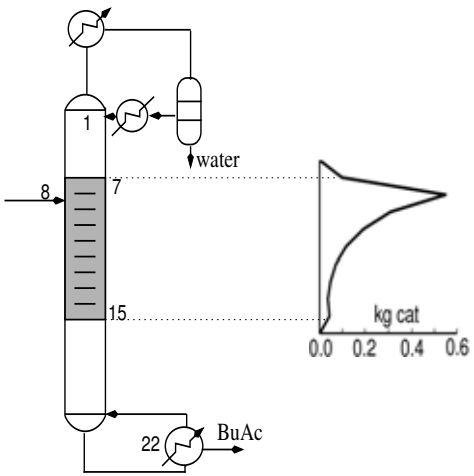

Figure 3.9: Optimum catalyst loading profile for RDC

Table 3.5: RDC - results of total cost optimization for 22 stages column and constant catalyst loading

$\mathbb{T}$	$\mathbb{C}$	$\mathbb{O}$	Q_{REB}	$Mcat_s$	$\mathcal{D}_{col}$	N_R	FTL
5737	5504	233	0.6924	0.0525	0.0371	2-18	7

SRC optimization

The side reactor configuration, as shown in Fig. 3.8 (b), is first optimized wrto. minimal reboiler heat duty. As can be seen from Table 3.6, for a moderate product purity, the optimizer could achieve a design that demands 30 % lower heat duty compared to the previous design given in section 3.5. The optimum solution for a higher BuAc purity in the bottoms, for example 0.9919, is also reported in Table 3.6. This indicates a significant rise in the reboiler heat duty. The value of 0.9919 is chosen so that the direct comparison can be made between the RDC and the SRC processes in following sub-sections.

In the next step, nSRCs are optimized wrto. minimal total cost. The optimization results are shown in Table 3.7 and optimized configurations are shown in Fig. 3.10. For each of the SRCs, in a first step, side reactor positions, feed tray location, catalyst loading and reboiler duty are optimized for a fixed number of 22 column stages. Afterwards, a

simultaneous optimization of the stage number and the other parameters is done. As it can be seen, the 1SRC with 36 stages column performs roughly 34 % better than the 1SRC with 22 stages. Also it consumes only 1.2 times higher reboiler duty compared to the optimal RDC. Further improvements are observed by increasing the number of reactors as can be seen for 2SRC, 3SRC and 4SRC. It is worth noting that the total cost required for the 4SRC is practically equivalent to that of the RDC.

As can be seen from Fig. 3.10, none of the optimal SRC shows nested coupling of reactors. The nested loop of reactors coupled with a column is one of the possibilities in the SRC configuration according to Baur and Krishna [3]. Though the model presented in the Appendix B for the nSRC configuration is capable of determining such a nested loop, the optimal solution does not show any nested loop. That means, there can be two possibilities: 1.) either the solution with nested loops is inferior or 2.) suitable initial values are not available determining a better local solution with nested loops. Another possible reason could be the difference in the objectives of these two work. That is, in their work the objective was to maximize the conversion, whereas in this work the objective is to minimize total annual costs.

The SRC models involve many possible combinations of binary variables, which represent discrete design decisions. For e.g., for 22 column stages the number of integer variables in the 1SRC model is 66, leading to a large number of possible binary combinations. This number goes significantly up in case of the 4SRC, where the number of integer variables is 198. Further research is required for rigorously solving these problems up to global optimality. Some details are presented in the next section on global optimization.

Multiplicities in SRC

As discussed in section 3.5, multiple steady states are known to exist for the case of 1SRC. Hence, it needs to be ensured that the local solution found by the optimizer lies

Table 3.6: SRC - results of reboiler duty optimization for 22 stages column

Q_{REB}	$Mcat_R$	F_R	FTL	fb/sd	bottoms composition			remarks
					x_{AcH}	x_{BuAc}	x_{DBE}	
1.0	4.0	1.0	6	6/7	0.0024	0.9872	0.0103	taken from section 3.5, moderate BuAc purity
0.7139	1.4674	1.0	4	5/6	0.0026	0.9872	0.0101	moderate BuAc purity
3.4056	0.6968	1.0	6	7/7	0.0004	0.9919	0.0077	increased BuAc purity

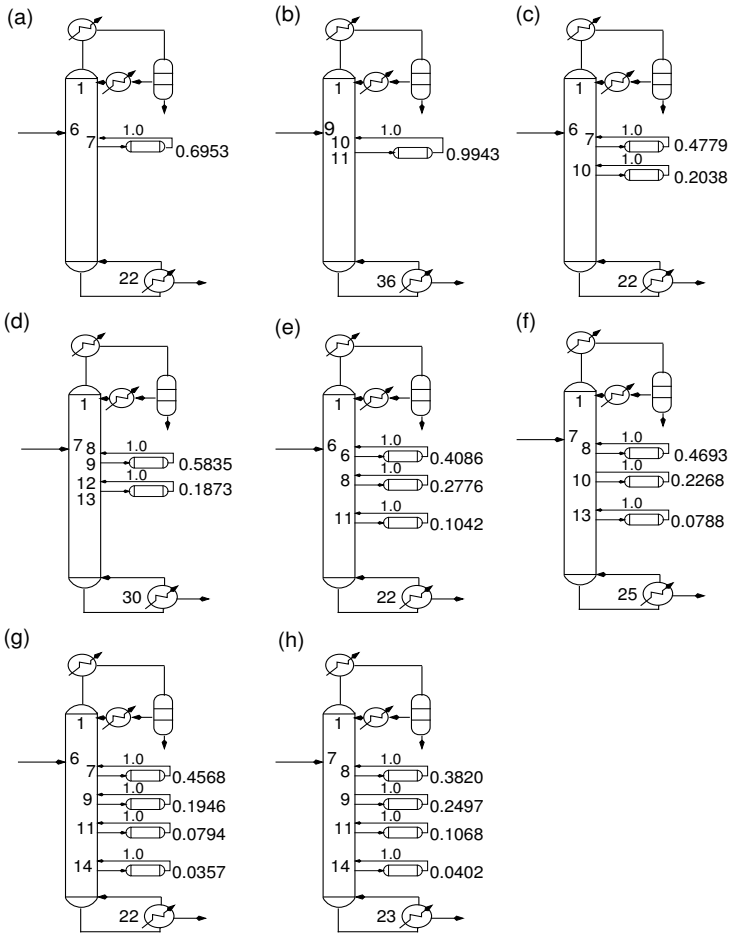

Figure 3.10: Optimal SRC configurations corresponding to Table 3.7. Numbers close to the reactor blocks indicate the catalyst loadings in Kg, number on reactor outlets indicates flow through reactor in kmol/hr and numbers inside the column indicate locations of corresponding inlets or outlets

Table 3.7: Comparison of optimal total cost for SRCs

Nr.	N_T	$N_{reactor}$	$\mathbb{T}$	$\mathbb{C}$	$\mathbb{O}$	Q_{REB}	$\mathcal{D}_{col}$
(a)	22	1	13245	12098	1147	3.4056	0.0823
(b)	36	1	8702	8421	281	0.8209	0.0404
(c)	22	2	7919	7492	427	1.2427	0.0497
(d)	30	2	7079	6841	238	0.6793	0.0368
(e)	22	3	6466	6180	286	0.8067	0.0401
(f)	25	3	6090	5870	222	0.6151	0.0350
(g)	22	4	5953	5706	247	0.6760	0.0367
(h)	23	4	5795	5572	223	0.6041	0.0347

on the desirable steady state branch. Fig. 3.11 (a) shows the solution branches and the location of the optimum for the 36 stages 1SRC column. The solution branches in this figure are computed using a one parameter continuation method in DIVA [52]. The round mark on the curve indicates the optimum solution obtained using GAMS. In this case, the optimum is lying on the upper solution branch due to the higher purity constraint set on the bottoms BuAc composition. The continuation calculation is also performed for the 2SRC case with 30 column stages, as shown in Fig. 3.11 (b). Here, interestingly, the multiplicity regions are found to be shrinking. Furthermore, the continuation with the 3SRC did not show any multiplicity. For a more detailed discussion of optimization for problems with multiple steady states, we refer to [15].

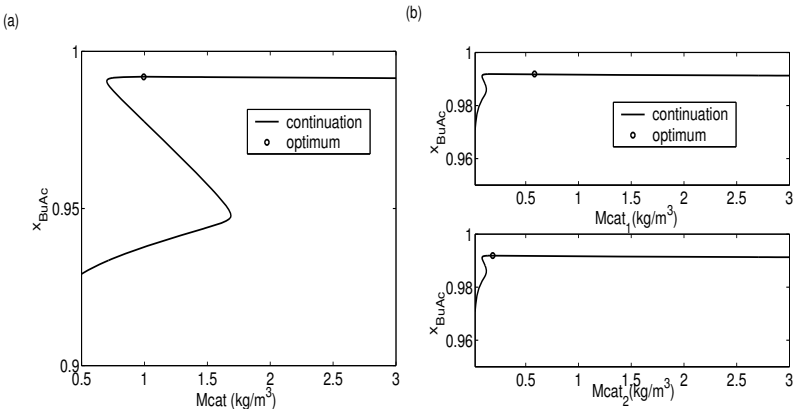

Figure 3.11: Multiple steady states: (a) 1SRC - BuAc mole fraction in bottoms vs. $Mcat_R$; (b) 2SRC - BuAc mole fraction in bottoms vs., at top first reactor catalyst loading and at bottom second reactor catalyst loading

Optimal reactor temperature in SRC

It is found that the performance of the 1SRC configuration can be improved by optimizing the reactor temperature (Fig. 3.12). The isothermal mode of operation is assumed for the CSTR. The upper limit of the reaction temperature is set to 400 K, which happens to be the highest temperature the catalyst Amberlyst-15 can survive without deactivating. The reactor temperature hits the upper limit of 400 K in the optimal solution. The result in Table 3.8 indicates that the 1SRC configuration with an external heater performs economically better than the one without heater (Table 3.7, case (a)).

Table 3.8: SRC - result of total cost optimization with optimal reactor temperature

N_T	$\mathbb{T}$	$\mathbb{C}$	$\mathbb{O}$	Q_{REB}	$Q_{reactor}$	$\mathcal{D}_{col}$
22	12469	11080	1389	2.7782	1.3484	0.0744

The optimization of the side reactor type is not the purpose of this work, as there can be many of such choices. However, it can be said that the reactor type can change the course of the side reaction and hence can affect the process economy.

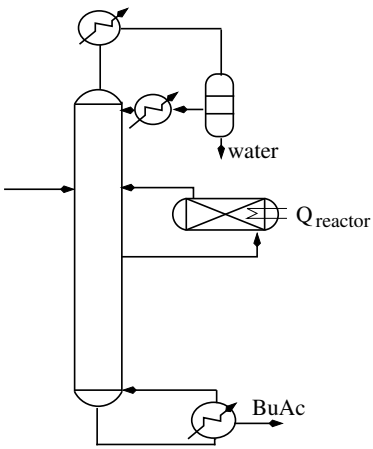

Figure 3.12: SRC with optimal reactor temperature

RDC coupled to the side reactor (RDCSR)

Fig. 3.13 shows a reactive distillation column coupled with a side reactor. Apparently, this configuration will eliminate all the advantages offered by the SRC, viz., easier catalyst regeneration and the elimination of the tedious column hardware design. However, as shown in Table 3.9, the total cost for the RDCSR is less than that of the RDC and the SRC due to the synergistic effects.

Table 3.9: RDCSR - result of total cost optimization for 22 stages column

$\mathbb{T}$	Q_{REB}	$Mcat_s$	N_R	FTL	$Mcat_R$	F_R	$\mathcal{D}_{col}$	fb/sd
4895	0.4658	0.0353	6-21	8	0.7485	0.9169	0.0304	10/10

Effect of the feed compositions

In this section, optimizations of the RDC and the 1SRC configuration are carried out for different feed compositions as shown in Table 3.10. The base case feed composition is taken from Table 3.1. In addition, a stoichiometric feed without a pre-reactor (SF) and

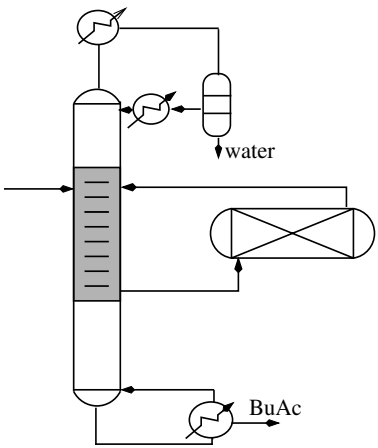

Figure 3.13: Reactor coupled to reactive distillation

a feed with equilibrium composition (EF), where a pre-reactor is used to achieve equilibrium conversion, are considered. Additional feed cases include a stoichiometric feed (SAB) and an equilibrium feed (EAB) with slight excess of BuOH, which is frequently used in practice to avoid any AcH in the bottom products. The results are shown in Table 3.11 and 3.12. It is obvious from these results that the feed compositions has a significant impact on the total cost of RDC and 1SRC configuration. For e.g., if the EF is used instead of the base case feed, then the total cost is roughly lowered by 40 %. Note that in this study the pre-reactor is not accounted explicitely into the cost functions. Therefore, the total cost for the EF case in Table 3.11 and 3.12, could actually be little higher. If one considers the SF, then also nearly a 40 % reduction in the total cost is gained. These gains are even bigger for the 1SRC configuration, where the EF saves 64 % on the total cost, whereas the SF saves up to 55 %.

Table 3.10: Various feed compositions

FC	X_{AcH}	X_{BuOH}	X_{BuAc}	X_{H2O}	X_{DBE}
base case feed	0.1535	0.1676	0.4491	0.2297	0.0001
Hanika et al. [34]	0.1665	0.1797	0.3211	0.3327	0.0000
SAB	0.4950	0.5050	-	-	-
EAB	0.1733	0.1831	0.3218	0.3218	-
SF	0.5	0.5	-	-	-
EF	0.175	0.175	0.325	0.325	-

Table 3.11: Effect of feed compositions on RDC, 22 stages column

FC	$\mathbb{T}$	$\mathbb{C}$	$\mathbb{O}$	Q_{REB}	$Mcat_s$	N_R	FTL
base case feed	5737	5504	233	0.6924	0.0525	2-18	7
Hanika et al. [34]	5119	4932	187	0.5532	0.0419	2-19	8
SAB	3674	3574	100	0.2832	0.0214	6-21	8
EAB	3628	3533	95	0.2798	0.0211	8-21	8
SF	3412	3325	87	0.2420	0.0184	3-21	5
EF	3349	3269	80	0.2366	0.0103	10-21	4

Table 3.12: Effect of feed compositions on 1SRC, 22 stages column

FC	$\mathbb{T}$	$\mathbb{C}$	$\mathbb{O}$	Q_{REB}	$Mcat_s$	FTL	fb/sd
base case feed	13245	12097	1147	3.4056	0.6953	6	7/7
Hanika et al. [34]	8798	8270	528	1.5579	0.5587	5	6/7
SAB	7994	7558	436	1.2706	0.7794	7	6/7
EAB	6122	5864	258	0.7520	0.6090	4	5/7
SF	5845	5606	239	0.6863	0.4588	4	3/4
EF	4727	4567	160	0.4601	0.1598	4	6/7

3.7 Global optimization

In this section, two optimization problems are solved to determine the globally optimal RDC and 4SRC designs. To do that, the stochastic approach introduced in the previous chapter is used. The deterministic approach based on the polyhedral relaxations is not applied in this section, because, it is not yet fully developed to tackle complexity of these problems.

3.7.1 Local optimization from multiple starting points

For RDC, optimizing the total annual costs by applying the combination of the OQNLP - CONOPT - SBB solvers as explained in chapter 2, results in total number of 91 distinct local solutions of the relaxed problem. As can be seen from Fig. 3.14 (a), there exists an optimal number of column stages, for which total annual costs are lowest. The best local solution is indicated by an open "six star". The design variables for the best solutions are given in Table 3.13. Table 3.13 also indicates that 0.5 % in the total costs can be saved by this new design compared to that presented in the previous section. Fig. 3.14 (b) shows the plot of various costs vs. reboiler vapor flow.

Table 3.13: RDC final design

$\mathbb{T}$	$\mathbb{C}$	$\mathbb{O}$	Q_{REB}	$Mcat_s$	$\mathcal{D}_{col}$	N_T	N_R	FTL	%age improvement
5709	5510	199	0.5916	0.0448	0.0343	25	4-22	9	0.5 %

For 4SRC, a total number of 502 distinct local solutions are obtained (Fig. 3.15). In this case, however, it is found that the solution reported in the previous section, solution (h) in Table 3.7 is the best solution.

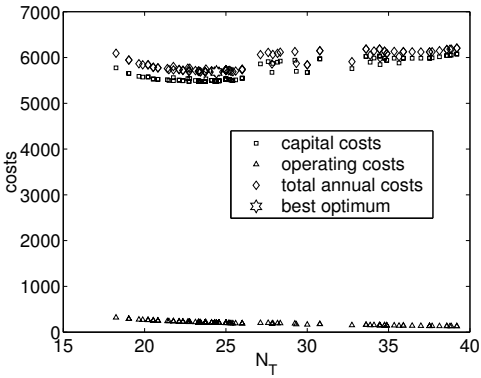

(a)

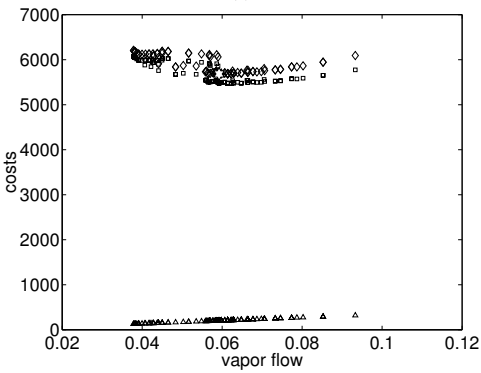

(b)

Figure 3.14: Local solutions ($\diamond$) from multiple starting points for RDC problem: local solutions plotted in terms of (a) various costs vs. number of column stages; (b) various costs vs. vapor flow from reboiler

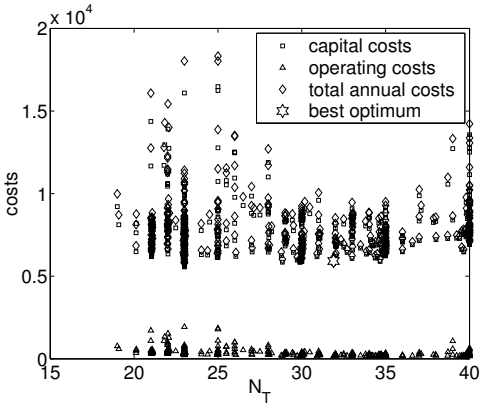

(a)

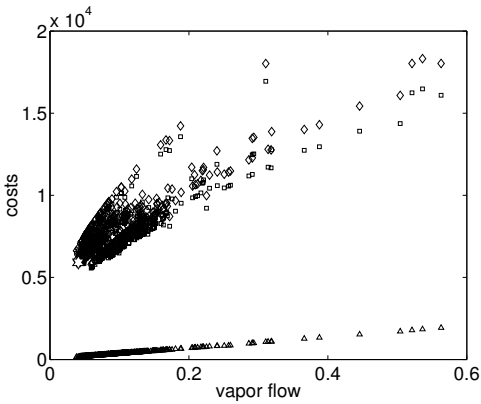

(b)

Figure 3.15: Local solutions ($\diamond$) from multiple starting points for 4SRC problem: local solutions plotted in terms of (a) various costs vs. number of column stages; (b) various costs vs. vapor flow from reboiler

3.8 Summary

In this chapter, the economically optimal designs of a reactive distillation column and side reactors coupled to a nonreactive column have been proposed for the BuAc synthesis problem using MINLP optimization. It is found that the MINLP optimization results clearly outweigh the results of the one parameter optimization. The optimal designs from the former approach consume 5 % and 30% less reboiler heat duty for the RDC and SRC, respectively, compared to the designs obtained by using the one parameter optimization. The local optimization performed for rigorous total costs minimization suggests that the RDC configuration is the most economical option. The other interesting finding is that the 4SRC configuration performs economically similar to the RDC with a difference of $\approx$ 1.0 % in total annual costs. 4SRC offers additional benefits like easy regeneration of catalyst and elimination of a tedious column hardware design, which will clearly lead to reduced maintenence cost. Since this is not explicitely taken into account in the cost functions, 4SRC may perform practically better than RDC. Other designs, in particular, a pre-reactor for RDC or SRC are also considered indirectly by using the equilibrium feed. Their optima show significant improvement in the objective. In these cases, however, final total annual costs may be little higher than the presented one as the costs of the pre-reactor are not taken into account. In the end, if combination of RDC and SRC is considered, then economically better configuration emerges. Although this combination results in increased complexity and loss of individual benefits of SRC. The total annual costs of this configuration is $\approx$ 14 % lower than RDC. Improvements are also observed by operating a side reactor at the optimal reaction temperature.

The stochastic method employed in the second step, determines an improved solution with 0.5 % lesser costs for RDC and gives a better assurance for the 4SRC solution. In recent years, an alternative deterministic local optimization procedure based on the disjunctive programming has also been found to be efficient [91, 51]. The other important tool for treating general nonlinear functions occurring in the MINLP model is to resort to convex underestimators for the corresponding functions. Following this approach, interesting global bounds on the optimal value of the synthesis problem can be given if one is able to derive good convex underestimators. An alternative strategy based on polyhedral relaxations discussed in chapter 2 requires further research to extend that method to complex problems like those considered in this chapter.

Chapter 4

Reactive distillation with potential phase splitting of the liquid phase

4.1 Introduction

This chapter deals with a complex process example – reactive distillation process with potential phase splitting of the liquid phase. As an interesting application new process for the removal of acetic acid from waste waters by esterification with butanol is considered. In the present case, the involved concentration ranges exhibit potential liquid phase splitting on many column stages. The reaction system is the five component system from the previous chapter.

Acetic acid (AcH) is widely used as a solvent or as a reagent in many chemical or petrochemical processes. Some of these processes, such as manufacturing of terephthalic acid, cellulose esters or dimethyl terephthalate, produce dilute AcH streams in compositions ranging from 1 - 65 wt% [63]. It is necessary to recover this acid for re-use and to produce an aqueous stream free of organic contaminants to be discarded to the environment. This can be achieved by separating acid and water conventionally by using simple distillation or extraction, or in a modified way by using azeotropic distillation or extractive distillation. Though a simple distillation column can produce high purity acid at one end and high purity water at the other end (because of the absence of an azeotrope), this operation is uneconomic. The main reasons are: 1. the presence of a tangent pinch on the water end in the x-y diagram and 2. large portions of water possessing a large latent heat of vaporization have to be vaporized (see Fig. 4.1). Extraction can not produce high purity

acid and water streams because of the limited phase separation and component distributions. The more customary approach therefore is to use an extra entrainer or solvent in an azeotropic distillation column [12] or extractive distillation column [14]. These modified approaches can save up to 45 % of estimated total costs of the simple distillation operation.

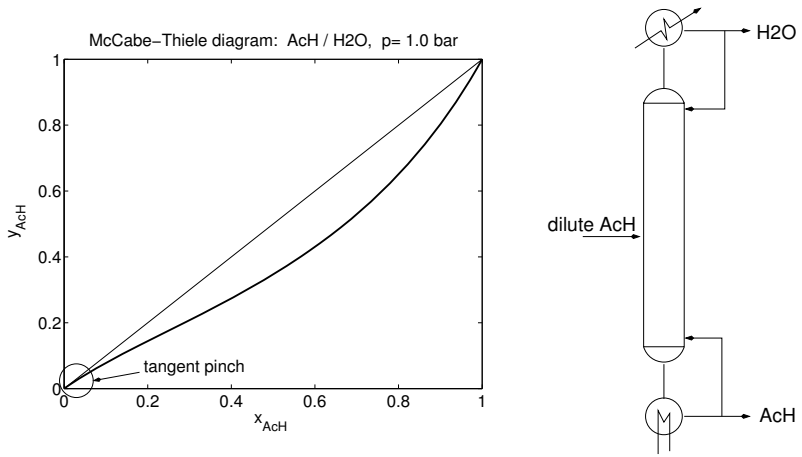

Figure 4.1: (a) McCabe Thiele diagram for a binary mixture of AcH-H_2O; (b) conventional distillation column for the treatment of dilute AcH stream

This chapter deals with another interesting approach, where the present AcH from dilute stream is reacted away in a reactive distillation (RD) column with a suitable alcohol to produce a valuable acetate. This approach was originally suggested by Saha et al. [63]. Saha et al. [63] proposed to use butanol (BuOH) or iso-amyl alcohol (i-AmOH), producing either butyl acetate (BuAc) or iso-amyl acetate (i-AmAc). In their RD column experiments for the treatment of 30 wt% dilute AcH stream, they could achieve 58% AcH conversion with a 2 : 1 mole ratio of BuOH to AcH and 51 % AcH conversion with a 2 : 1 mole ratio of i-AmOH to AcH.

The objective, in this chapter, is to demonstrate a modeling based design procedure for RD columns exhibiting a potential liquid-liquid phase split on column stages. For that purpose, the assumptions of a phase equilibrium and equal reaction extent in both phases

are used. These are rather restrictive assumptions, especially for heterogeneously catalyzed process and should be viewed as a first step. As a starting point, the design of Saha et al. [63] is investigated to determine whether any further improvements are possible.

Unlike the esterification of a pure AcH stream with BuOH, for the esterification of a dilute AcH stream, higher conversions have not been achieved yet. In the latter process, a significant amount of water enters the column with the feed, which apart from being a product of the esterification possesses the potential to form two immiscible liquid phases with the other reacting components. It is, therefore, likely that on many column stages the overall liquid will split into two distinct liquid phases. Design of such a column is complicated due to increased complexity. The design complicacy comes not only from the reaction-separation interactions, as experienced in the previous chapter, but also from the presence of a three phase regime. There is not much work available in literature on this category of design problems.

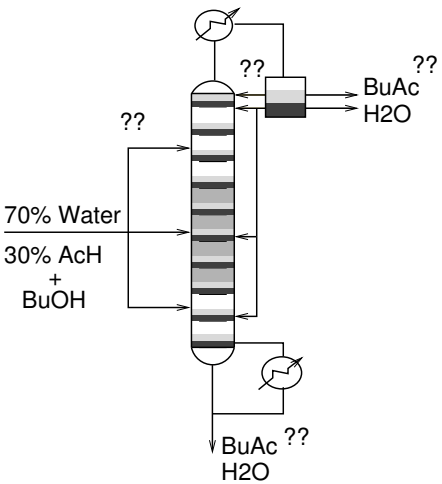

Figure 4.2: Multiphase reactive distillation column for the esterification of a dilute AcH stream

Fig-4.2 shows a typical RD column for the reactive AcH removal process. The precise detection of single or double liquid phases on every single tray is a crucial step for the success of the design procedure. This is done by combining the main column model (MESH equations) with an extra routine for the phase split calculation [61]. The main

design decision variables are, single or double feeds, aqueous or organic reflux at the top, positions of feed trays, reflux trays and reactive trays.

The remainder of the chapter is organized as follows. At first, algorithmic issues like, model formulation, verification and solution procedure are presented. Then various process candidates are introduced and the simulation results for the same are presented. Later dynamic simulations of the selected column designs are presented in order to gain insight of the process operability and sensitivity wrto. disturbances.

4.2 Mathematical model

The mathematical model of a RD column with phase split calculations has been written in two parts (see Fig. 4.3). The first part, the main model, contains the classical MESH equations of a reactive distillation column model [85, 82, 58]. The vapor-liquid equilibrium calculation is slightly adapted for the provision of a second liquid phase [61]. The reaction kinetics for the main and side reactions are taken from the section 3.2. To account for the liquid-liquid phase splitting, the UNIQUAC activity coefficient model was used. The binary interaction parameters for the homogeneous pairs (i.e AcH-BuOH, AcH-BuAc, AcH-H_2O, BuOH-BuAc) were fitted to predictions of the Wilson activity coefficient model known from section 3.3. The binary interaction parameters for the heterogeneous pairs (i.e BuOH-H_2O, BuAc-H_2O) were obtained from a UNIQUAC-LLE model, again known from section 3.3. The binary interaction parameters for dibutyl ether (DBE) pairs were fitted to predictions generated by the UNIFAC model. The new binary interaction parameters for the UNIQUAC model are shown in Table 4.1. The azeotropes for the five component nonreactive system (AcH-BuOH-BuAc-H_2O-DBE), calculated with the parameters in Table 4.1 at atmospheric pressure, are listed in Table 4.2. Table 4.2 also shows normal boiling points of pure components.

For the reaction rate calculations, equal reaction extent is assumed for both liquid phases according to Eq. 4.1 due to the iso-activity condition.

$$r_i^{overall} = Mcat_{tot}^{st} \cdot f(a_i^I) = Mcat_I^{st} \cdot f(a_i^I) + Mcat_{II}^{st} \cdot f(a_i^{II}) \quad \forall \quad \text{reactive trays} \quad (4.1)$$

Table 4.1: UNIQUAC model parameters

Volume parameters		
component	r	q
AcH (1)	2.2024	2.072
BuOH (2)	3.4543	3.052
BuAc (3)	4.8274	4.196
H_2O (4)	0.9200	1.400
DBE (5)	6.0925	5.176

Binary interaction parameters for the UNIQUAC equation u_{ij} Kcal/Kmol						
i	j	1	2	3	4	5
1		0.0	-533.8135	-150.9514	-490.2368	-289.1820
2		533.7985	0.0	-73.1426	41.4492	-130.9375
3		273.4758	218.2952	0.0	999.3043	98.3067
4		490.2274	463.1690	232.8096	0.0	-94.3710
5		289.2317	367.4297	-51.5701	1252.8446	0.0

Table 4.2: Stationary points of a nonreactive mixture of AcH-BuOH-BuAc-H_2O-DBE at 1 atm

pure components or azeotropes	mole fractions					T_b [K]	liquid phase
	x_{AcH}	x_{BuOH}	x_{BuAc}	x_{H_2O}	x_{DBE}		
AcH	1.0	-	-	-	-	391.05	-
BuOH	-	1.0	-	-	-	390.85	-
BuAc	-	-	1.0	-	-	399.25	-
H_2O	-	-	-	1.0	-	373.15	-
DBE	-	-	-	-	1.0	415.15	-
AcH-BuOH	0.5260	0.4740	-	-	-	395.40	homogeneous
BuOH-BuAc	-	0.7329	0.2671	-	-	389.41	homogeneous
BuOH-H_2O	-	0.2218	-	0.7782	-	366.99	heterogeneous
BuAc-H_2O	-	-	0.2866	0.7134	-	364.05	heterogeneous
BuOH-DBE	-	0.8885	-	-	0.1115	389.9	homogeneous
H_2O-DBE	-	-	-	0.8025	0.1975	367.25	heterogeneous
AcH-BuOH-BuAc	0.4520	0.2019	0.3462	-	-	394.07	homogeneous
BuOH-BuAc-H_2O	-	0.0551	0.2400	0.7049	-	363.88	heterogeneous
BuOH-H_2O-DBE	-	0.1249	-	0.7618	0.1132	366.18	heterogeneous

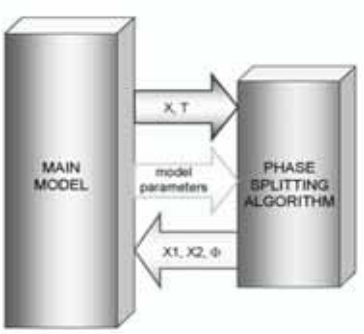

Figure 4.3: Components of a dynamic RD model with potential liquid phase splitting.

The second part, a phase splitting algorithm, basically identifies the existence of a phase split on a considered tray. This algorithm has been developed by Steyer et al. [78] based on the vapor-liquid-liquid flash algorithm proposed by Bausa and Marquardt [4]. When phase split is reported to occur on the considered tray, this routine returns to the main model a state vector $\{x^I, x^{II}, \phi\}$. Fig. 4.3 shows the phase split routine and its interaction with the main column model.

Note that all the simulations presented in this chapter are performed with the process simulator DIVA [52]. The external phase split routine written in Fortran77 is interfaced to a main column model in the DIVA kernel. All simulations are performed at 650 mbar pressure to avoid 1-butene formation, a product of BuOH dehydration according to Janowsky et al. [43].

4.2.1 Model verification

Due to the lack of comprehensive experimental data, the model is verified by reproducing the results of Brüggemann et al. [10]. In their work, they presented modeling and simulations for a homogeneously catalyzed batch reactive distillation process for BuAc synthesis in a three phase regime. This practical example was taken from Venimadhavan et al. [89]. In particular, they examined the following operating scenarios:

1. ternary nonreactive batch distillation (initial reboiler loading: 40 % H_2O, 20 % BuOH and 40 % BuAc), at a constant reflux ratio (0.9)

2. reactive batch distillation (initial reboiler loading: 51 % BuOH and 49 % AcH), homogeneously catalyzed with sulfuric acid, at a constant reflux ratio (0.9)

3. second scenario except at a variable-adaptive reflux ratio (0.9 and 0.99)

In order to reproduce these scenarios, the model presented in this work is adapted for a 33 stage batch column, including the condenser plus decanter and the still pot (with internal reboiler). At top, the reflux from the decanter comes to the first column tray. The holdup on each tray is 0.001 kmol, the combined holdup of the condenser and the decanter is 0.01 kmol and the initial holdup of the still pot is 2 kmol. A constant vapor flowrate of 2 kmol/h from the reboiler is considered. To maintain the consistency with Brüggemann's work, the thermodynamic data and reaction kinetics were taken from Venimadhavan et al. [89] which are slightly different from the data presented in Table 4.1. All three operating strategies presented in Brüggemann et al. [10] were investigated with our model implementation, but due to the lack of space only the results for the first scenario are shown here. Figs. 4.4 and 4.5 depict the global composition in the decanter and the reboiler, respectively. The results are found to be in a very good agreement with those from Brüggemann's paper.

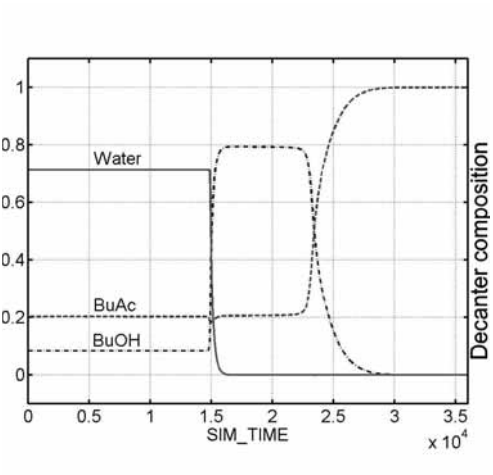

Figure 4.4: Reproduction of the first scenario from Brüggemann et al. [10], decanter composition (mole fraction) vs. simulation time (s).

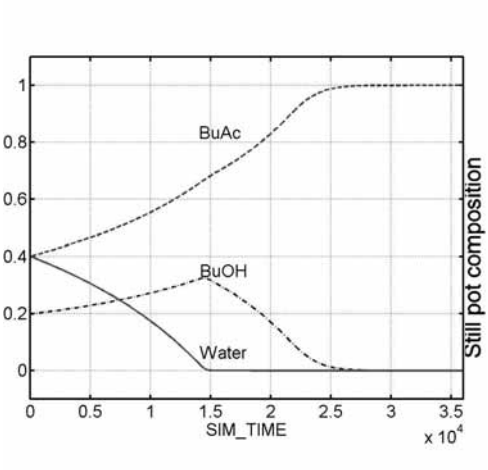

Figure 4.5: Reproduction of the first scenario from Brüggemann et al. [10], bottom composition (mole fraction) vs. simulation time (s).

For a homogeneously catalyzed RD column the phase split algorithm precisely detects the existence of two liquid phases. In the remainder, a heterogeneously catalyzed process will be considered.

4.2.2 Model with phase split vs. model without phase split

For a theoretical understanding of the phenomena of liquid-liquid phase splitting occurring in the RD column, the liquid-liquid equilibrium boundary shown in Fig. 3.2 is useful. It can be seen that binary pairs of BuOH-H_2O and BuAc-H_2O have miscibility gaps. As a result, there is a miscibility region in the present system. This miscibility region is close to the water corner. The liquid-liquid phase splitting is expected to occur when the overall composition on the column trays will fall inside the liquid-liquid phase boundary. In other words, a mixture with higher water concentration and high enough concentration of BuOH or BuAc or both of them, will most likely split into two separate liquid phases. In the esterification of a dilute stream of AcH, ample amount of water enters the column with the feed. Hence, on many column trays, it is likely that the overall composition falls inside the miscibility region.

As a result of the phase split on the column trays, the activities of the components on these trays will be significantly different from those calculated based on a model without liquid-liquid phase split. This might lead to severe errors due to the wrong reaction rate calculations based on the wrong values of the activities. For example, Fig. 4.6 shows a comparison between the composition profiles for a RD column model with phase split (PHSP) and without phase split of the liquid phase (NPHSP) for the same set of operating parameters (see Table 4.3). Here, the NPHSP model composition profiles are completely different from the PHSP model near the lower part of the column. The NPHSP model wrongly predicts 95 % AcH conversion instead of 13 % conversion predicted by the PHSP model. The phase split occurs almost entirely in the column from the column top down to the 19^{th} tray, as can be seen from the value of the phase fraction ϕ. These results clearly indicate the need for a PHSP model to design such a process.

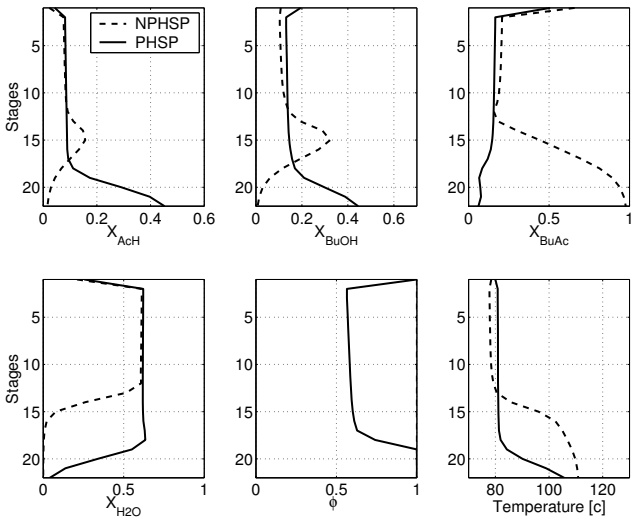

Figure 4.6: Column profiles indicating big differences between NPHSP and PHSP model composition profiles

Table 4.3: operating conditions for Fig. 4.6

Feed compositions	
Feed (kmol/hr)	0.006125
x_{AcH}	0.1021
x_{BuOH}	0.1021
x_{BuAc}	0.0
x_{H2O}	0.7958
x_{DBE}	0.0

Configurational details	
Q_{REB}(kW)	0.0938
$Mcat_{st}$ (kg/tray)	0.0005
N_R	3-21
N_T	22
FTL	2^{nd}

4.2.3 Solution procedure

Obtaining an appropriate initialization vector for a PHSP model which gives convergence to a desired steady state is a non-easy task. The large solution time requirement (of the order of few hours) presents a major difficulty. The close numerical interaction between the main column model and the phase split algorithm increases the complexity of the solution procedure. The phase split routine performs a homotopy continuation from the different starting points corresponding to different convex regions of the three phase region. In the present example, two starting points are provided for two binary pairs showing miscibility gaps, namely, BuOH-H_2O and BuAc-H_2O. The homotopy steps need to be performed from these starting points for each of the column stages.

Here, four different approaches based on engineering insight are applied to achieve the final designs.

1. Using the NPHSP model results as starting values

   In cases where a liquid-liquid phase split is not occurring or occurring on a relatively small number of column stages, the NPHSP model solution provides good starting values.

2. Dynamic simulation to a new steady state

3. Continuation in one parameter to achieve a desired steady state

4. GAMS [9] optimization to obtain a rough estimation of the desired states yielding 99 % AcH conversion

   A preliminary GAMS model is written where binary variables acting as switches for the phase split, are kept ON (=1) for specific column trays. This information can be a priori obtained from the the previous simulation results. The GAMS model is then optimized for a 99 % conversion of AcH setting as a constraint. Though not very elegant, this approach helps significantly to reduce the simulation effort.

4.3 Alternative process candidates

In this section, at first, a few possible column configurations are presented with the aim to obtain a preliminary ranking based on the maximum achievable conversions. These process candidates are generated based on the following main design features (see Fig-4.2): 1. organic reflux or aqueous reflux or both; 2. positions of reflux streams into the column; 3. position of reaction zone; 4. single feed or double feed; and 5. positions of feed trays. The other important design factor is the molar ratio of alcohol to acid in the feed. In general, if alcohol is higher in the feed, the conversion of AcH to acetate will be higher. As recommended by Saha et al. [63], here, at first a BuOH to AcH molar feed ratio of 2 : 1 is used. Later, BuOH concentration is reduced to further improve the process design.

Fig. 4.7 shows six different process candidates which include:

1. Configuration 1 having a total organic reflux at the top

2. Configuration 2 having a total aqueous reflux at the top

3. Configuration 3 having a total organic reflux and partial aqueous reflux at the top

4. Configuration 4 having a partial organic and partial aqueous reflux at the top

5. Configuration 5 having a total aqueous reflux fed into the reboiler and a partial organic reflux at the top

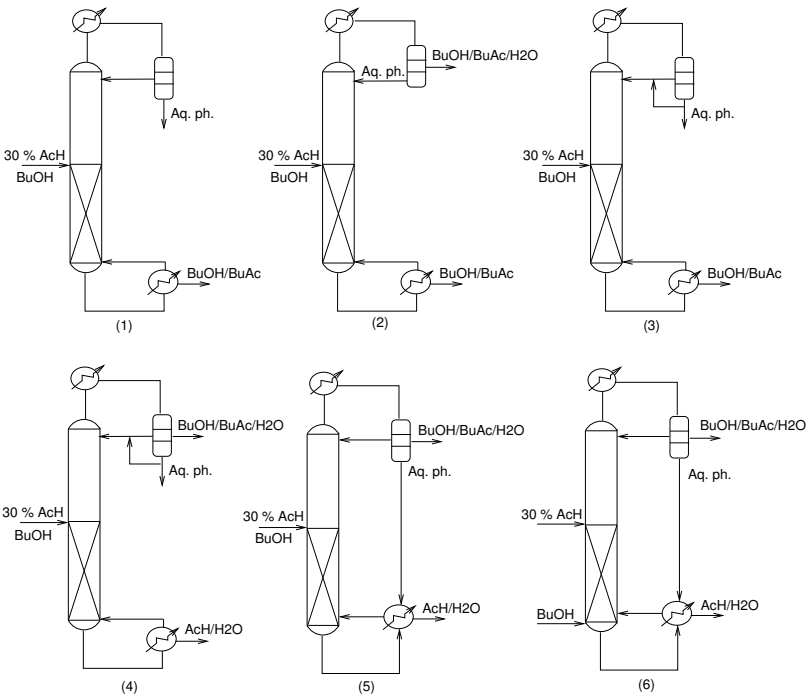

Figure 4.7: Different process alternatives based on different combinations of design variables

6. Configuration 6 having reflux features similar to the configuration 5 but with two feed streams: a dilute AcH feed at the top of the reaction zone and pure alcohol feed at the bottom of the reaction zone

Obviously many other process variations are viable. However, in this section, the attention is focused on these six configurations only, which were inspired by the work of Saha et al. [63].

For the feed conditions shown in Table 4.4, using the PHSP model and the solution procedure explained in the preceding section, the maximum achievable AcH conversions for the six process alternatives were determined (see Table 4.5). As can be seen, the configurations 1 and 6 achieve 99 % conversion, configuration 5 achieves 92 % conversion and

Table 4.4: Feed compositions, BuOH : AcH is 2 : 1

	configurations 1 to 5	configuration 6	
		Feed I	Feed II
Feed (kmol/hr)	0.00675	0.0055	0.00125
x_{AcH}	0.0926	0.1137	0.0
x_{BuOH}	0.1854	0.0	1.0
x_{BuAc}	0.0	0.0	0.0
x_{H2O}	0.7220	0.8863	0.0
x_{DBE}	0.0	0.0	0.0

very little conversion levels are achieved by the other configurations. Due to numerical difficulties, for configuration 4 no steady state solution could be obtained.

Table 4.5: Configurational details

configurations	1	2	3	5	6
AcH conversion (%)	99	63.7	9.0	91.92	99
Q_{REB}(kW)	0.1033	0.14	0.107	0.362	0.1244
$Mcat_{st}$ (kg/tray)	0.00265	6.90	0.0027	0.8381	1.3637
N_R	8-21	12-21	12-21	12-21	9-21
N_T	22	22	22	22	22
FTL	8^{th}	11^{th}	11^{th}	11^{th}	9^{th} and 21^{st}

Now onwards, the focus will be on the configurations 1 and 6 only, because only these two process alternatives give high AcH conversions. In the following sections, a detailed model based analysis is presented to evaluate the performance of configurations 1 and 6.

4.4 Proposed process candidates

Configuration 1 has a single feed stream and no aqueous reflux. The aqueous phase is obtained as a distillate and a mixture of BuOH and BuAc or high purity BuAc can be obtained in the bottoms. Configuration 6, on the other hand, has two feed streams and an aqueous reflux entering into the column reboiler. The product streams are reversed com-

pared to configuration 1, water is obtained at the bottom and the organic phase containing acetate is obtained as distillate.

4.4.1 Configuration 1

In this section, steady state simulation results for configuration 1 for three different feed compositions are presented. These feed cases include: a 2 : 1 mole ratio BuOH to AcH; a stoichiometric mole ratio of BuOH to AcH (i.e. 1 : 1) and a 4 % excess of BuOH (i.e. 1.04 : 1).

Table 4.6: Optimal design: configuration 1 - simulations at 650 mbar

	2 : 1 BuOH to AcH	stoichiometric BuOH	4 % excess BuOH
Feed			
feed (Kmol/hr)	0.00675	0.006125	0.00615
x_{AcH}	0.0926	0.1021	0.1017
x_{BuOH}	0.1854	0.1021	0.1057
x_{H_2O}	0.7220	0.7958	0.7926
Bottoms			
bottoms (Kmol/hr)	0.0012	0.00061	0.000608
x_{AcH}	0.0001	0.0451	0.0031
x_{BuOH}	0.4892	0.0058	0.0028
x_{BuAc}	0.5094	0.9489	0.9940
x_{H_2O}	0.0	0.0001	0.0
x_{DBE}	0.0013	0.0001	0.0001
Distillate			
distillate (Kmol/hr)	0.00555	0.005515	0.005542
x_{AcH}	0.0	0.0014	0.0014
x_{BuOH}	0.0062	0.0058	0.0058
x_{BuAc}	0.0020	0.0020	0.0020
x_{H_2O}	0.9918	0.9908	0.9908
x_{DBE}	0.0	0.0	0.0
Configurational details			
AcH conversion (%)	99	94.3	98.5
Q_{REB} (kW)	0.1033	0.0999	0.1004
$Mcat_{st}$ (kg/tray)	0.00265	0.0036	0.004
N_R	8-21	13-21	22-26
N_T	22	22	27
FTL	8^{th}	4^{th}	4^{th}

2 : 1 molar ratio of BuOH to AcH

The feed composition and feed flow rate can be read from Table 4.6. The composition profiles for the obtained design are presented in Fig. 4.8. Fig. 4.8 also shows the phase fraction ϕ and the temperature profile inside the column. It can be seen that a phase split occurs for trays 8, 9 and 10. For comparison the concentration profiles obtained for the NPHSP model are also shown in Fig. 4.8. For the NPHSP model the value of ϕ is equal to one. The top and bottom product compositions are presented in Table 4.6. As mentioned earlier, the distillate is the aqueous phase from the decanter carrying more than 99 % water. BuOH and BuAc are present only in traces. The bottom product is approximately a 50 - 50 mixture of BuAc and BuOH. It is obvious that unreacted BuOH in excess of AcH has shown up in the bottom products.

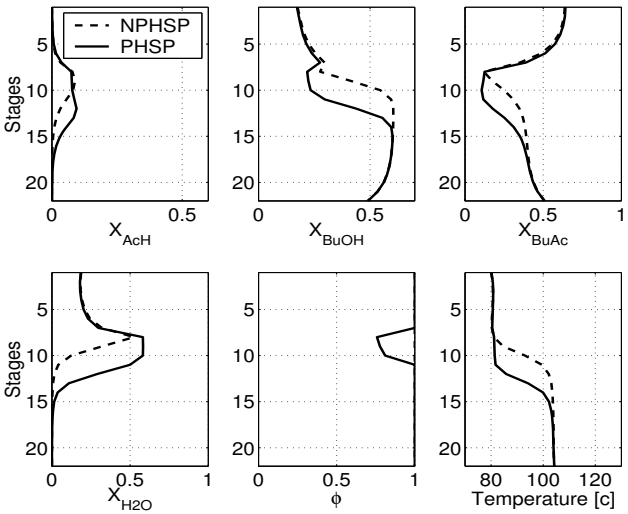

Figure 4.8: Column profiles for configuration 1 calculated at 650 mbar: 2 : 1 mole ratio of BuOH to AcH

1 : 1 molar ratio of BuOH to AcH

Fig. 4.9 presents the composition profile for this case with 94.3 % conversion of AcH. As can be seen from the figure the three phase region is longer than in the previous case covering trays from 4 to 16. For this case, the differences in the concentration profiles for a PHSP model and NPHSP model are even larger. The bottom product compositions as

can be seen from Table 4.6 indicates that around 95 % BuAc stream can be produced. The distillate product still contains more than 99 % water. A possible reason for the limited conversion of AcH can be the loss of alcohol through the aqueous phase.

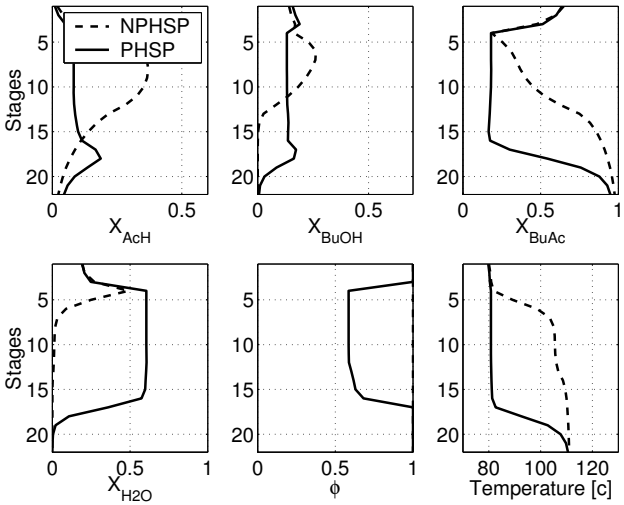

Figure 4.9: Column profiles for configuration 1 calculated at 650 mbar: stoichiometric BuOH

1.04 : 1 molar ratio of BuOH to AcH

In order to obtain higher conversion of AcH, a 4 % excess of BuOH in the feed stream is used that will make up for the loss occurring in the distillate stream. Fig. 4.10 presents the composition profile for the excess BuOH case with close to 99 % conversion of AcH. The distillate stream contains 99 % water and the bottom stream contains more than 99 % of BuAc. In this case too, a large region of the column exhibits three phases, i.e trays from 4 to 19.

In summary we find for this configuration: 1. the NPHSP model can mislead the process design, 2. close to 100 % AcH conversion is possible 3. high purity water can be produced as a distillate which after simple processing can be discarded to the environment, 4. for a 2 : 1 molar ratio of BuOH to AcH, a 50 - 50 mixture of BuOH and BuAc is obtained which needs down stream processing to separate the two organics; for 1 : 1 and 1.04 : 1 molar

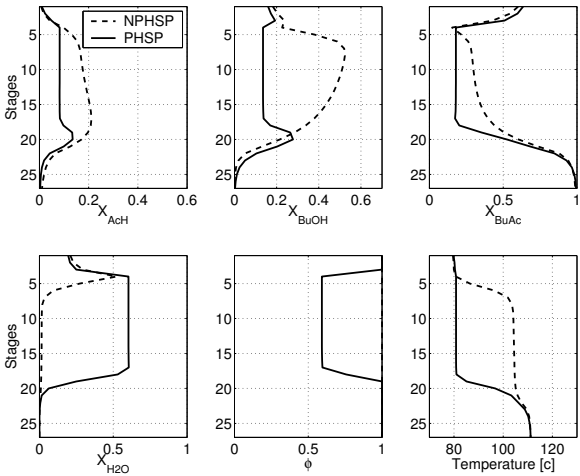

Figure 4.10: Column profiles for configuration 1 calculated at 650 mbar: 4 % excess BuOH

ratios, high purity BuAc (95 % and 99 %, respectively) can be obtained at the column bottom.

The design variables and operating conditions for all three scenarios can be read from the last section of Table 4.6. For a 2 : 1 molar feed ratio, a 22 stage column with a reaction zone in the stripping section between the trays 8 and 21; and a feed tray at the top of the reaction zone can achieve the desired goal of 99 % acid conversion. The three phase region starts at the feed tray location and goes down into the stripping section. For a 1 : 1 molar ratio a 22 stage column with a reaction zone between the trays 13 and 21; and a feed position at the 4^{th} tray is required to achieve a maximum conversion of 94.3 %. Here again the three phase region starts from the feed tray and goes down into the stripping section. For the 4 % excess BuOH case, to achieve close to 99 % conversion, a 27 stage column with a reaction zone between the trays 22 and 26 and a feed position at the 4^{th} tray is required. In this case again, the three phase region starts from the feed tray and extends down in the stripping section.

4.4.2 Configuration 6

Here, two different feed cases have been investigated, namely 2 : 1 and 1 : 1 (BuOH : AcH). The overall feed compositions are exactly the same as used in configuration 1.

Table 4.7: Optimal design: configuration 6 - simulations at 650 mbar

	2 : 1 mole ratio of BuOH to AcH	stoichiometric BuOH
Feed		
BuOH feed (Kmol/hr)	0.00125	0.00062534
AcH feed (Kmol/hr)	0.0055	0.0055
x_{AcH}	0.1137	0.1137
x_{H_2O}	0.8863	0.8863
Bottoms		
bottoms (Kmol/hr)	0.00535	0.005421
x_{AcH}	0.0011	0.0032
x_{BuOH}	0.0227	0.0001
x_{BuAc}	0.0	0.0
x_{H_2O}	0.9762	0.9967
x_{DBE}	0.0	0.0
Distillate		
distillate (Kmol/hr)	0.0014	0.0007
x_{AcH}	0.0001	0.0029
x_{BuOH}	0.2597	0.0256
x_{BuAc}	0.4433	0.8604
x_{H_2O}	0.2444	0.1106
x_{DBE}	0.0525	0.0005
Configurational details		
AcH conversion (%)	99.01	96.91
Q_{REB} (kW)	0.1244	0.3497
$Mcat_{st}$ (kg/tray)	1.3637	0.5289
Rf_{org}	0.6646	0.9288
N_R	9-21	16-29
N_T	22	30
FTL	$9^{th}$and 21^{st}	10^{th} and 29^{th}

2 : 1 molar ratio of BuOH to AcH

The composition profiles for the obtained design are presented in Fig. 4.11 and feed compositions and product compositions are presented in Table 4.7. In the bottoms water with a purity of 97.6 % is obtained. The top product is the organic phase of the decanter containing a mixture of 44 % BuAc, 26 % BuOH and 24 % water. A significant amount of side product DBE is also present in the top product.

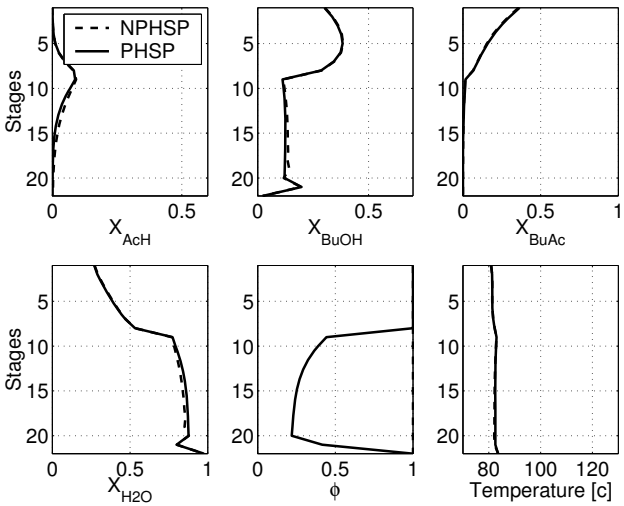

Figure 4.11: Column profiles for configuration 6 calculated at 650 mbar: 2 : 1 mole ratio of BuOH to AcH

1 : 1 molar ratio of BuOH to AcH

For a 1 : 1 molar ratio, configuration 6 can achieve up to 97 % conversion of AcH. The composition profiles can be seen in Fig. 4.12 and feed compositions and product compositions in Table 4.7. Here the bottom contains more than 99 % of water. The distillate is predominantly a mixture of BuAc and water. The unreacted BuOH is present in small amounts in the distillate stream. It would be possible to separate high purity BuAc from the distillate using a membrane separator, for example.

The design variables are shown in the lower section of Table 4.7. For a 2 : 1 molar ratio a 22 stage column with a reaction zone in the stripping section and feed tray at the 9^{th}

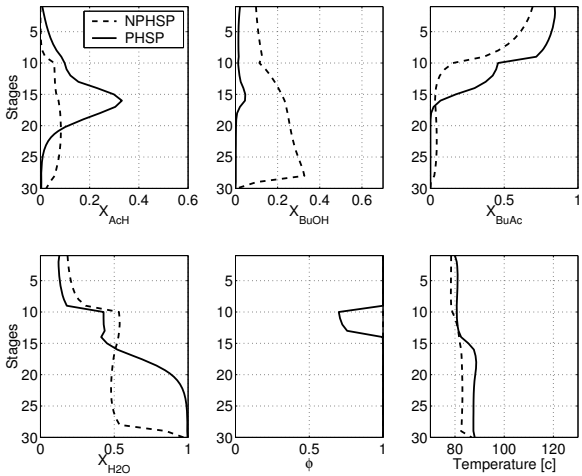

Figure 4.12: Column profiles for configuration 6 calculated at 650 mbar: stoichiometric BuOH

position can achieve 99 % AcH conversion. The reboiler heat duty requirement for this scenario is comparable to the one required in configuration 1. For a 1 : 1 molar ratio 30 column stages with a reaction zone located between the trays 16 and 29 and a feed tray position at the 10^{th} tray is required to achieve 97 % AcH conversion. The reboiler duty requirement for this scenario is significantly higher compared to those required in configuration 1.

4.4.3 Extreme AcH concentrations (1 wt% and 65 wt%)

In the previous section, it is shown that RD processes yield close to 100 % conversion of AcH for a 30 wt% AcH streams. It is also interesting to find out whether these processes are also suitable for extreme AcH streams, i.e. with 1 wt% and 65 wt%. To investigate this, a scenario with 2 : 1 mole ratio of BuOH to AcH is considered as a base case. However, any other scenario could have also been simulated accordingly. The results of simulations giving very high AcH conversion are shown in Table 4.8. For a 65 wt% AcH stream configurations 1 and 6 both yield more than 99 % conversion. Whereas, for a 1 wt% AcH streams configuration 1 yields only 89.3 % conversion and configuration 6 yields 96.9 % conversion. Configuration 6 on the other hand requires a very large heat

duty to fulfill this task. It can be seen that design of 65 wt% AcH stream is relatively easier to achieve than that of 1 wt% AcH stream. This is expected since 1 wt% AcH stream possesses significantly less AcH (0.3 mole%) which potentially contributes to form BuAc in the reaction zone. BuAc in turn acts as an entrainer, like in an extractive distillation column by forming a low-boiling azeotrope with water. This means that a very high internal flow of organic phase is required to satisfy the need of BuAc forming an azeotrope with very large amount of water. For this reason, it is recommended not to

Table 4.8: Simulations of configurations 1 and 6 for the extreme compositions (1 and 65 wt%) of AcH for a 2 : 1 mole ratio of BuOH to AcH, 650 mbar and 22 stages column

	configuration 1		configuration 6	
	65 wt%	1 wt%	65 wt%	1 wt%
Feed				
BuOH feed (Kmol/hr)	-	-	0.003936	0.000033
AcH feed (Kmol/hr)	0.009436	0.005533	0.0055	0.0055
x_{AcH}	0.2086	0.003	0.3578	0.003
x_{BuOH}	0.4172	0.006	-	-
x_{H_2O}	0.3742	0.991	0.6422	0.997
Bottoms				
bottoms (Kmol/hr)	0.003834	0.4e-05	0.005357	0.005493
x_{AcH}	0.0003	0.0018	0.0023	0.0001
x_{BuOH}	0.4764	0.0	0.1359	0.0004
x_{BuAc}	0.5102	0.9979	0.0002	0.0
x_{H_2O}	0.0	0.0	0.8614	0.9995
x_{DBE}	0.0131	0.0003	0.0002	0.0
Distillate				
distillate (Kmol/hr)	0.005602	0.005529	0.004079	0.4e-5
x_{AcH}	0.0	0.0003	0.001	0.0
x_{BuOH}	0.0078	0.0033	0.2608	0.2946
x_{BuAc}	0.0020	0.0020	0.4782	0.4034
x_{H_2O}	0.9901	0.9944	0.2366	0.2659
x_{DBE}	0.0	0.0	0.0234	0.0361
Configurational details				
AcH conversion (%)	99.91	89.3	99.17	96.9
Q_{REB} (kW)	0.1087	0.0994	0.2895	0.2840
$Mcat_{st}$ (kg/tray)	0.1588	0.0007	1.6332	1.0
Rf_{org}	1.0	1.0	0.5896	0.9956
N_R	8-21	5-21	9-21	6
PHSP trays	-	1-6	10-22	3-5
FTL	8^{th}	3^{rd}	9^{th} and 21^{st}	3^{rd} and 7^{th}

process extreme low concentrations of AcH streams in an RD process.

4.4.4 Comparison of estimated total annual costs (TAC)

The total annual costs, i.e. equipment costs and operating costs, are estimated for configurations 1 and 6 based on the cost functions obtained from Appendix B. The comparison of the estimated TAC are given in Table 4.9. For the same feed composition, i.e 30 wt% AcH, and same feed flow rate, the simple distillation process (Fig. 4.1) separating AcH as well as water with 99 mole % purity, is also optimized with respect to the total annual costs. It has total annual costs of 7250 money units. The optimal total number of stages are 29 and the feed position is at the 19^{th} tray from the top. The optimal reflux ratio is 15.64 and the reboil ratio is 218.17. These costs are compared with the costs of a 4 % excess BuOH case for configuration 1 and the 1 : 1 molar ratio of BuOH to AcH for configuration 6, because these are the cases where high conversions of AcH are achieved and high purity end products are obtained. Note that the configurations 1 and 6 are not optimized with respect to TAC. They represent only feasible designs. Even though, as can be seen from Table 4.9, configuration 1 saves up to 66 % and configuration 6 saves up to 56 % on the total annual costs.

Table 4.9: Comparison of estimated total annual costs (TAC)

Process	Estimated TAC	%age savings
distillative separation	7250	-
Conf. A, 4 % excess BuOH	2500	66 %
Conf. B, 1 : 1 BuOH to AcH	3200	56 %

The cost calculations do not consider reactant costs, however, it is assumed that the profit from selling the valuable esters will recover the cost of reactants in the latter cases. For the optimization of the conventional distillative separation process, the problem was formulated as a MINLP and was subsequently solved by using a SBB solver from GAMS. To solve internal NLP problems CONOPT3 was used. The obtained solution is a local solution and no guarantee can be given for its globality. Optimization of the reactive distillation process with potential liquid-liquid phase split is a challenging task and beyond the scope of this work.

4.4.5 Dynamic simulations

Besides steady state design and economics, also the sensitivity wrto. disturbances is important for operability. For this purpose, dynamic responses to a $\pm$ 5 % disturbance in the feed flow rate and $\pm$ 5 % disturbance in the AcH composition of the feed are evaluated for the configurations 1 and 6. For a concise presentation, only a few interesting results are reported. The results of dynamic simulations for the configurations 1 and 6 with a 2 : 1 mole ratio of BuOH to AcH, i.e case of Figs. 4.8 and 4.11, are reported elsewhere [27]. The brief summary of these results are given in Table 4.10.

Fig. 4.13 shows the dynamic simulation results for configuration 1 with 4 % excess BuOH around the steady state profiles shown in Fig. 4.10, for a 5 % increase in the feed flow rate. Here, the dynamic response of the column is drawn over a time length between an old steady state (gray line) and a new steady state (dark line). It can be seen that even

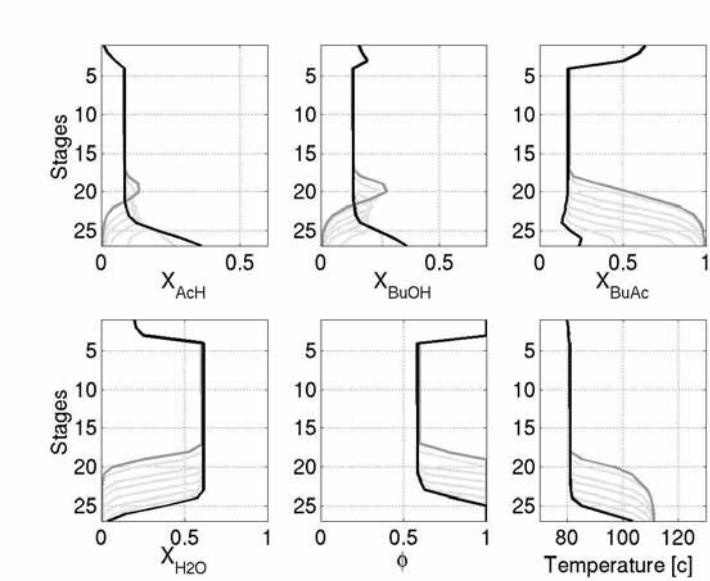

Figure 4.13: Dynamic simulation of configuration 1 with 4 % excess BuOH: transient response to a 5 % increase in the feed flow rate. Gray line - initial steady state; dark line - final steady state; light gray lines - intermediate states

with a small disturbance (here, + 5 %) in the feed flow rate, the column profiles change significantly. Though the top products remain unchanged, the bottom products deteriorate significantly. This is a result of the movement of concentration fronts inside the column due to a disturbance in the feed flow rate. In this case the concentration fronts are moving towards the bottom. The conversion of AcH reduces from 99 % at the old steady state to 40 % at the new steady state (Fig. 4.14). The three phase region extends in the column as can be seen from the ϕ profiles.

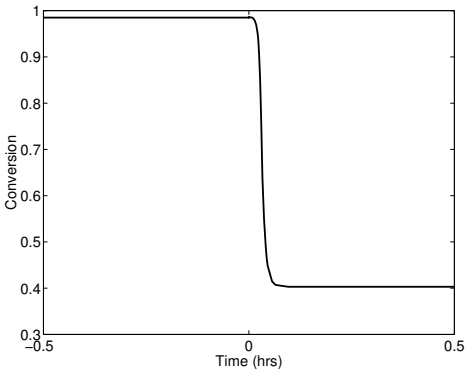

Figure 4.14: Dynamic response in conversion to a 5 % increase of the feed flow rate

For the same case, Fig. 4.15 shows a dynamic response to a 5 % increase in the AcH composition in the feed. The AcH conversion drops to 93 % at the new steady state (Fig. 4.15). In this case, unlike the previous case, the concentration fronts travel towards the column top. The three phase region shrinks to a single stage in the new steady state.

If a 5 % decrease in the feed flow rate or a 5 % decrease of AcH composition in the feed is applied, as expected the concentration fronts move towards the column top in the former case and towards the column bottom in the latter case, yielding 97 % and 96 % AcH conversion, respectively.

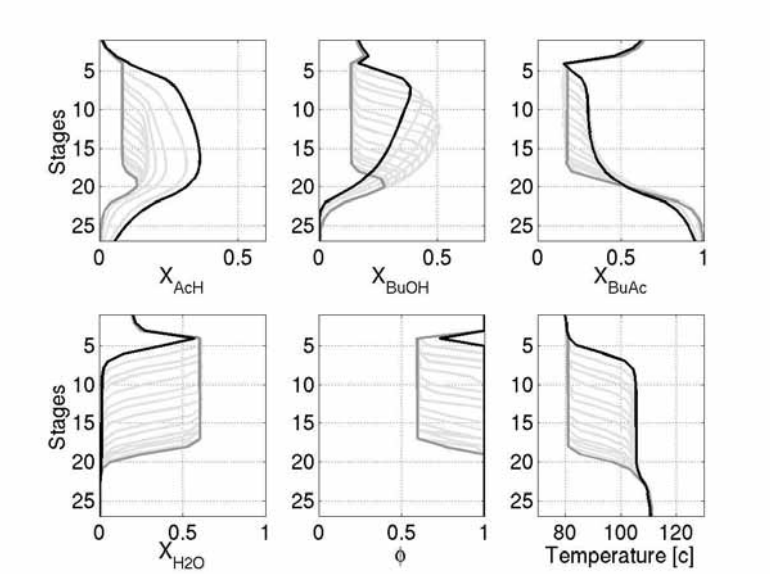

Figure 4.15: Dynamic simulation of configuration 1 with 4 % excess BuOH: transient response to a 5 % increase in AcH composition in feed. Gray line - initial steady state; dark line - final steady state; light gray lines - intermediate states

Table 4.10: Summary of dynamic simulation results for configurations 1 and 6

	Disturbance	AcH conversion at new steady state	
		4 % excess BuOH	2 : 1 BuOH to AcH
configuration 1	+ 5 % feed flow	40.0 %	38.0 %
	- 5 % feed flow	97.2 %	99.9 %
	+ 5 % AcH mole fraction	93.3 %	99.9 %
	- 5 % AcH mole fraction	96.0 %	98.4 %
		Stoichiometric BuOH	2 : 1 BuOH to AcH
configuration 6	+ 5 % feed flow	77.2 %	98.9 %
	- 5 % feed flow	67.0 %	99.2 %
	+ 5 % AcH mole fraction	66.6 %	98.49 %
	- 5 % AcH mole fraction	84.2%	99.0 %

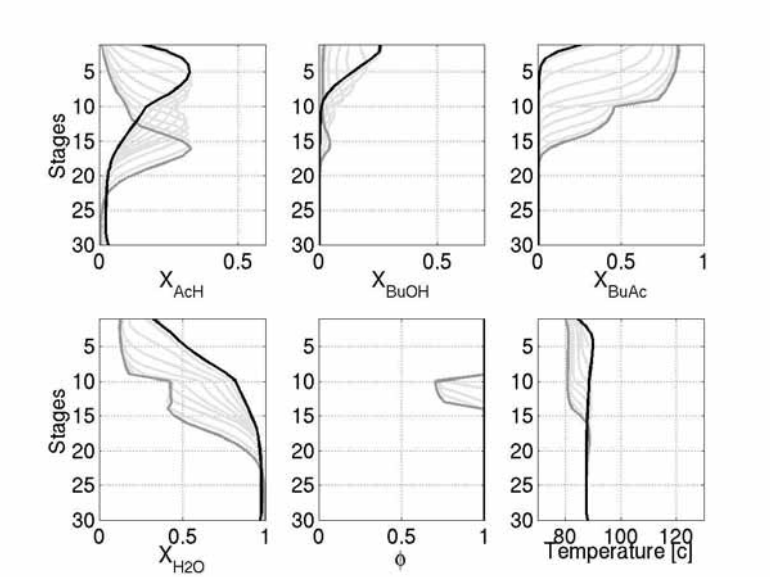

Figure 4.16: Dynamic simulation of configuration 6 with stoichiometric molar ratio of BuOH to AcH: transient response to a 5 % decrease in both feed flow rate. Gray line - initial steady state; dark line - final steady state; light gray lines - intermediate states

Fig. 4.16 shows an open loop dynamic response around the steady state profile shown in Fig. 4.12 to a 5 % decrease in the feed flow rate. In this case, the concentration fronts expectedly move towards the column top, thus adversely effecting the AcH conversion (Fig. 4.17). The three phase region vanishes at the new steady state. In a like wise manner, for a 5 % increase in the AcH composition, the concentration fronts in the column again move towards the top (Fig. 4.18). The AcH conversion drops to a new level of 67 %. The three phase region vanishes completely, like in the previous case. These results clearly indicate that also configuration 6 is very sensitive to disturbances. Hence, in both cases suitable concentration control seems to be crucial for practical operation.

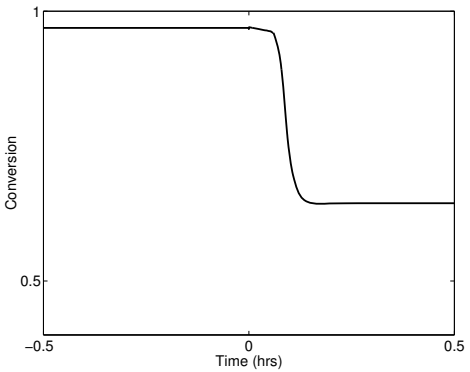

Figure 4.17: Dynamic response in conversion to a 5 % decrease of the feed flow rate

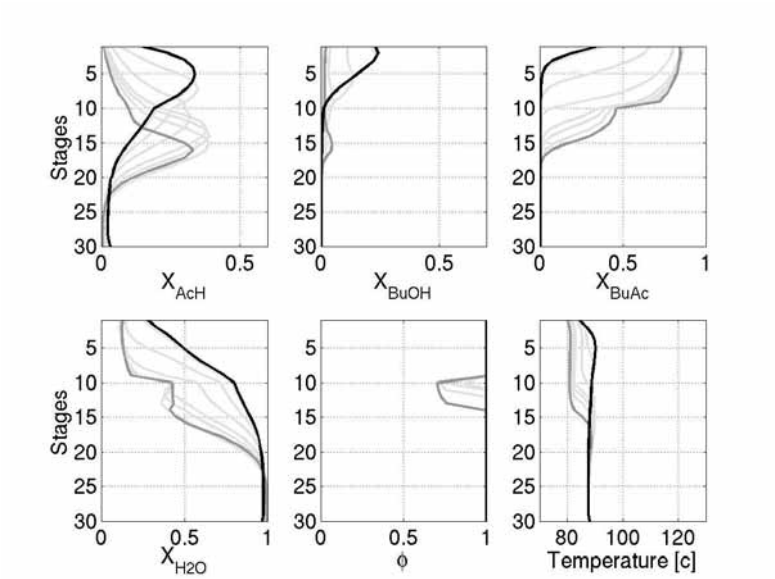

Figure 4.18: Dynamic simulation of configuration 6 with stoichiometric molar ratio of BuOH to AcH: transient response to a 5 % increase in the AcH composition of AcH feed stream. Gray line - initial steady state; dark line - final steady state; light gray lines - intermediate states

4.4.6 Nonlinear dynamic analysis

The dynamics simulation results indicate that configurations 1 and 6 are sensitive to disturbances (see Table 4.10). Configuration 1 is especially sensitive to a + 5 % disturbance in the feed flow rate. Configuration 6 is insensitive for a 2 : 1 BuOH feed case and highly sensitive for a stoichiometric BuOH case. In order to have a better insight of these transient responses, the nonlinear dynamic analysis in the vicinity of the nominal steady states is performed.

Fig. 4.19 shows one parameter continuation diagrams for both process candidates as the reboiler duty is varied from its nominal values, represented by an open circle on these curves. In Fig. 4.19 the AcH conversion is plotted against the reboiler duty. For configuration 1, both feed compositions, namely 2 : 1 BuOH to AcH and 4 % excess of BuOH, possess a single stable steady state over the entire range of the reboiler duty. In contrast, configuration 6 shows multiple steady states in the form of a hysteresis loop for the feed case of stoichiometric BuOH. In particular, the nominal operating point lies within a multiplicity region. It is lying on a very small stable branch, which is hardly visible in Fig. 4.19 (b). A similar stable branch is shown, however, for a higher value of organic reflux (Rf_{org} = 0.97) by an open rectangle. For the feed case of 2 : 1 BuOH, configuration 6 shows a stable steady states branch. It is clear from Figs. 4.19 (a) and (b) that for all feed cases, the desired nominal operating points are lying at the steep hill position. It is expected that a slight process disturbance will deteriorate the process performance significantly.

For configuration 1 (Fig. 4.19 (a)), an operation of the process at a slightly higher reboiler duty will ensure the process insensitivity wrto. the studied process disturbances. On the contrary, configuration 6 (Fig. 4.19 (b)) poses difficulty to be operated at the stoichiometric feed case. It will require a good control strategy. For the feed case of 2 : 1 BuOH, there exists a flat steady state region for Q_{REB} values between 0.11 to 0.15 kW. Since the nominal value is residing well in this range, it has shown insensitivity to disturbances. However, for large process disturbances, a good control strategy will be required for this case too.

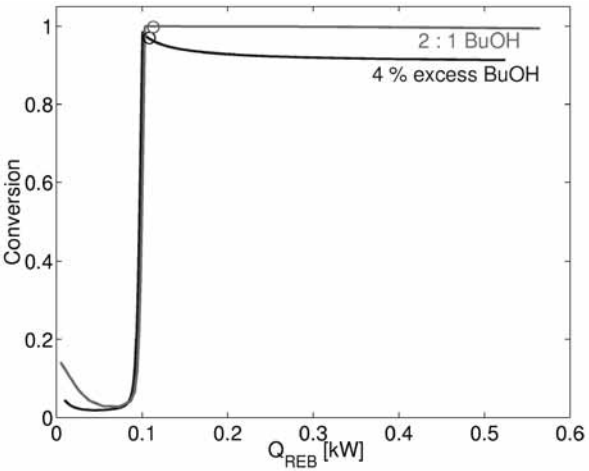

(a)

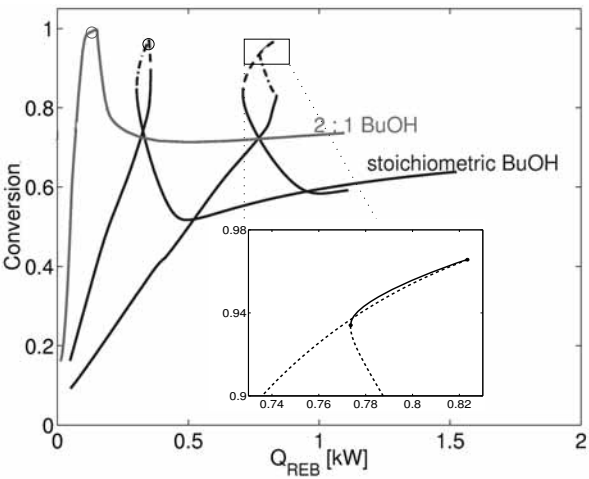

(b)

Figure 4.19: Continuation diagram for (a) configuration 1 and (b) configuration 6

4.5 Summary

A new mathematical approach for the design of reactive distillation column with potential phase split of the liquid phase has been devised. Out of the six selected process candidates, two promising candidates for the removal of AcH from waste water are proposed based on the maximum achievable conversion of acetic acid. Reversed product streams are obtained in case of configuration 1 and configuration 6, both achieving 99 % conversion of AcH. The configuration 1 yields a high purity water stream as distillate and a high purity BuAc stream as bottoms, whereas the configuration 6 yields a high purity water stream as bottoms and a BuAc rich stream as distillate. Their cost comparison with the optimized traditional distillative separation shows 66 % costs reduction with the configuration 1 and 56 % costs reduction with the configuration 6. These values are better than those of the modified approaches appearing in literature, namely, extractive or azeotropic distillations. It should be mentioned, however, that fair comparison with those processes is not possible because previous work considered different concentrations of AcH. Influence of the alcohol to acid ratio on the final process design is also investigated. The results suggest that high alcohol to acid ratio yields higher conversion with less resources (energy costs and number of stages). However, if a high purity ester stream is required, then a feed close to the stoichiometric ratio should be preferred. Configurations 1 and 6 are also investigated for extreme high (65 %) and extreme low (1 %) concentrations of AcH in waste water stream. For a 65 % AcH stream, both configurations yield 99 % AcH conversion, on the other hand, for a 1 % AcH stream, both perform poorly.

Among other interesting features the operability issues are addressed. In this study, insight of the process response to disturbances has been obtained through dynamic simulation and nonlinear dynamic analysis. The results clearly show the complexity involved in maintaining the desired steady states for these two configurations. Some suitable control strategy will be required to operate them. This is a topic of further investigation. It is also important in future to validate the model results experimentally. Another issue is process optimization which is not considered in this chapter, that also requires further investigation.

Chapter 5

Conclusions

Optimization of combined reaction and distillation processes is a challenging but rewarding task. The major challenge is – how to effectively handle present nonlinearities and combinatorial complexities. The field of discrete mathematical optimization offers good tools that are able to provide some answers. In this thesis new solution strategies have been explored to tackle these complex design problems. Summarizing the design strategy, it includes three main steps: 1. selection of suitable process candidates, 2. modeling and simulation for parameter studies and 3. optimization from local to global methods. The design strategy is demonstrated for three practical benchmark problems with increasing level of model complexities, each representing a wide class of process applications.

State-of-the-art local optimization methods are found to be effective when appropriate variable bounds and good initialization are provided. To gain a better assurance, if necessary, local optimizers with multiple restart strategy can be applied. The first global method employing the multi-start algorithm OQNLP is found to be promising for that purpose. Apart from giving a better assurance for the obtained solution, it provides multiple local solutions allowing the user to interpret them in order to make an informed decision. A disadvantage of the single start or multi-start strategy is that no guarantee can be given for the solution to be global. The second global method explored in this thesis is deterministic in nature. Unlike the first global method, it is capable of providing a rigorous global bound on optimal solutions based on the polyhedral relaxation technique. To this end, this method involves a tedious procedure to obtain polyhedral relaxations for the present nonlinear terms. To extend its application to more complex practical examples and to simplify the relaxation procedure, further developments are required. At the end, it is important to determine the inherent risk in the final optimized design with respect to pa-

rameter uncertainties as this design is based on the given values of the model parameters which are subjected to uncertainties. For that purpose, a relatively new method, namely, global sensitivity analysis (GSA) is explored. Though computationally much more demanding than the local sensitivity analysis, the GSA provides an unbiased and reliable estimate of the risk. If the risk is unacceptable then more laboratory experiments can be performed to reduce the uncertainty in sensitive parameters. This at the end also lowers the risk. If the risk is still unacceptable then other process candidates can be analyzed in a similar manner to make a better choice for the design. The GSA problems are difficult to solve for complex practical applications such as esterification necessitating further developments.

For the simple isomerization system, for given constraints and assumed costs, a reactive distillation column is found as the most economical option. For this example, the single start and multi-start strategy converge to the same best solutions. The deterministic optimization method also provides a global confirmation that a reactor coupled with a nonreactive column can not be superior to the reactive distillation column for given costs and constraints. The global sensitivity analysis with respect to the forward rate constant K_f and the equilibrium constant K_{eq} suggests that the final design is operated close to equilibrium bearing higher sensitivity wrto. K_{eq}. The optimized RDC configuration has a lower risk than the optimized RPLUSC configuration.

In case of the esterification process the complexity has increased considerably. This process is still solvable using MINLP optimization techniques. Proper initialization is obtained by using the CMO model in order to effectively use local solvers. The solution times increased from a few seconds for the isomerization example to a few minutes/hours for the esterification example on a 2.0 GHz AMD 64.0 processor. This is not surprising as the number of variables has increased approximately by 10 times. Moreover, in case of nSRCs the number of discrete variables increases drastically with n. In essence, the local optimizers suggest that the RDC configuration is the most economical option marginally better than the 4SRC. The global optimizer based on the multi-start strategy could determine an improved solution with 0.5 % lesser costs for RDC. However, it obtains the same best solution as obtained by using the local optimizer with good initialization and variable bounds for 4SRC.

The third benchmark example, a new process for the removal of acetic acid from waste waters exhibits potential phase splitting of the liquid phase on many column stages. For this problem, optimization methods have not been applied due to increased modeling complexity. A novel and reliable modeling approach applied to detect phase splitting

of the liquid phase involves an external Fortran routine which is difficult to interface with GAMS. Further study is required to explore the external function facility available in GAMS to enable the use of local or global optimizers. For the purpose of this thesis the final designs are obtained based on modeling and simulation performed in DIVA. In particular, two new feasible process candidates are proposed which are found economically favorable compared to a distillative separation of AcH and water. Nonetheless, the new processes are difficult to operate at their nominal steady states requiring a suitable control strategy. However, design and cost estimation of controllers are beyond the scope of this thesis. That should be considered for future work.

Future directions

The gradient based local methods or stochastic methods are often applied to optimally design chemical processes. However, in both cases no guarantee can be given that the solution found by the algorithm is the global optimum. On the other hand, the deterministic global approach based on polyhedral relaxation is limited to problems of moderate complexity due to tricky mixed-integer linear relaxations. Further research is required to extend this method to deal with complex practical applications of combined reaction distillation processes.

On the chemical engineering front more complex and more advanced configurations, for example, a dividing wall reactive distillation column [67] remains to be fully understood. Their design problems will be addressed in future. Secondly, this work employed equilibrium stage column models. A possible extension to rather complex non-equilibrium stage models is interesting for future work as it offers advantage of simultaneous optimization of column internals [30].

Chemical processes could exhibit highly nonlinear steady state and dynamic behavior with output multiplicities, oscillatory behavior and high parameter sensitivity. Therefore, optimization of the steady state design does not guarantee that it is the best process to operate. It is important to extend the design problem by addressing the parameters uncertainty, operability and controllability issues in the early design stage. An excellent work dealing with these aspects is published by Marquardt and Mönnigmann [53]. Another approach based on advance mixed integer dynamic optimization (MIDO) problem is proposed by Panjwani et al. [59].

Appendix A

Cost functions for isomerization example

RDC

Total number of stages:

$$N_T = N_{max} - \sum_{i=1}^{N_{max}} i \cdot IR_i + 2 \tag{A.1}$$

Number of reactive stages:

$$N_R = \sum_{i=1}^{N_{max}} Icat_i \tag{A.2}$$

Column diameter and height:

$$\mathcal{D}_{col} = \sqrt{\frac{4 \cdot V}{\pi F_c} \sqrt{\frac{MW \cdot R \cdot T}{P}}} \tag{A.3}$$

where, F_c is well known F-factor. Its value for 1 bar pressure and 12 inch tray spacing is $\approx$ 1.6 [Pa$^{0.5}$]. The vapor flow in this formula should have to be converted into kmol/s.

$$\mathcal{H}_{col} = (N_T - 2)\mathcal{H}_s + \mathcal{H}^0 \tag{A.4}$$

Constraint on maximum catalyst loading on a tray:

$$Mcat_S \leq 150.0 \frac{\pi}{4} \mathcal{D}_{col}^2 \mathcal{H}_s \tag{A.5}$$

Total catalyst loading in column:

$$Mcat = Mcat_S N_R \tag{A.6}$$

Capital cost calculation:

$$C_{rp} = C_9 \mathcal{D}_{col}^2 \mathcal{H}_s N_R \tag{A.7}$$

$$C_p = C_6 \mathcal{D}_{col}^{C_7} \mathcal{H}_s^{C_8} (N_T - N_R - 2.0) \tag{A.8}$$

$$C_{sh} = C_3 \mathcal{D}_{col}^{C_4} \mathcal{H}_{col}^{C_5} \tag{A.9}$$

$$Q_{REB} = V(H_1^v x_B + H_2^v (1 - x_B)) \tag{A.10}$$

$$Q_{CON} = V H_1^v \tag{A.11}$$

$$A_{REB} = \frac{Q_{REB}}{K_W \Delta T_{REB}} \tag{A.12}$$

$$A_{CON} = \frac{Q_{CON}}{K_W \Delta T_{CON}} \tag{A.13}$$

$$C_{he} = C_1 (A_{REB}^{C_2} + A_{CON}^{C_2}) \tag{A.14}$$

$$\mathbb{C} = C_{rp} + C_p + C_{sh} + C_{he} \tag{A.15}$$

Operating cost calculation:

$$C_{CW} = C_{11} Q_{CON} \tag{A.16}$$

$$C_{HW} = C_{10} Q_{REB} \tag{A.17}$$

$$\mathbb{O} = C_{CW} + C_{HW} \tag{A.18}$$

Total cost:

$$\mathbb{T} = C_{12} C_{13} \mathbb{C} + \mathbb{O} \tag{A.19}$$

Specification

C_1= 3800.0	C_{10} = 250.0	ΔT_{CON} = 35.0 K
C_2= 0.65	C_{11} = 100.0	K_W = 0.8 kJ/s m^2 K
C_3= 8200.0	C_{12} = 0.25	R = 8.314 kJ/kmol K
C_4= 0.9	C_{13} = 4.0	T = 335.0 K
C_5= 1.0	H_1^v = 27405.0 kJ/kmol	P = 101.325 kPa
C_6= 3600.0	H_2^v = 29635.0 kJ/kmol	F_c = 1.6 [Pa$^{0.5}$]
C_7= 1.5	$\mathcal{H}_s$ = 0.33 m	MW = 84.162 kg/kmol
C_8= 1.0	$\mathcal{H}^0$= 4.0 m	N_{max} = 60
C_9= 25000.0	ΔT_{REB} = 35.0 K	

Here, the cost parameters C_1 to C_{13}, $\mathcal{H}_s$, $\mathcal{H}^0$, K_W and F_c are taken from Frey, 2001[19] and ΔT_{REB}, ΔT_{CON} and T are assumed based on a practical considerations.

RPLUSC

$$\mathcal{V}_R = 2\frac{Mcat_R}{\rho_{cat}} \tag{A.20}$$

$$\mathcal{H}_R = \mathcal{D}_R = \left(\frac{4}{Pi}\mathcal{V}_R\right)^{\frac{1}{3}} \tag{A.21}$$

$$Creac = C_3\mathcal{D}_R^{C_4}\mathcal{H}_R^{C_5} + C_{14}Mcat_R \tag{A.22}$$

Capital cost calculation:

$$\mathbb{C} = Creac + C_p + C_{sh} + C_{he} \tag{A.23}$$

Operating cost calculation:

$$\mathbb{O} = C_{CW} + C_{HW} + C_{15}B \tag{A.24}$$

Specification

C_{14} = 20.0
C_{15} = 100.0
ρ_{cat} = 730.0
Here, the cost parameters C_{14} and C_{15} are assumed based on a practical considerations.

REACREB

For the REACREB configuration, cost functions and cost parameters given for the RDC configuration can be directly used with only a single reactive tray at the reboiler.

Appendix B

MINLP model formulation for esterification example

The MINLP model for the RDC and the SRC is based on the assumptions stated in section 3.4. This Appendix shows how integer variables are incorporated in the balance equations. Let i be the index for the number of components, i.e. $i \in n_c$ and j be the index for the number of stages, i.e. $j \in N_T$, such that $j = 1$ represents the top tray in the column and $j = N_T$ represents the reboiler. The total condenser and the decanter models are coupled to the column at the top. The binary variables IN_j, $Icat_j$ and IR_j decide whether a tray 'j' is a feed tray (IN_j = 1), a reactive tray ($Icat_j$ = 1) or the top tray receiving the reflux (IR_j = 1). Additional logical constraints need to be provided on the integer variables as shown in Eq. (B.4).

RDC

Total material balances:

$$\begin{aligned}
&-L_j + V_{j+1} - V_j + FIN_j + Icat_j \sum_{l=1}^{nr} \nu_{Tl} r_{lj} + LorgIR_j = 0 && (j = 1) \\
&-L_j + L_{j-1} + V_{j+1} - V_j + FIN_j + Icat_j \sum_{l=1}^{nr} \nu_{Tl} r_{lj} + LorgIR_j = 0 \\
& && (j = 2, \ldots, N_T - 1) \\
&-L_j + L_{j-1} - V_j + FIN_j + Icat_j \sum_{l=1}^{nr} \nu_{Tl} r_{lj} + LorgIR_j = 0 && (j = N_T)
\end{aligned} \tag{B.1}$$

Component material balances ($\forall i = 1, \ldots, n_c - 1$):

$$\begin{aligned}
&-L_j x_{ij} + V_{j+1} y_{ij+1} - V_j y_{ij} + Fx_{F_i} IN_j + Icat_j \sum_{l=1}^{nr} \nu_{li} r_{lj} + Lorg\ xorg_i IR_j = 0 \\
&\qquad\qquad\qquad\qquad\qquad\qquad\qquad\qquad\qquad\qquad (j = 1) \\
&-L_j x_{ij} + L_{j-1} x_{ij-1} + V_{j+1} y_{ij+1} - V_j y_{ij} + Fx_{F_i} IN_j + Icat_j \sum_{l=1}^{nr} \nu_{li} r_{lj} \\
&\quad + Lorg\ xorg_i IR_j = 0 \qquad\qquad\qquad\qquad\qquad\qquad (j = 2, \ldots, N_T - 1) \\
&-L_j x_{ij} + L_{j-1} x_{ij-1} - V_j y_{ij} + Fx_{F_i} IN_j + Icat_j \sum_{l=1}^{nr} \nu_{li} r_{lj} + Lorg\ xorg_i IR_j = 0 \\
&\qquad\qquad\qquad\qquad\qquad\qquad\qquad\qquad\qquad\qquad (j = N_T)
\end{aligned} \tag{B.2}$$

Energy balances:

$$\begin{aligned}
&-L_j H_j^l + V_{j+1} H_{j+1}^g - V_j H_j^g + FH_j^f IN_j + LorgH_j^{lorg} IR_j = 0 \qquad\qquad (j = 1) \\
&-L_j H_j^l + L_{j-1} H_{j-1}^l + V_{j+1} H_{j+1}^g - V_j H_j^g + FH_j^f IN_j + LorgH_j^{lorg} IR_j = 0 \\
&\qquad\qquad\qquad\qquad\qquad\qquad\qquad\qquad\qquad\qquad (j = 2, \ldots, N_T - 1) \\
&-L_j H_j^l + L_{j-1} H_{j-1}^l - V_j H_j^g + FH_j^f IN_j + LorgH_j^{lorg} IR_j + Q_{REB} \cdot 3600.0 = 0 \\
&\qquad\qquad\qquad\qquad\qquad\qquad\qquad\qquad\qquad\qquad (j = N_T)
\end{aligned} \tag{B.3}$$

Logical constraints:

$$\begin{aligned}
\text{a single feed tray:} \quad & \sum_{j=1}^{N_{max}} IN_j = 1 \\
\text{relative feed location:} \quad & \sum_{j=1}^{N_{max}} j \cdot IN_j \geq \sum_{j=1}^{N_{max}} j \cdot IR_j \\
\text{relative reaction zone location:} \quad & Icat_j \cdot (j \cdot Icat_j - \sum_{j=1}^{N_{max}} j \cdot IR_j) \geq 0.0 \\
\text{a single top tray:} \quad & \sum_{j=1}^{N_{max}} IR_j = 1
\end{aligned} \tag{B.4}$$

Note that for a fixed number of column stages, IR_1 = 1

nSRCs

For the nSRC models, only the component balances are shown in the following. The total material balance and the energy balance equations can be modified accordingly. The reactor model is a standard CSTR model. Let k be the index for the number of reactors, i.e. $k \in N_{Rx}$. Here, the binary variables IN_j and IR_j make the same decisions as in the previous case, whereas the additional binary variables $IN^I_{R_{jk}}$ and $IN^O_{R_{jk}}$ decide whether a tray j is a sidedraw tray of k^{th} reactor ($IN^I_{R_{jk}}$ = 1) or a feedback tray ($IN^O_{R_{jk}}$ = 1).

Component material balances($\forall\ i = 1, \ldots, n_c - 1$):

$$\begin{aligned}
&-L_j x_{ij} + V_{j+1} y_{ij+1} - V_j y_{ij} - \sum_{k=1}^{N_{Rx}} F^I_{R_k} x_{ij} IN^I_{R_{jk}} + \sum_{k=1}^{N_{Rx}} F^O_{R_k} x^O_{R_{ik}} IN^O_{R_{jk}} \\
&\quad + F x_{F_i} IN_j + Lorg\ xorg_i IR_j = 0 \qquad\qquad (j = 1) \\
&-L_j x_{ij} + L_{j-1} x_{ij-1} + V_{j+1} y_{ij+1} - V_j y_{ij} - \sum_{k=1}^{N_{Rx}} F^I_{R_k} x_{ij} IN^I_{R_{jk}} \\
&\quad + \sum_{k=1}^{N_{Rx}} F^O_{R_k} x^O_{R_{ik}} IN^O_{R_{jk}} + F x_{F_i} IN_j + Lorg\ xorg_i IR_j = 0 \\
&\qquad\qquad (j = 2, \ldots, N_T - 1) \\
&-L_j x_{ij} + L_{j-1} x_{ij-1} - V_j y_{ij} - \sum_{k=1}^{N_{Rx}} F^I_{R_k} x_{ij} IN^I_{R_{jk}} + \sum_{k=1}^{N_{Rx}} F^O_{R_k} x^O_{R_{ik}} IN^O_{R_{jk}} \\
&\quad + F x_{F_i} IN_j + Lorg\ xorg_i IR_j = 0 \qquad\qquad (j = N_T)
\end{aligned} \tag{B.5}$$

Logical constraints:
Constraints for a single feed tray, a single sidedraw tray and a single feedback tray:

$$\sum_{j=1}^{N_{max}} IN_j = 1\ ; \sum_{j=1}^{N_{max}} IN^I_{R_{jk}} = 1\ ;\quad \sum_{j=1}^{N_{max}} IN^O_{R_{jk}} = 1\ ;\quad \forall k \tag{B.6}$$

Constraint on a relative feed location:

$$\sum_{j=1}^{N_{max}} j \cdot IN_j \geq \sum_{j=1}^{N_{max}} j \cdot IR_j \tag{B.7}$$

Constraint on a relative reaction zone location:

$$\sum_{j=1}^{N_{max}} j \cdot IN^{I}_{R_{jk}} \geq \sum_{j=1}^{N_{max}} j \cdot IR_j \text{ and } \sum_{j=1}^{N_{max}} j \cdot IN^{O}_{R_{jk}} \geq \sum_{j=1}^{N_{max}} j \cdot IR_j \quad \forall k \tag{B.8}$$

Constraint for a single top tray:

$$\sum_{j=1}^{N_{max}} IR_j = 1 \tag{B.9}$$

Once again note that for a fixed number of column stages, IR_1 = 1

Cost functions

In this appendix, detailed cost functions determining the equipment cost viz. the cost of column shell, column internals, heat exchangers and reactors; and the operating cost involving the cost of hot and cold utilities are described. The values of the cost coefficients appearing in the following equations are adopted from Frey [19].
Total number of stages:

$$N_T = N_{max} - \sum_{j=1}^{N_{max}} j \cdot IR_j + 1 \tag{B.10}$$

Number of reactive stages:

$$N_R = \sum_{j=1}^{N} Icat_j \tag{B.11}$$

Column diameter and height:

$$\mathcal{D}_{col} = \sqrt{\frac{V_{N_T}\, 4}{\pi\, F_c} \sqrt{\frac{(\sum_{i=1}^{n_c} MW_i\, y_{iN_T})\; R\, T_{N_T}}{P}}} \tag{B.12}$$

where, F_c is a well known F-factor. Its value for 1 bar pressure and 12 inch tray spacing is $\approx$ 1.5 [Pa$^{0.5}$]. The vapor flow in this formula should have to be converted into kmol/s.

$$\mathcal{H}_{col} = (N_T - 2)\, \mathcal{H}_s + \mathcal{H}^0 \tag{B.13}$$

Constraint on maximum catalyst loading on a tray:
For the commercially available Amberlyst-15 catalytic packing (e.g. Katapack-s), the packing density is around 0.21 (vol/vol). Therefore, there is a maximum limit on kg of catalyst that can be loaded on a tray with a given diameter.

$$Mcat_S \leq 150.0 \, \frac{\pi}{4} \, \mathcal{D}_{col}^2 \, \mathcal{H}_s \tag{B.14}$$

Total catalyst loading in column:

$$Mcat = Mcat_S \, N_R \tag{B.15}$$

Capital cost calculation:

$$C_{rp} = C_9 \, \mathcal{D}_{col}^2 \, \mathcal{H}_s \, N_R \tag{B.16}$$

$$C_p = C_6 \, \mathcal{D}_{col}^{C_7} \, \mathcal{H}_s^{C_8} \, (N_T - N_R - 2.0) \tag{B.17}$$

$$C_{sh} = C_3 \, \mathcal{D}_{col}^{C_4} \, \mathcal{H}_{col}^{C_5} \tag{B.18}$$

$$Q_{CON} = V_1 \sum_{i=1}^{n_c} H_i^v \, y_{i1} \tag{B.19}$$

$$A_{REB} = \frac{Q_{REB}}{K_W \, \Delta T_{REB}} \tag{B.20}$$

$$A_{CON} = \frac{Q_{CON}}{K_W \, \Delta T_{CON}} \tag{B.21}$$

$$C_{he} = C_1 \, (A_{REB}^{C_2} + A_{CON}^{C_2}) \tag{B.22}$$

$$\mathbb{C} = C_{rp} + C_p + C_{sh} + C_{he} \tag{B.23}$$

Operating cost calculation:

$$C_{CW} = C_{11} \, Q_{CON} \tag{B.24}$$

$$C_{HW} = C_{10} \, Q_{REB} \tag{B.25}$$

$$\mathbb{O} = C_{CW} + C_{HW} \tag{B.26}$$

Total cost:

$$\mathbb{T} = C_{12} \, C_{13} \, \mathbb{C} + \mathbb{O} \tag{B.27}$$

Specification

C_1= 3800.0
C_2= 0.65
C_3= 8200.0
C_4= 0.9
C_5= 1.0
C_6= 3600.0
C_7= 1.5
C_8= 1.0
C_9= 25000.0
C_{10} = 250.0
C_{11} = 100.0
C_{12} = 0.25
C_{13} = 4.0
$\mathcal{H}_s$ = 0.33 m
$\mathcal{H}^0 = 4.0$ m
ΔT_{REB} = 35.0 K
ΔT_{CON} = 35.0 K
K_W = 0.8 kJ/s m^2 K
R = 8.314 kJ/kmol-K
T = 335.0 K
P = 0.65 bar
H_1^v = 23700.0 kJ/kmol
H_2^v = 43760.0 kJ/kmol
H_3^v = 35500.0 kJ/kmol
H_4^v = 40660.0 kJ/kmol
H_5^v = 40210.0 kJ/kmol

Cost functions for the side reactors

The coefficients appearing here are estimated on practical considerations.

$$\mathcal{V}_{R_k} = 2\,\frac{Mcat_{R_k}}{\rho_{cat}} \quad \forall k \tag{B.28}$$

$$\mathcal{H}_{R_k} = \mathcal{D}_{R_k} = \left(\frac{4}{Pi}\,\mathcal{V}_{R_k}\right)^{\frac{1}{3}} \quad \forall k \tag{B.29}$$

$$Creac_k = C_3\,\mathcal{D}_{R_k}^{C_4}\,\mathcal{H}_{R_k}^{C_5} + C_{14}\,Mcat_{R_k} \quad \forall k \tag{B.30}$$

Capital cost for nSRCs:

$$\mathbb{C} = \sum_{k=1}^{N_{Rx}} Creac_k + C_p + C_{sh} + C_{he} \tag{B.31}$$

Operating cost for nSRCs:

$$\mathbb{O} = C_{CW} + C_{HW} + C_{15} \sum_{k=1}^{N_{Rx}} F_{R_k}^I \tag{B.32}$$

Specification

C_{14} = 15.0
C_{15} = 5.0
ρ_{cat} = 730.0

Bibliography

[1] V. H. Agreda, L. R. Partin, and W. H. Heise. High-purity methyl acetate via reactive distillation. *Chem. Eng. Prog.*, 40:40–46, 1990.

[2] D. Barbosa and M. F. Doherty. The influence of equilibrium chemical reactions on vapor-liquid phase diagrams. *Chem. Eng. Sci.*, 43:529–540, 1988.

[3] R. Baur and R. Krishna. Distillation column with reactive pump arounds: an alternative to reactive distillation. *Chem. Eng. Process.*, 43:435–445, 2003.

[4] J. Bausa and W. Marquardt. Quick and reliable phase stability test in VLLE flash calculations by homotopy continuation. *Comput. Chem. Eng.*, 24:2447–2456, 2000.

[5] B. Bessling. *Zur Reaktivdestillation in der Prozesssynthese*. PhD thesis, University of Dortmund, 1998.

[6] B. Bessling, G. Schembecker, and K. Simmrock. Design of processes with reactive distillation line diagrams. *Ind. Eng. Chem. Res.*, 36:3032, 1997.

[7] B. Bessling, R. Welker, J. W. Knab, B. Lohe, and W. Disteldorf. Continuous preparation of esters and apparatus therefore. *Ger. Offen.*, 6, 1999. CA: 130: 11832v.

[8] P. Bratley and B. L. Fox. Algorithm 659: Implementing Sobol's quasirandom sequence generator. *ACM Trans. Math. Softw.*, 14:88–100, 1988.

[9] A. Brooke, D. Kendrick, and A. Meeraus. *GAMS A User's Guide, Release 2.25*. GAMS Development Corp., Washington D.C., 1996.

[10] S. Brüggemann, J. Oldenburg, P. Zhang, and W. Marquardt. Robust dynamic simulation of three-phase reactive batch distillation columns. *Ind. Eng. Chem. Res.*, 43:3672–3684, 2004.

[11] M. F. Cardoso, R. L. Salcedo, S. F. de Azevedo, and D. Barbosa. Optimization of reactive distillation processes with simulated annealing. *Chem. Eng. Sci.*, 55:5059–5078, 2000.

[12] I. L. Chien, K. L. Zeng, H. Y. Chao, and J. H. Liu. Design and control of acetic acid dehydration system via heterogeneous azeotropic distillation. *Chem. Eng. Sci.*, 59:4547–4567, 2004.

[13] A. R. Ciric and D. Gu. Synthesis of nonequilibrium reactive distillation processes by MINLP optimization. *AIChE J.*, 40:1479–1487, 1994.

[14] H. Demiral and M. E. Yildirim. Recovery of acetic acid from waste streams by extractive distillation. *Water Sci. Technol.*, 47:183–188, 2003.

[15] E. Doedel. *AUTO: Software for continuation and bifurcation problems in ordinary differential equations*. Pasadena, 1986.

[16] J. Douglas. *Conceptual design of chemical processes*. McGraw-Hill, New York, 1988.

[17] A. S. Drud. CONOPT-A large scale GRG code. *ORSA Journal on Computing*, 6:207–216, 1994.

[18] M. A. Duran and I. E. Grossmann. An outer approximation algorithm for a class of mixed-integer nonlinear programs. *Math. Prog.*, 36:307–339, 1986.

[19] Th. Frey. *Synthese und Optimierung von Reaktivrektifikationsprozessen*. PhD thesis, TU München, 2001.

[20] Th. Frey, D. Brusis, J. Stichlmair, M. H. Bauer, and S. Glanz. Systematische Prozesssynthese mit Hilfe mathematischer Modelle. *Chemie-Ing.-Techn.*, 72:813–821, 2000.

[21] Th. Frey and J. Stichlmair. Thermodynamic fundamentals of reactive distillation. *Chem. Eng. Technol.*, 22:11–18, 1999.

[22] S. B. Gadewar, L. Tao, M. F. Malone, and M. F. Doherty. Process alternatives for coupling reaction and distillation. *Chem. Eng. Res. Des.*, 82:140–147, 2004.

[23] GAMS. *The Solver Manuals*. GAMS Development Corp., Washington D.C., 2006.

[24] J. Gangadwala, A. Kienle, U.-U. Haus, D. Michaels, and R. Weismantel. Global bounds on optimal solutions for the production of 2,3-dimethylbutene-1. *Ind. Eng. Chem. Res.*, 45:2261–2271, 2006.

[25] J. Gangadwala, A. Kienle, E. Stein, and S. Mahajani. Production of butyl acetate by catalytic distillation: Process design studies. *Ind. Eng. Chem. Res.*, 43:136–143, 2004.

[26] J. Gangadwala, S. Mankar, S. Mahajani, A. Kienle, and E. Stein. Esterification of acetic acid with butanol in the presence of ion exchange resins as catalysts. *Ind. Eng. Chem. Res.*, 42:2146–2155, 2003.

[27] J. Gangadwala, G. Radulescu, A. Kienle, F. Steyer, and K. Sundmacher. New processes for recovery of acetic acid from waste water. In *Paper H4.4, CHISA'06, 29.8. - 3.9., Prague*, 2006.

[28] S. Giessler, R. Y. Danilov, R. Y. Pisarenko, L. A. Serafimov, S. Hasebe, and I. Hashimoto. Feasibility study of reactive distillation using the analysis of the statics. *Ind. Eng. Chem. Res.*, 37(11):4375–4382, 1998.

[29] J. Gmehling, J. Li, and M. Schiller. A modified UNIFAC model. 2. present parameter matrix and results for different thermodynamics properties. *Ind. Eng. Chem. Res.*, 32:178–193, 1993.

[30] J. M. Gomez, J.-M. Reneume, M. Roques, M. Meyer, and X. Meyer. A mixed integer nonlinear programming formulation for optimal design of a catalytic distillation column based on a generic nonequilibrium model. *Ind. Eng. Chem. Res.*, 45:1373–1388, 2006.

[31] B. S. Greenberg and L. S. Lasdon. Using global optimization to estimate population class sizes. *J. Glob. Optim.*, 36:319–338, 2006.

[32] I. E. Grossmann and L. T. Biegler. Part II. Future perspective on optimization. *Comput. Chem. Eng.*, 28:1193–1218, 2004.

[33] R. F. Blanco Gutierrez, C. C. Pantelides, and C. S. Adjiman. Risk analysis and robust design under technological uncertainty. In W. Marquardt and C. Pantelides, editors, *European Symposium on Computer Aided Process Engineering – 16*, pages 191–196. Elsevier Science B.V., 2006.

[34] J. Hanika, J. Kolena, and Q. Smejkal. Butyl acetate via reactive distillation: Modeling and experiments. *Chem. Eng. Sci.*, 54:5205–5209, 1999.

[35] J. Hanika, M. Kucharova, J. Kolena, and Q. Smejkal. Multi-functional trickle bed reactor for butyl acetate synthesis. *Catal. Today*, 79-80:83–87, 2003.

[36] E. R. Hansen. Global optimization using interval analysis: The multi-dimensional case. *Numerische Mathematik*, 34:247–270, 1980.

[37] H. Hartig and H. Regner. Verfahrenstechnische Auslegung einer Veresterungskolonne. *Chemie-Ing.-Techn.*, 43:1001–1007, 1971.

[38] S. Hauan, A. W. Westerberg, and K. M. Lien. Phenomena based analysis of fixed points in reaction separation systems. *Chem. Eng. Sci.*, 55:1053, 1999.

[39] D. M. Himmelblau and J. Riggs. *Basic Principles and Calculation in Chemical Engineering*. Prentice Hall PTR, New Jersey, 2003.

[40] T. Homma and A. Saltelli. Importance measures in global sensitivity analysis of nonlinear models. *Reliab. Eng. Syst. Safe.*, 52:1–17, 1996.

[41] ILOG. CPLEX, 1997–2005. url: http://www.ilog.com/products/cplex/.

[42] J. R. Jackson and I. E. Grossmann. A disjunctive programming approach for the optimal design of reactive distillation columns. *Comput. Chem. Eng.*, 25:1661–1673, 2001.

[43] R. Janowsky, M. Groebel, and U. Knippenberg. Nonlinear dynamics in reactive distillation – phenomena and their technical use. Final Report, FKZ : 03D0014 B0, Huels Infracor GmbH: experSCience, Marl, 1997.

[44] L. Jimenez, A. Garvin, and J. Costa-Lopez. The production of butyl acetate and methanol via reactive and extractive distillation. I. Chemical equilibrium, kinetics and mass transfer issues. *Ind. Eng. Chem. Res.*, 41:6663–6669, 2002.

[45] A. Kent, M. Lawrenson, and D. Macalpine. Process for the production of 2,3-dimethylbutene-1 from propene, 1989. U.S. Patent 4,835,328.

[46] A. Kienle, K. D. Mohl, and E. D. Gilles. Nichtlineare Dynamik bei Reaktivdestillationsprozessen. In *Nichtlineare Dynamik bei chemischen Prozessen*, pages 1–6. Dechema e.V., 1997.

[47] R. Krishna. Hardware selection and design aspects of reactive distillation columns. In K. Sundmacher and A. Kienle, editors, *Reactive Distillation – Status and Future Directions*, pages 241–281. Wiley-VCH, Weinheim, 2003.

[48] R. Kumar, H. Nanavati, S. B. Noronha, and S. M. Mahajani. A continuous process for the recovery of lactic acid by reactive distillation. *Journ. Chem. Tech. Biotechno.*, 81:1767–1777, 2006.

[49] M. Laguna and R. Marti. *Scatter search, methodology and implementations in C*. Kluwer Academic, Dordrecht, 2003.

[50] J. W. Lee, S. Brüggemann, and W. Marquardt. Shortcut method for kinetically controlled reactive distillation systems. *AIChE J.*, 49:1471, 2003.

[51] S. Lee and I. E. Grossmann. A global optimization algorithm for nonconvex generalized disjunctive programming and applications to process systems. *Comput. Chem. Eng.*, 25:1675–1697, 2001.

[52] M. Mangold, A. Kienle, K. D. Mohl, and E. D. Gilles. Nonlinear computation using DIVA – Methods and applications. *Chem. Eng. Sci.*, 55:441–454, 2000.

[53] W. Marquardt and M. Mönnigmann. Constructive nonlinear dynamics in process systems engineering. *Comput. Chem. Eng.*, 29:1265–1275, 2005.

[54] J. Marriott and E. Sorensen. The optimal design of membrane systems. *Chem. Eng. Sci.*, 58:4991–5004, 2003.

[55] C. D. McGregor, D. Glasser, and D. Hildebrandt. Process synthesis of a reactive distillation system using attainable region results. *Distillation & Absorption'97, Trans. IChem E. Symposium Series*, 142:663, 1997.

[56] M. Minotti, M. F. Doherty, and M. F. Malone. Design for simultaneous reaction and liquid-liquid extraction. *Ind. Eng. Chem. Res.*, 37:4748–4755, 1998.

[57] A. Nisoli, M. F. Malone, and M. F. Doherty. Attainable regions for reaction with separation. *AIChE J.*, 43:374, 1997.

[58] C. Noeres, E. Kenig, and A. Gorak. Modelling of reactive separation processes: reactive adsorption and reactive distillation. *Chem. Eng. Process.*, 42:157–178, 2003.

[59] P. Panjwani, M. Schenk, M. C. Georgiadis, and E. N. Pistikopoulos. Optimal design and control of a reactive distillation system. *Eng. Optim.*, 37:733–753, 2005.

[60] Z. Qi, A. Kolah, and K. Sundmacher. Residue curve maps for reactive distillation systems with liquid-phase splitting. *Chem. Eng. Sci.*, 57:163–178, 2002.

[61] G. Radulescu, J. Gangadwala, A. Kienle, F. Steyer, and K. Sundmacher. Dynamic simulation of reactive distillation processes with liquid liquid phase splitting. In Iulian Nistor, editor, *Buletinul universitatii petrol-gaze din ploiesti*, pages 1–12, Ploiesti, 2006.

[62] R. C. Reid, J. M. Prausnitz, and B. E. Poling. *The Properties of Gases and Liquids*. McGraw-Hill, New York, 4. edition, 1987.

[63] B. Saha, S. P. Chopade, and S. M. Mahajani. Recovery of dilute acetic acid through esterification in a reactive distillation column. *Catal. Today*, 60:147–157, 2000.

[64] S. Saltelli, S. Tarantola, F. Campolongo, and M. Ratto. *Sensitivity Analysis in Practice*. John Willey & Sons, West Sussex, 2004.

[65] G. Sand, S. Barkmann, P. Scherpian, M. Tylko, S. Engell, and G. Schembecker. MINLP - optimization in the integration of reaction and separation processes. In P. Jansen, A. Stankiewicz, and A. Green, editors, *Sustainable (Bio) Chemical Process Technology incorporating Process Intensification 6*, pages 317–324, Cranfield UK, BHR Group, 2005.

[66] G. Sand, S. Barkmann, C. Schmidt, and S. Engell. Global optimization in the conceptual design of reactive distillation columns. In *Proc. 7th World Congress of Chemical Engineering*, Glasgow, 2005.

[67] S. Sander, C. Flisch, E. Geissler, H. Schoenmakers, O. Ryll, and H. Hasse. Methyl acetate hydrolysis in a reactive divided wall column. *Chem. Eng. Res. Des.*, 85:149–154, 2007.

[68] H. Sato, H. Tojima, and K. Ikimi. Studies on nickel-containing ziegler-type catalysts V. dimerization of propylene to 2,3-dimethylbutenes. Part III. 1,1,1,3,3,3-hexafluoro-2-propanol as a new efficient activator. *J. Mole. Cat. A: Chem.*, 144:285–293, 1999.

[69] H. Schoenmakers and W. Buehler. Distillation column with external reactors - an alternative to the reaction column. *Ger. Chem. Eng.*, 5:292–296, 1982.

[70] H. G. Schoenmakers and B. Bessling. Reactive distillation process development in the chemical process industries. In K. Sundmacher and A. Kienle, editors, *Reactive Distillation – Status and Future Directions*, pages 241–281. Wiley-VCH, Weinheim, 2003.

[71] M. M. Sharma and S. Mahajani. Industrial application of reactive distillation. In K. Sundmacher and A. Kienle, editors, *Reactive Distillation – Status and Future Directions*. Wiley-VCH, Weinheim, 2003.

[72] A. Singh, R. Hiwale, S. Mahajani, R. D. Gudi, J. Gangadwala, and A. Kienle. Production of butyl acetate by catalytic distillation: Theoretical and experimental studies. *Ind. Eng. Chem. Res.*, 44:3042–3052, 2005.

[73] L. A. Smith. Catalytic distillation process, 1981. US Patent No. 4,307,254.

[74] I. M. Sobol'. Uniformly distributed sequences with an additional uniform property. *USSR Comput. Math. Math. Phys.*, 16:236–242, 1976.

[75] I. M. Sobol'. Global sensitivity indices for nonlinear mathematical models and their Monte Carlo estimates. *Math. Comput. Simulat.*, 55:271–280, 2001.

[76] E. Stein. *Synthesis of reactive distillation processes*. PhD thesis, OvGU Magdeburg, 2003.

[77] S. Steinigeweg and J. Gmehling. n-Butyl acetate synthesis via reactive distillation: Thermodynamic aspects, reaction kinetics, pilot-plant experiments, and simulation studies. *Ind. Eng. Chem. Res.*, 41:5483–5490, 2002.

[78] F. Steyer, D. Flockerzi, and K. Sundmacher. Equilibrium and rate-based approaches to liquid-liquid phase splitting calculations. *Comput. Chem. Eng.*, 30:277–284, 2005.

[79] J. Stichlmair and Th. Frey. Mixed-integer nonlinear programming optimization of reactive distillation processes. *Ind. Eng. Chem. Res.*, 40:5978–5982, 2001.

[80] E. H. Stitt. Multifunctional reactors? "Up to a point Lord Copper". *Chem. Eng. Res. Des.*, 82:129–139, 2004.

[81] K. Sundmacher. *Reaktivdestillation mit katalytischen Füllkörpern – ein neuer Prozeß zur Herstellung der Kraftstoffkomponente MTBE*. PhD thesis, Technische Universität Clausthal, 1995.

[82] K. Sundmacher and A. Kienle. *Reactive Distillation – Status and Future Trends*. Wiley-VCH, Weinheim, 2003.

[83] K. Sundmacher and Z. Qi. Conceptual design aspects of reactive distillation processes for ideal binary mixtures. *Chem. Eng. Process.*, 42:191–200, 2003.

[84] M. Tawarmalani and N. V. Sahinidis. Global optimization of mixed-integer nonlinear programs: A theoretical and computational study. *Math. Program.*, 99 (3, Ser. A):563–591, 2004.

[85] R. Taylor and R. Krishna. Modelling reactive distillation. *Chem. Eng. Sci.*, 55:5183–5229, 2000.

[86] Z. Ugray, L. Lasdon, J. Plummer, F. Glover, J. Kelly, and R. Marti. A multistart scatter search heuristic for smooth NLP and MINLP problems. 2003. submitted to *INFORMS J. Comput.* or on the web at www.utexas.edu/courses/lasdon, link to papers.

[87] S. Ung and M. F. Doherty. Vapor-liquid phase equilibrium in systems with multiple chemical reactions. *Chem. Eng. Sci.*, 50:23–48, 1995.

[88] G. Venimadhavan, G. Buzad, M. F. Doherty, and M. F. Malone. Effect of kinetics on residue curve maps for reactive distillation. *AIChE J.*, 40:1814–1824, 1994.

[89] G. Venimadhavan, M. F. Malone, and M. F. Doherty. A novel distillate policy for batch reactive distillation with application to the production of butyl acetate. *Ind. Eng. Chem. Res.*, 38:714–722, 1999.

[90] J. Viswanathan and I. E. Grossmann. An alternate MINLP model for finding the number of trays required for a specified separation objective. *Comput. Chem. Eng.*, 17:946–955, 1993.

[91] H. Yeomans and I. E. Grossmann. Optimal design of complex distillation columns using rigorous tray by tray disjunctive programming models. *Ind. Eng. Chem. Res.*, 39:4326–4335, 2000.

[92] Y. Zhicai, C. Xianbao, and G. Jing. Esterification - distillation of butanol and acetic acid. *Chem. Eng. Sci.*, 53:2081–2088, 1998.